DEVELOPMENT AND EVALUATION OF INTEGRATED CHASSIS CONTROL SYSTEMS

by

Youseok Kou

A dissertation submitted in partial fulfillment
of the requirements for the degree of
Doctor of Philosophy
(Mechanical Engineering)
in The University of Michigan
2010

Doctoral Committee:

Professor Huei Peng, Chair
Professor Timothy J. Gordon
Professor Jing Sun
Professor A. Galip Ulsoy

To my family

ACKNOWLEDGMENTS

I would like to especially thank my advisor, Prof. Huei Peng, for his support, persistence, and motivation throughout my doctorial studies. He provided great inspiration and devoted guidance, both of which stimulated me to pursue my interests throughout my research. I would also like to express my deep appreciation to the other members of my committee, Prof. Galip Ulsoy, Prof. Dr. Timothy J. Gordon and Prof. Jing Sun, for their valuable advice and comments, which helped guide the direction of my work.

I gratefully acknowledge the sincere cooperation of Dr. Dohyun Jung, Korean Automotive Technical Center, and Mando Corporation conducting my dissertation research in University of Michigan.

I will remember my colleagues and friends in the Automotive Laboratory but not limited to Dae-Kyun Kim, Min Joong Kim, Jinming Liu, Jing Zhou, Yongsong Chen, Jeong-Seok Kim, Dongsuk Kum, Hsin-Hsiang Yang, Changsun Ahn, Chiao-Ting Li and JongHwa Yoon, whose friendship and inspiring ideas were a great source of encouragement.

I would like to express my loving appreciation to my wife, Eunkyoung Youn, my sons, Byoungjune and Byoungheon, my father, mother, father-in-law, and mother in law for their love and prayer. I appreciate the affection and prayer of Ann Arbor Hope church members. Finally, I give all honor and glory to God.

TABLE OF CONTENTS

LIST OF FIGURES

LIST OF TABLES

LIST OF APPENDICES

LIST OF SYMBOLS

a	distance of center gravity to front axle	[m]
a_x	longitudinal acceleration at center gravity	[m/s^2]
a_y	lateral acceleration at center gravity	[m/s^2]
b	distance of center gravity to rear axle	[m]
$C_{\phi f}$, $C_{\phi r}$	front and rear damping rate	[N-m-s/rad]
F_{xi}, F_{yi} and F_{zi}	tire forces in the *x*, *y* and z directions of the *i*-th tire	[N]
g	gravitational acceleration	[m/s^2]
h_{cg}	center gravity height	[m]
h_{rf}	height of the front roll center	[m]
h_{rr}	height of the rear roll center	[m]
h_0	distance from ground to roll axis	[m]
h_1	distance from h_{cg} to h_0	[m]
I_{xx}	roll moment of inertia w.r.t. x-axis	[kg-m^2]
I_{zz}	yaw moment of inertia w.r.t. z-axis	[kg-m^2]
$K_{\phi f}$, $K_{\phi r}$	front and rear roll stiffness	[N-m/rad]
m	vehicle mass	[kg]
p	roll angular velocity of center gravity	[rad/s]
r	yaw angular velocity of center gravity	[rad/s]
r_d	desired yaw rate	[rad/s]
$\dot{r}$	yaw acceleration of center gravity	[rad/s^2]
R_w	effective wheel rolling radius	[m]
t_f, t_r	track width of front and rear axle	[m]
T_{bi}	brake torque at the *i*-th wheel	[Nm]

u_0	nominal longitudinal velocity of center gravity	[m/s]
β	vehicle sideslip angle	[rad]
δ	steering angle at the front wheels	[rad]
ϕ	roll angle	[rad]
μ	road friction coefficient	
ω_i	angular velocity of the *i*-th wheel	[rad/s]

ABSTRACT

Integrated chassis control (ICC) systems can be used to reduce the economic and social costs of road accidents. If these systems are to achieve their full potential for improved safety, however, two critical issues must be resolved: (i) the design of a controller integrating all sub-control systems, and (ii) rigorous evaluation to ensure their functionalities.

A decentralized design that coordinates the commands from sub-chassis control systems is achieved under the current business practice, in which suppliers provide OEMs with proprietary controllers. For effective coordination of sub-control commands and for avoidance of liability, the coordination strategy of saturating sub-control commands is used. A coordinator based on a hybrid approach--an offline model predictive control and an online fixed-point control allocation method--is designed, which has superior computational efficiency and flexibility. The effectiveness of the decentralized ICC system is verified via commercial software, CarSim. The simulation results show that ICC can resolve conflicts among subsystems and achieve improved stability. Reconfiguration in the control, for dealing with actuator failure in sub-control systems and robust control under uncertainties is presented.

For the evaluation of ICC, the worst-case scenario evaluation (WCSE) method is enhanced and applied to find the worst possible scenarios, for rigorous evaluation of vehicles, especially vehicles with chassis control systems. Two optimization methods (Sequential Quadratic Programming and Mesh Adaptive Direct Search) are used because of their convergence and computation efficiency. The worst allowable persistent bounded disturbance input generation method is applied to populate the initial points for

the optimization problem. The effectiveness of the proposed WCSE method was shown through a rollover prevention case study.

CHAPTER 1

INTRODUCTION

1.1 MOTIVATION

Both public and private agencies have demonstrated sustained interest in active safety technologies for ground vehicles to reduce the economic and social cost of road accidents (see Table 1-1). The direct and indirect cost resulting from road accidents was estimated to amount to 160 billion euro, which is 2% of the European Union's GNP (Commission, 2005). The commission on the European Road Safety Action Program suggests that the EU should target halving the number of road deaths by 2010. This seemingly high goal is achievable through integrated chassis control systems. The National Highway Traffic Safety Administration (NHTSA) of the US estimates that the installation of electronic stability control (ESC) reduced single vehicle crashes of passenger cars by 34 [%] and single vehicle crashes of sport utility vehicles (SUVs) by 59 [%], with a much greater reduction in rollover crashes (NHTSA, 2007a).

Table 1-1 Number of traffic fatalities and injuries (2008)

	Fatalities	**Injuries**
United States of America	37,000	2,250,000
European Union	39,000	1,700,000
China	73,000	3,000,000

The role of chassis control systems should be reconsidered especially in light of current trends toward reduction in vehicle weight to increase fuel efficiency. The

demand for highly fuel-efficient vehicles is growing because of increased oil prices and green house gas regulation (DeCicco et al., 2001; An and Sauer, 2004). Innovation in engine and power-train system design and optimal power-management control techniques have been widely studied (Kleimaier and Schroder, 2000; Lin et al., 2003). Among factors that affect the fuel efficiency of vehicles, vehicle weight is the critical design parameter (An and Sauer, 2004; WorldAutoSteel, 2009). However, reduction of vehicle weight often leads to reduction of vehicle safety. Under these circumstances, active safety chassis control systems become more important.

A wide array of chassis control functions have already been commercialized including ESC, anti-lock braking systems (ABS), traction control systems (TCS), four wheel steer (4WS), active front steer (AFS) and semi-active suspension systems (Karnopp, 1983; Furukawa and Abe, 1997; Zanten, 2000). These chassis control devices aim to improve vehicle safety, convenience, and comfort. NHTSA mandated the installation of ESC as standard equipment for all new light vehicles in the US by 2012 (Forkenbrock et al., 2005). Advanced chassis control systems such as X-by wire and electronic brake systems have been attempted. As these devices become mature and widely available, integration of these chassis control functions becomes necessary for better cost-leveraging and improved reliability and performance. The integration of the chassis control functions is loosely referred to as Integrated Chassis Control (ICC) systems. The benefits of ICC as compared to stand-alone, non-integrated safety systems include improved safety and comfort, reduced system cost and enhanced system reliabilities (Chang, 2007). In addition, reducing the complexity of control design and providing design flexibility are major objectives of ICC systems (Gordon et al., 2003).

We can observe efforts in industry and government regarding the development of ICC system in the following examples. Major auto suppliers such as Delphi, Continental Teves and Bosch seek to achieve enhanced active safety systems by integrating their products such as ESC, AFS and suspension control systems. Many suppliers and

automakers consider ICC systems the next step in the safety technology road-map (Koehn et al., 2006) for higher performance and improved vehicle stability. Thus government agencies, car manufacturers and other research institutes have made continuous efforts to develop and integrate sub-chassis control systems (Ghoneim et al., 2000; Hac and Bodie, 2002; Gordon et al., 2003).

The realization of ICC systems depends on the successful treatment of the two critical issues (i) designing a real-time master controller integrating all sub-control systems and (ii) ensuring their functionality under all circumstances through rigorous evaluations. This research focuses on the following problems, which are essential to design and evaluation of ICC systems. ICC system developers must integrate sub-chassis control systems under the current business practice, in which suppliers provide OEMs with proprietary controllers. By 'proprietary', this means devices for which the suppliers guard details of the design and makes only limited information about their internal systems available. Evaluation of ICC systems has been challenging because the existing approaches involve risky and high- cost field tests and have difficulties evaluating the vehicle with advanced safety control systems.

This research provides solutions for developing the ICC system under the current business environments and simulation-based evaluation approaches to complement current evaluation methods.

1.2 MAJOR CHALLENGES OF ICC

1.2.1 DEVELOPMENT OF INTEGRATED CHASSIS CONTROL (ICC) SYSTEMS

First, this research investigates existing ICC design approaches, which can be classified into two types: centralized and decentralized. In the centralized approach, one supervisory controller is designed to make all control decisions. The centralized ICC design can achieve the optimal solution because all control inputs can be computed using

available information from subsystems under full authority. In the decentralized approach, sub-chassis control systems that were designed individually are integrated together. These sub-chassis control systems are in many cases developed by different companies, and information sharing among them may not always happen smoothly.

The centralized control systems can be designed on the basis of various control theories: model predictive control (MPC) schemes (Chang, 2007; Falcone, 2007 b), sliding mode control (Lim and Hedrick, 1999; Mokhiamar and Abe, 2005), model reference (Komatsu et al., 2000), and fuzzy logic (Zeyada et al., 2000). These approaches mainly follow the basic principle that the desired vehicle motion commands are derived in the supervisory controller while individual sub-controllers manipulate the actuators to follow the commands. Much of the recent major researche on centralized ICC design is based on the optimal control allocation method via enhanced computing power (Webers and Busch, 2003; Tondel and Johansen, 2005). Simulation results of these centralized ICCs demonstrate superior results compared with their un-integrated counterparts or individual systems.

Despite the benefit of the centralized ICC design suggested above, there are several roadblocks to real-world implementation. First, centralized controllers require faster and more costly real-time embedded control units (Falcone, 2007 b). Second, the centralized architecture is more demanding in terms of engineering design and maintenance (Costlow, 2008). Third, the centralized approach works against the current business practice, in which suppliers develop individual chassis control systems and provide the finished products to automakers. This means that the centralized supervisory designs are constrained by the level of encapsulation of currently available chassis control systems (Webers and Busch, 2003).

The commercialized chassis control systems usually include large numbers of spaghetti codes that contain ad-hoc patches, exception handling, hand-shaking and coordination with other control systems (e.g., the engine), and sensor/actuator error

checking and diagnosis. It is therefore quite a leap of faith to think that any OEM (automaker) would throw away all these features of the sub-control systems and launch a new centralized controller. It is also hard to imagine that suppliers would be willing to provide the source codes knowing that by doing so they will lose business to the centralized controller (designed by either a single supplier or the OEM).

In the decentralized approach, the integration of these sub-systems involves coordination of the chassis control functions in an add-on unit. This add-on controller either modifies the control commands downstream of the individual controllers or modifies the feedback signals or set points upstream of the individual controllers. The coordination control can be used to overcome the current practical limitations of the centralized controllers discussed above. In making the actuation decision, the controller uses the knowledge regarding the characteristics of the steering and braking systems under the road surface friction (Bedner and Chen, 2004). In (He et al., 2004), a rule-based integration scheme is proposed to minimize conflicts between the individually designed chassis controllers for improved vehicle handling. Therefore, it seems apparent that we should establish systematic approaches rather than the ad-hoc rule-based approaches.

In this research, a coordinator for integrating a set of sub-control systems is developed. The proposed coordinator is designed to integrate existing sub-chassis control systems for implementation under the current business environment.

1.2.2 EVALUATION OF ICC

The performance of vehicles (such as rollover propensity and drivability) are usually assessed by government agencies through well-defined standard tests (NHTSA, 2003). As new safety control systems such as anti-lock brake systems (ABS) and electronic stability control (ESC) have been introduced, NHTSA has been forced to come

up with new methods to evaluate performances of vehicles with those systems installed. The standard tests developed to evaluate the performance of vehicles cannot adequately evaluate the performance of the vehicles with ICC systems. The NHTSA now faces a new and difficult problem: designing a simple, repeatable, and reliable way to assess the performance of vehicles with smart chassis control systems.

The need for a new assessment tool becomes evident through examining the current test procedures for rollover propensity. In the US, rollover propensity is assessed through a 5-star rating system based on the static stability factor (SSF) of the vehicle along with modifications based on a dynamic test result. The fishhook maneuver was selected for dynamic testing by NHTSA because of objectivity, repeatability, performability and discriminatory capability. With the advent of active safety control system such as ESC, however these standard tests and approaches to identify vehicle rollover propensity face a new situation: Starting in the late 1990s, ESC systems quickly penetrated the market as an active safety device. Automotive companies soon realized that ESC is a relatively cost-effective way to boost the rollover star-ratings of SUVs and light trucks. If wheel lift-off occurs during the given sine-with-dwell test, the rollover star rating will be reduced. Instead of redesigning the vehicle chassis or weight distributions, vehicle developers can simply calibrate the ESC systems to prevent wheel lift-off under the test conditions and thus improve the rollover star rating.

The problem of this evaluation process is analogous to assessing the learning of students. Traditional "standard test" procedures are similar to announcing the exam questions ahead of time and then assessing learning by grading the exam papers. Is it possible that some "students" will do a great job answering the exam questions but otherwise learn very little about the rest of the course material? With "students" armed with advanced chassis control systems that can be easily tuned for any pre-announced standard tests, the "teacher" (NHTSA) needs to find a new way to assess learning (safety performance). Additional problems with the current rollover propensity tests include the

high cost of empirical testing, limited test conditions, and the inherent risk of this type of field tests.

As an alternative to the standard NHTSA tests, the automakers have applied their own homogulation regulation to qualify the manufactured vehicles based on their own test standards before putting them on the market. In these approaches, mission-critical safety systems are examined and fixed before the production of vehicles. The automakers or the developers have applied their own standard evaluation methods in addition to ISO standards (Corno et al., 2003) and NHTSA tests (Bedner et al., 2007) as well as the subjective evaluation of experienced test drivers. These approaches will not provide comprehensive procedures that are generally applicable because they depend heavily on knowledge and experience specific to particular products.

For increasing numbers of vehicles with chassis control-based safety systems such as ESC, evaluation of vehicle performance and functionality of the safety system under extreme circumstances is important. The evaluation method should not miss a single potential failure. To improve reliability of the vehicle safety evaluation, large test matrices applying iterative processes have been defined, but these depend on time-consuming and expensive field tests (Forkenbrock et al., 2005; NHTSA, 2007a).

The proposed evaluation method will evaluate the performance of vehicles with active safety systems under a broad range of maneuvers in contrast to current standard methods, which evaluate performance under only a small set of pre-defined maneuvers. It uses computer simulations to systematically identify worst-case scenarios, i.e., potential cases when the active safety systems fail to perform satisfactorily.

To obtain a thorough understanding of the worst-case scenario evaluation (WCSE) its theoretical basis method is explored through a review of the literature on the relevant issues. In this research, the WCSE is treated as a trajectory optimization problem to solve for a trajectory (a sequence of steering inputs) that minimizes or maximizes defined performance (e.g. rollover index). The goal of searching for the

optimal disturbance is essentially the same as that of searching for the optimal control inputs. Several prior studies investigated disturbance generation of control systems (Jayasuriya, 1995; Georgiou and Fialho, 1999). When the system is linear, the worst bounded inputs are derived from the impulse responses (Jayasuriya, 1995). The solution of the Hamilton-Jacobi-Bellman equations for nonlinear systems is derived by variational calculus to solve the optimal trajectory problem (Georgiou and Fialho, 1999).

More recently, the worst case generation method was used to study vehicle behaviors (Ma, 1998; Ungoren, 2003). The work in (Ma, 1998) focuses on rollover and jackknifing of articulated vehicles using the worst-case generation methodology. This approach is based on a dynamic game theory, in which control inputs and disturbances inputs compete in an optimal setting and this completion leads to the two-player solution. The other approach (Ungoren, 2003) is based on various numerical schemes, with the vehicle plus its control system treated as a modified dynamic system. The one-player problem is solved numerically through the iterative dynamic programming method. These studies illustrate the theoretical basis of the WCSE and its implementation in vehicle systems with preliminary results.

Review of these studies suggests that further research may yield results that are more meaningful for practical application and extension of optimal disturbance generation. Such research should focus on advanced optimization schemes and generation of a good initial point for efficient searching with more reliable computational vehicle models. Good initial points suitable for searching optimal disturbance of dynamic vehicles must be investigated through theoretical and practical means. The results are expected to demonstrate practical significance in comparison to the results of standard tests and to provide guidance for design of ICC.

1.3 PROPOSED APPROACH

1.3.1 DEVELOPMENT OF ICC

An efficient and effective **decentralized ICC design** must have the following characteristics:

(i) It should be developed through coordination of the sub-control systems in the sense that the original functionalities of the sub-control systems are respected while at same time improved performance is realized.

(ii) The coordinator developed to achieve this coordination should eliminate redundancy and resolve conflicts among subsystems by modifying control commands of different system combinations.

(iii) The coordination should be realizable with limited real-time computational power.

Based on these requirements, the design of the coordinator is attempted as follows. A strategy of coordination, in which coordinators saturate the control commands of individual sub-systems, is used. This is based on the assumption that the appropriate combination of sub-systems is achieved by scaling down sub-control commands. For computation efficiency, a hybrid approach is accomplished by an offline desired value computation and an online control allocation. A lookup table scheme obtained through offline model predictive control (MPC) provides a way to replace real-time computations to obtain virtual control commands. An online control allocation applying the computationally efficient fixed-point iteration method makes flexible and reconfigurable control of the coordinator possible via an on-board controller.

1.3.2 EVALUATION OF ICC

Any **new evaluation** method for ICC needs to have three major characteristics:

(i) The test maneuver cannot be one-size-fits-all. Instead, we need to create customized test maneuvers for each vehicle.

(ii) The test needs to be simulation-based, instead of experiment-based.

(iii) The test needs to be based on various comprehensive scenarios instead of relying on a small number of test maneuvers.

Based on the above three characteristics a new method, "worst-case scenario evaluation'' (WCSE) is applied. The WCSE method in this research aims to solve the worst-case disturbance problem as a one-player problem (Ma, 1998), with the driver steering input treated as the only disturbance signal in an effort to optimize a selected cost function.

Development of the WCSE should encompass the following key elements. First, the vehicle model must be accurate enough under extreme maneuvers. The accuracy of the model under severe maneuvers is crucial because ICC systems operate under near-incident conditions. Second, the simulation model should provide compatibility with any given ICC controller model and WCSE optimization software. Third, the optimization method needs to be fast and yet capable of achieving acceptable convergence even with nonlinear dynamics and constraints. In other words, well-developed local search methods should be used instead of global optimization methods such as dynamic programming. This is because those global optimization methods are not suitable for ill-conditioned problems including high dimensional models with their nonlinearities and complex dynamics.

In this research, two numerical methods (Mesh Adaptive Direct Searching and Sequential Quadratic Programming) are selected. For effective local searching by the developed numerical method, good initial point generation is essential. To generate initial points, we can deploy standard testing maneuvers such as NHTSA tests and also apply the worst allowable persistent bounded disturbance (WAPBD), which is based on the impulse response of a linear time invariant system (Jayasuriya, 1995). The

effectiveness of the worst-case scenarios method developed in this study is investigated by comparing its results with those of standard tests. Rollover prevention control of ESC is presented as evaluation of ICC systems via the proposed WCSE.

1.4 CONTRIBUTION

This dissertation examines the development and evaluation of an integrated chassis control (ICC) systems. The major contributions are summarized below.

Development: The development of the proposed ICC systems is based on current automotive industry practices. This ICC design, composed of a set of proprietary subsystems, is in contrast to the centralized approaches based on the assumptions that all control commands are calculated by a supervisory controller with full authority. It is developed to be compatible with the current business practice, where automotive suppliers develop individual chassis control systems and provide the finished products to automakers. The current business practice gives rise to an encapsulation problem: limited communication and interaction among sub-control systems. In the face of these technical difficulties, the ICC system is designed to solve the problem through coordination of the subsystems, which are treated as black boxes.

The main contributions of development of ICC systems are the following:

• Development of electronic stability control (ESC) applying a sliding mode control (SMC) scheme. The SMC scheme is applied through linearization of a tire model including combined slip. Rollover index for control performance is developed through the application of dynamic energy conservation.

• Analysis of the feasibility of decentralized diagonal control to the ICC systems. The analysis results demonstrate that the diagonal decoupling approaches is not suitable

for ICC systems (ESC+AFS and ESC+RWS). The relative gain array analysis can provide theoretical grounds for the feasibility of the diagonal decoupling approaches to vehicle control systems that encompass different combinations of sub-systems.

• Formulation & application of a control strategy for the coordination. The coordination approach is investigated by analysis of optimal feedback gains in a two DOF ICC LQ problem. Under such a coordination strategy, control commands from subsystems are saturated appropriately to prevent conflict among chassis subsystems and eliminate redundancy.

• Design of a coordinator based on a hybrid approach--an offline model predictive control (MPC) and an online fixed-point (FP) control allocation method--for its computational efficiency and flexibility. Simulation results suggest that the proposed coordinator leads to an improved system with robust and reconfigurable control. This approach allows ICC designers the flexibility to choose subsystems that will become part of the ICC on the basis of performance and cost without having to overhaul their entire systems even if they change suppliers. This hybrid approach can be applied to develop modular control strategy, which is frequently used in integrated control systems.

Evaluation: Because the worst-case scenario evaluation (WCSE) is a rigorous method for evaluating chassis control systems, results from the evaluation can accelerate the development of the system by clearly showing its strengths and weakness. The development of the WCSE proceeds by way of generation of worst-case disturbances, which in turn are closely related to optimal control. Improvement and extended application of the WCSE, a simulation-based evaluation method via dynamic optimization schemes, are achieved. The method can serve as a valuable surrogate for the current field tests that are costly and risky to conduct. It is expected to provide a

better solution for various evaluation objectives such as determination of rollover and spinout potential. The selection of optimization methods and initial points is critical because the WCSE is an optimization problem including complex and nonlinear functions with vehicle and control models.

The contributions of the WCSE method development are the following.

• Development of the WCSE method via two optimization methods (Sequential Quadratic Programming and Mesh Adaptive Direct Search). The selection of these two was based on a review of possible optimization methods and on comparison simulations via a simple optimization problem. Both optimization methods show convergence and reasonable computational efficiency under dynamic optimization including the high nonlinearity.

• Application of the worst allowable persistent bounded disturbance (WAPBD) (Jayasuriya, 1995) to disturbance input generation of vehicle motion. Development of the initial point generation method is critical because these nonlinear optimization methods rely primarily on local searches. In this research, the WAPBD approach is used effectively as a new method of providing an initial guess for the worst steering input that generates rollover of a mid-size SUV. The WAPBD can be applied for robust control design by identifying the worst-case disturbance of dynamic systems.

• Application of the developed WCSE to provide design engineers with evaluation results to demonstrate limits of for rollover prevention (ROP) control strategies. The developed WCSE served as an important engineering tool by showing evaluation results of ICC systems that previous studies and the present tests methods (sine-with-dwell and fishhook test) could not generate. The WCSE results regarding the ROP control systems provide a boundary condition that permits the maximum steering input at the specific speed without rollover in steer-by-wire systems.

1.5 THESIS OUTLINE

Chapter 2 presents the development of vehicle models and sub-chassis control systems, and demonstrates the effectiveness of the developed models and systems through the simulation.

Chapter 3 proposes the decentralized ICC design for integrated chassis control. The benefits and limitation of ICC with regard to centralized and decentralized approaches are studied, and the feasibility of decoupling control of ICC systems is examined via a relative gain array analysis. A hybrid approach combining offline model predictive control and online control allocation computations is described for the coordination control in the decentralized ICC design. The effectiveness of the decentralized ICC is verified through simulations.

Chapter 4 demonstrates the application of the worst-case scenario evaluation (WCSE) method to assess the performance of ICC systems. The basic architecture and major components of the WCSE are described. The effectiveness of the WCSE is shown via assessment of rollover prevention performance of chassis control systems.

Chapter 5 summarizes overall conclusions from the study and presents possible future study.

CHAPTER 2

DESIGN OF VEHICLE MODELS & SUB CHASSIS CONTROL SYSTEMS

2.1 VEHICLE MODELS

Proper modeling of the target vehicle is a primary step for this research on the development and evaluation of integrated chassis control systems. Three vehicle models are used, each for a particular purpose in this research. The first one is a CarSim vehicle model, a multi-body dynamic model with 17 degrees of freedom (DOF), which is used for the overall evaluation of vehicle performance (MSC, 2009). The second one is a nonlinear 3 DOF vehicle model --lateral, yaw, and roll body motion--taking into account wheel dynamics and nonlinear characteristics of the tires for the ESC design (see Section 2.2.2). The third one is the well-known basic bicycle linear model, which is a 2 DOF model, used to describe the lateral/yaw body motion based on linear cornering stiffness (see Section 3.2.1 and 3.2.2).

The primary use of the CarSim model in this research is for the evaluation procedures including the WCSE method. The main challenge of constructing the CarSim model lies in the facts that (i) there are many parameters and (ii) tire/suspension tables need to be obtained to match the real vehicle characteristics.

In this research, the nonlinear 3 DOF model is developed for sliding mode control design. The nonlinear vehicle model comprises state variables such as vehicle lateral velocity, yaw rate, roll angle and roll rate, and parameters such as nonlinear tire models with load-transfer and mechanical delays. This nonlinear model has comprehensive accuracy, to be shown in Section 2.1.1, in addition to its expected computation efficiency and compatibility with other computation tools such as SIMULNK.

Despite the foregoing, it should be noted that this vehicle model is suitable for the control algorithm design and analysis process rather than for the rigorous evaluation of the vehicle systems. This is because the 3 DOF model has difficulties in appropriately simulating extreme vehicle motions such as rollovers or spinout in the manner that the evaluation required.

2.1.1 NONLINEAR 3 DOF (YAW/LATERAL/ROLL) VEHICLE MODEL

The nonlinear 3 DOF model is developed to describe only the lateral, roll and yaw motions (Figure 2.1). The variables and parameters all follow the ISO standard.

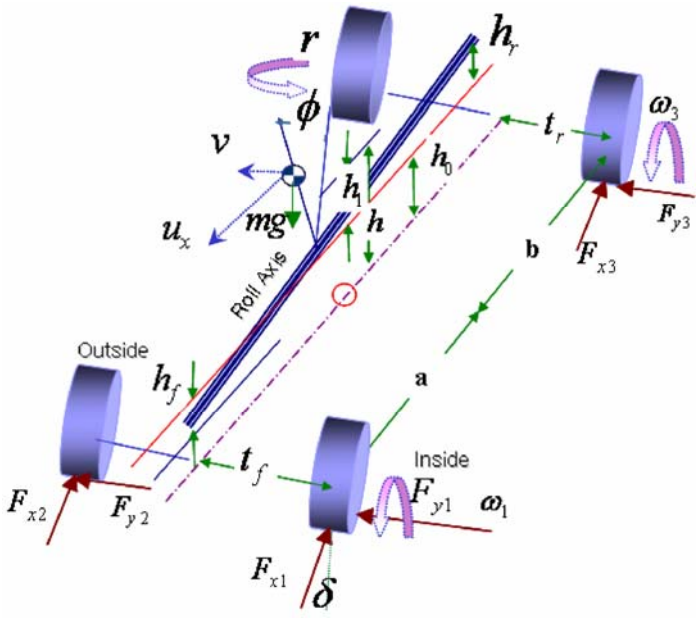

Figure 2.1 Vehicle model based on yaw, lateral and roll motions

The governing equations for the 3 DOF vehicle model are described by

$$
\begin{aligned}
&mh_1\dot{v} + I_{xx}\dot{p} + mh_1u_x r = L_\phi \phi + L_p p + h_{cf}\sum_{i=1}^{2} F_{yi} + h_{cr}\sum_{i=3}^{4} F_{yi} \\
&I_{zz}\dot{r} = a\sum_{i=1}^{2} F_{yi} - b\sum_{i=3}^{4} F_{yi} - t_f F_{x1} - t_r F_{x3} + t_f F_{x2} + t_r F_{x4} \\
&m\dot{v} + mh_1\dot{p} + mu_x r = h_f\sum_{i=1}^{2} F_{yi} + h_r\sum_{i=3}^{4} F_{yi}
\end{aligned} \tag{2.1}
$$

where $p = \dot{\phi}, L_\phi = mgh - K_R, L_p = -C_R$. K_R is the roll stiffness and C_R is the roll damping coefficient.

Eq. (2.1) can be written in the state space form. For this three DOF system, 4 state variables are needed. The state space model is

$$
M_1\dot{X} = M_{2m}X + M_y F_y + M_x F_x \tag{2.2}
$$

where

$$
X = \begin{bmatrix} r & v & \phi & p \end{bmatrix}^T \tag{2.3}
$$

$$
\begin{aligned}
F_y &= \begin{bmatrix} F_{y1} & F_{y2} & F_{y3} & F_{y4} \end{bmatrix}^T \\
F_x &= \begin{bmatrix} F_{x1} & F_{x2} & F_{x3} & F_{x4} \end{bmatrix}^T
\end{aligned} \tag{2.4}
$$

$$
M_1 = \begin{bmatrix} 0 & m & 0 & mh_1 \\ 0 & mh_1 & 0 & I_{xx} \\ I_{zz} & 0 & 0 & \varepsilon I_{zz} \\ 0 & 0 & 1 & 0 \end{bmatrix}, M_{2m} = \begin{bmatrix} -mu_x & 0 & 0 & 0 \\ -mh_1u_x & 0 & L_\phi & L_p \\ 0 & 0 & 0 & 0 \\ 0 & 0 & 0 & 1 \end{bmatrix} \tag{2.5}
$$

$$
M_x = \begin{bmatrix} 0 & 0 & 0 & 0 \\ 0 & 0 & 0 & 0 \\ -t_f & t_f & -t_r & t_r \\ 0 & 0 & 0 & 0 \end{bmatrix}, M_y = \begin{bmatrix} 1 & 1 & 1 & 1 \\ h_f & h_f & h_r & h_r \\ a & a & -b & -b \\ 0 & 0 & 0 & 0 \end{bmatrix} \tag{2.6}
$$

Brake torque, T_b and longitudinal tire force at the contact point on the ground are described in the wheel rotation dynamics shown in Figure 2.2:

$$
J_w\dot{\omega}_j = -T_{bj} + r_w F_{xj} \tag{2.7}
$$

$$\lambda_j = \frac{u_x - r_w \omega_j}{u_x},\ j = 1,2,3,4 \tag{2.8}$$

where J_w is the angular moment inertia of the wheel and r_w is the wheel radius.

The wheel slip, λ_i in Eq. (2.8) determines the tire longitudinal force applying the longitudinal velocity calculated from Eq.(2.9).

$$m(\dot{u}_x - r v_y) = \sum_{i=1}^{4} F_{xi} \tag{2.9}$$

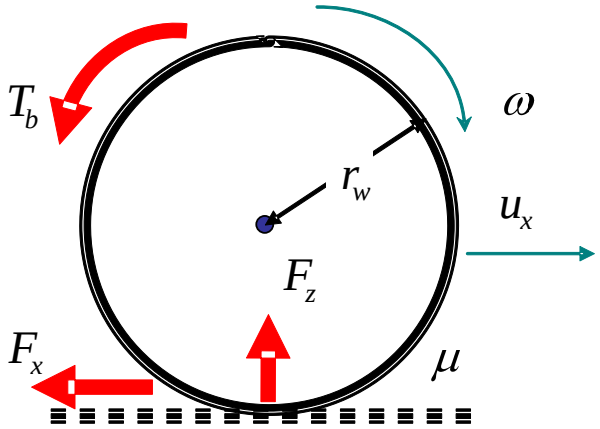

Figure 2.2 Wheel rotational dynamics

The lateral/longitudinal tire forces are computed via look-up tables identical to those used in the CarSim model as shown in Figure 2.3. It is based on the tire ellipse concept, which describes the correlation between both tire forces as function vertical load, side slip angle, slip ratio and road friction in Eq.(2.10) . Since these dynamic variables are included, the performance of brake control systems such as ABS and ESC can be included and evaluated.

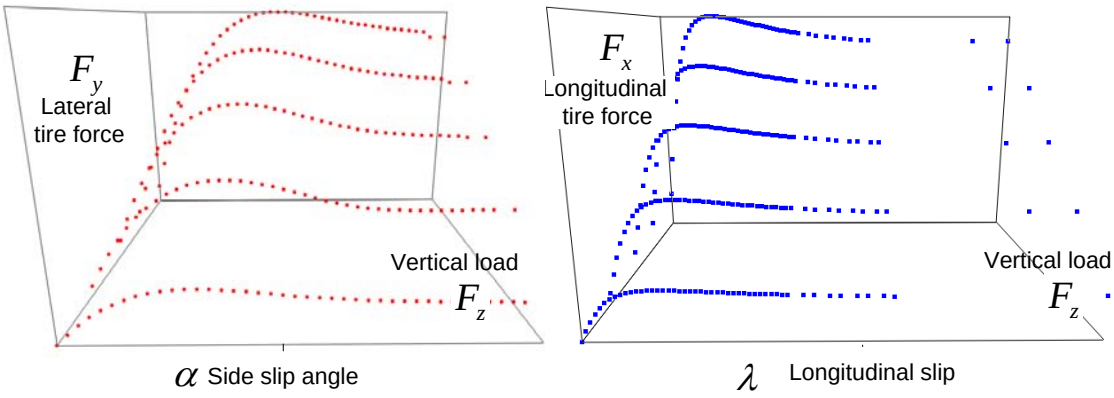

Figure 2.3 Lookup table of lateral/longitudinal tire force in CarSim model

Tire forces are described as follows

$$F_x = f_x(F_z, \mu, \alpha, \lambda) \text{ and } F_y = f_y(F_z, \mu, \alpha, \lambda) \tag{2.10}$$

where α : the side slip angle, μ : road friction coefficient and F_z : vertical force

The parameters used in the nonlinear 3 DOF vehicle model are shown in APPENDIX A. It should be noted that the nonlinear model captures the major dynamic variables such as vehicle forward speed and the wheel speeds even though this is referred as a 3 DOF model.

2.1.2 VEHICLE MODEL VALIDATION

The nonlinear 3 DOF vehicle model is written in Matlab SIMULNK. It has four major components for vehicle lateral/yaw/roll dynamics, longitudinal velocity, wheel dynamics, and tire force computations. In the state space block, the vehicle model is linearly computed based on nonlinear tire models. The longitudinal velocity and the wheel speeds are calculated separately based on wheel rotational dynamics and tire forces.

To verify the fidelity of the 3 DOF vehicle model, simulation comparison with the CarSim model is conducted. Open loop steering (i.e., without including a driver model) is given for the objective evaluation of the model accuracy.

The results in Figure 2.4 are obtained using a step steering input, 180 [deg] at the steering wheel. It can be seen that the maximum lateral acceleration is close to 0.8[g], while the maximum yaw rate is 33[deg/sec] under this maneuver. Even though there are some small differences, the response from the CarSim model and the nonlinear 3 DOF model are close.

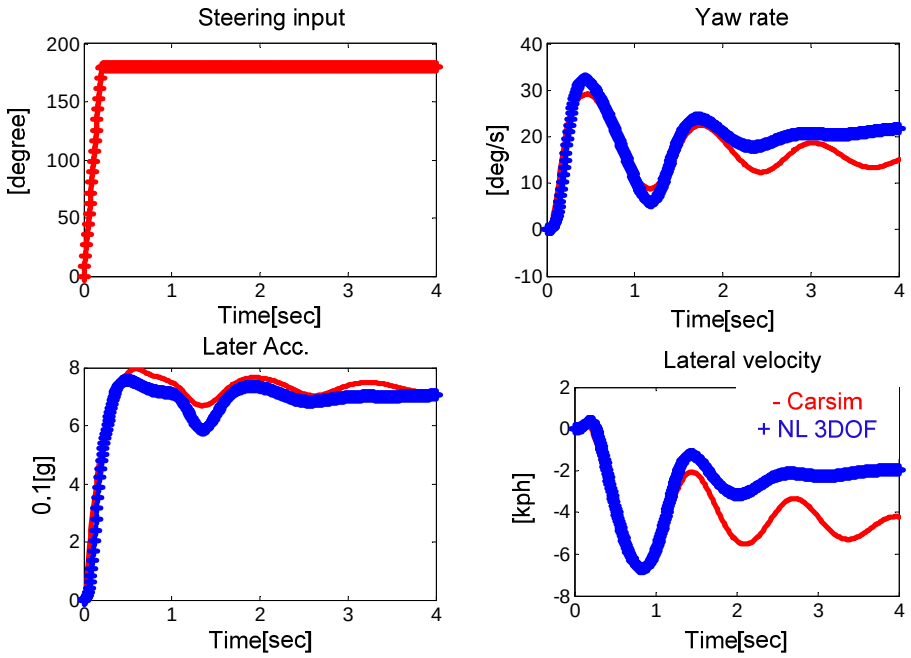

Figure 2.4 Comparison between CarSim and nonlinear (NL) 3 DOF model under step steering input @ 80[kph] and $\mu = 0.9$

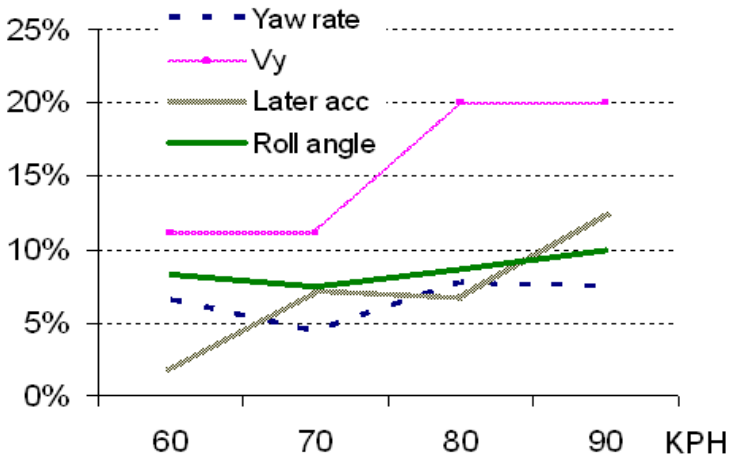

Figure 2.5 Errors between CarSim and the nonlinear 3 DOF model under step steer of 100 degrees.

Figure 2.5 shows the error (infinity-norm) between the two models. Given the simplicity of the nonlinear 3 DOF vehicle model, its accuracy is adequate for application despite the difference in the lateral velocity, v_y.

2.2 CHASSIS CONTROL SYSTEMS

In this section, the development of sub-chassis control systems will be described. The design features of chassis control systems developed by major automotive supplier companies are reviewed, and then representative chassis control functions with significant inter-dependency are selected.

Delphi Automotive Company developed a wide array of chassis control functions and has suggested a concept that called "Unified Chassis Control". This "UCC" concept consists of both active and passive safety control systems, many of which are already commercialized (Chandy, 2003). Another major auto supplier, Bosch, has focused on a vehicle dynamics management (VDM) concept. The main target of integrated chassis control in their suggested system is the resources management of the vehicle control systems to optimize the safety performance of the vehicle (Trachtler, 2004). The optimal tire force derived from the VDM contributes to shorter stopping distance, small steering input and yaw rate reduction. These two systems include (integrate) chassis control functions related to braking, steering, and damping. This research similarly focuses on the development of an ICC system with brake, suspension and steering elements. These correspond to electronic stability control (ESC), continuous damping control (CDC) and rear wheel steer (RWS) respectively. This is because clearly these systems are felt to be critical safety systems; furthermore, they are relatively mature systems and provide a better stability performance.

It should be noted that the chassis control systems to be developed in this research are based on a "place holder" algorithm. It should be noted that t the main goal of my

research is not to develop a chassis control algorithm. Rather, the goal is to develop integrating methods and a numerically efficient worst-case scenario evaluation method. Therefore, the sub-chassis control algorithm to be developed will have to work reasonably well i.e., it improve vehicle dynamic stability with regard to yaw, sideslip and roll behavior but it does not need to represent a new and breakthrough design.

In contrast to the algorithm of RWS and CDC, that of ESC includes various and complex functionalities (yaw motion control, lateral stabilization, rollover prevention, and wheel slip control). The simple placeholder algorithms (to the best of my knowledge) have limitations in encompassing all functionalities identified above. Furthermore, ESC has greater effectiveness than other chassis control systems in terms of stability control. Therefore, a new ESC controller shows reliable performance under a set of conditions that place high demands on the safety systems. The sliding mode control (SMC) scheme is applied as a servo control that ensures robustness under system uncertainties and stability in complex conditions.

2.2.1 ELECTRONIC STABILITY CONTROL (ESC)

The ESC system controls the braking forces of the four tires to stabilize the vehicle motions based on its working principle shown in

Figure 2.6. The functionalities of the ESC system are based on the follow objectives: i) following of the desired yaw rate, ii) regulation of the vehicle sideslip, iii) rollover prevention and iv) the slip control of the wheels. The controller uses sensor information for the four wheel speeds, lateral acceleration, steering input, roll angle and yaw-rate to detect the vehicle motions and to judge the driver's intention. Based on the above information, the controller derives the optimal braking force of four wheels and generates them independently. Bosch's ESC control algorithm is a good example of the ESC principle described above (Zanten, 2000). The ESC has been developed from basic

functionalities of anti-lock brake systems, which are designed to prevent the wheel from locking or skidding (Kade et al., 1987).

The switching rule will be derived to activate corresponding ESC control modules defined as i) wheel slip control, ii) yaw moment control, iii) side slip control, and iv) rollover prevention control. The control modules are active when control values crossed predefined thresholds as explained below.

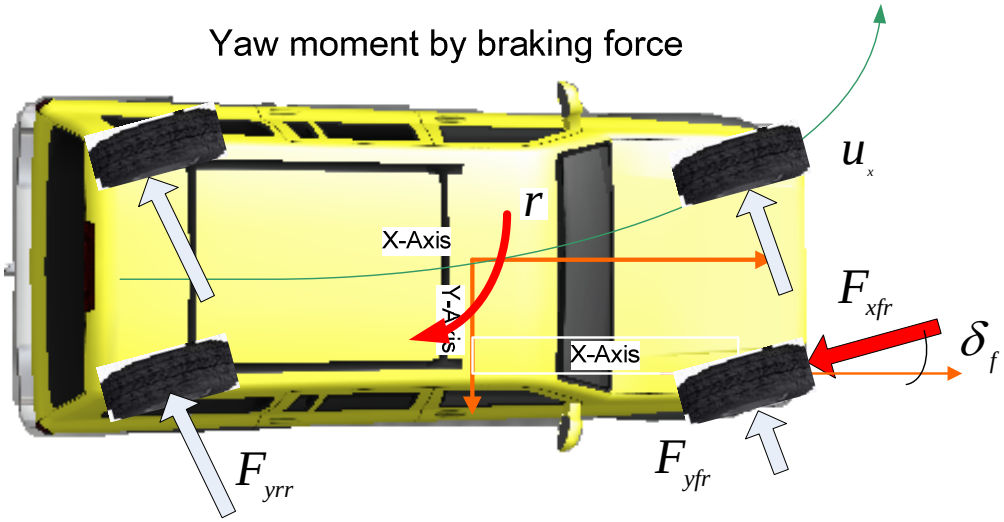

Figure 2.6 Working principle of ESC

The wheel slip control is imposed to keep magnitude of the wheel slip to remain close to the optimal value, 0.1~0.2 by taking into account relationship between the slip ratio and the adhesion coefficient .

A desired yaw rate is calculated first from linear vehicle steady state cornering:

$$r_d = \frac{\delta \cdot u_x}{1+\left(u_x / u_{ch}\right)^2} \cdot \frac{1}{L} \tag{2.11}$$

This value is then saturated based on a nominal road friction value and vehicle forward speed.

$$\left|r_d\right| \le r_{\lim} = \left|\frac{\mu \cdot g}{u_x}\right| = \left|\frac{a_y}{u_x}\right| \tag{2.12}$$

A yaw control command is based on a yaw error, $\Delta r = r_d - r_m$ where r_m is measured yaw rate.

The limit for the sideslip angle, β_{thresh} is chosen to be 5 degrees. When this threshold value is exceeded, yaw moment will be requested to reduce the magnitude of the side slip angle to maintain driver's control authority (Inagaki et al., 1995).

The rollover index is derived based on analysis of geometric characteristics during a rollover as shown in Figure 2.7. The rollover threat is measured by the total amount of energy stored in the vehicle including both potential energy and kinetic energy. Assuming that K_s is the suspension roll stiffness and ϕ_c is the roll angle, the vehicle critical roll rate, beyond which enough kinetic energy exists to roll over the vehicle, can be calculated from

$$\dot{\phi}_c = \frac{mg\left(\sqrt{4h^2 + T^2} - 2h\right)}{I_{xx}} = \frac{2mg(h_c - h_0)}{I_{xx}} + \frac{K_s \phi_c^{\,2}}{I_{xx}} \tag{2.13}$$

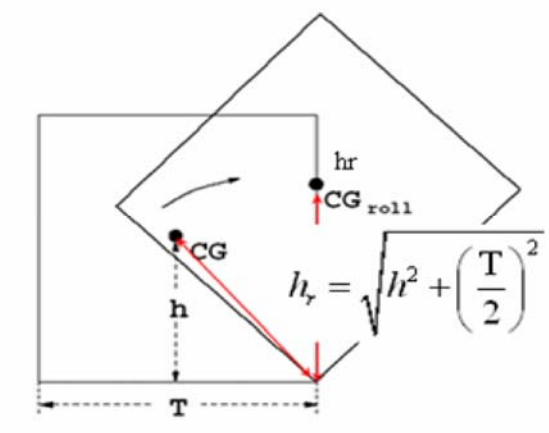

Figure 2.7 Schematic diagram of rollover phenomena

To improve the responsiveness of the control system, predicted vehicle roll rate, instead of measured vehicle roll rate, is used. The predicted roll rate is calculated based on roll rate at the present time and the roll acceleration as follow.

$$\dot{\phi}_p(t) = \dot{\phi}(t+\tau) = \dot{\phi}(t) + \ddot{\phi} \cdot \tau \tag{2.14}$$

where t is the present time and τ is the prediction time.

The roll acceleration is estimated from a simple roll dynamic model, shown below in Eq.(2.15).

$$\ddot{\phi}(t) = -\frac{k_\phi \cdot \phi(t) + b_\phi \cdot \dot{\phi}(t)}{I_{xx}} + \frac{mh_{Rc}}{I_{xx}} \cdot a_y \tag{2.15}$$

The predicted roll rate is used by the final form as

$$\dot{\phi}_p(t) = \dot{\phi}(t) + \left(-\frac{k_\phi \cdot \phi(t) + b_\phi \cdot \dot{\phi}(t)}{I_{xx}} + \frac{mh_{Rc}}{I_{xx}} \cdot a_y \right) \cdot \tau \tag{2.16}$$

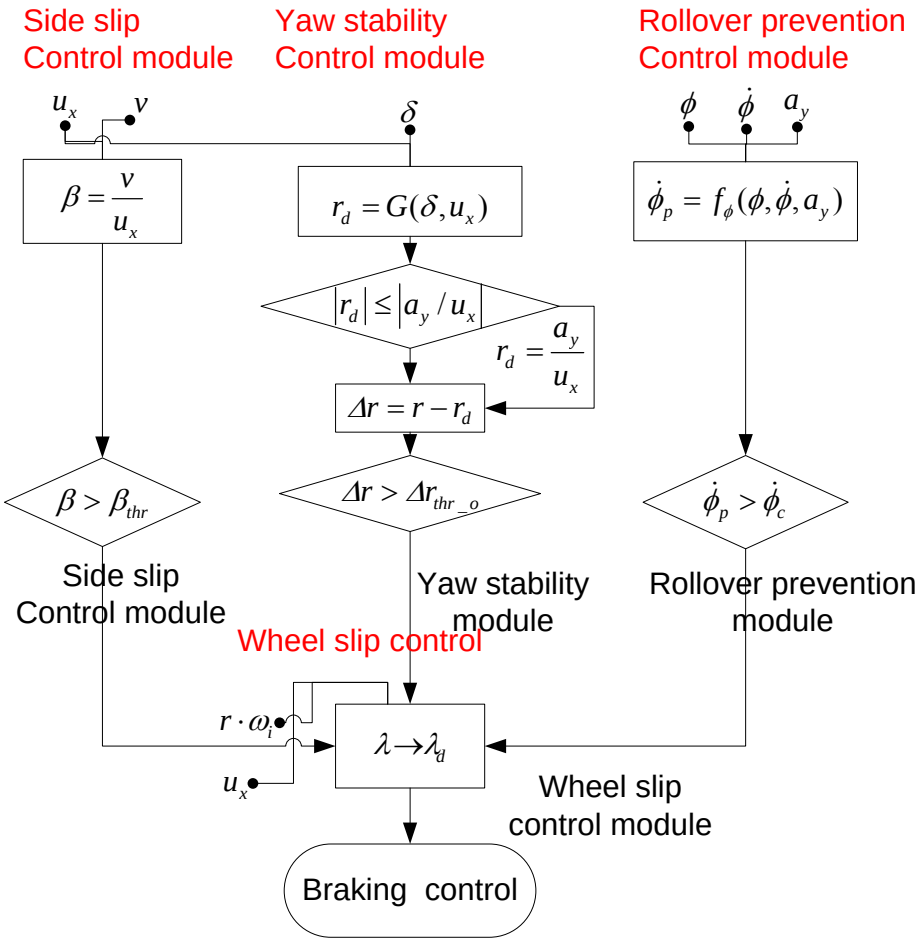

Figure 2.8 Flow chart of the ESC control algorithm

The overall ESC control logic is shown in Figure 2.8. The desirable yaw rate is first inferred from steering input and forward speed, which is saturated according to Eq. (2.12). In parallel, the sideslip threshold and the critical roll rate of the vehicle are derived according to the dynamic characteristics of the vehicle. The differences between yaw rates, sideslip, and roll rate and their threshold values are then calculated. If the difference is larger than the threshold gaps, $\Delta\beta_{thr}, \Delta r_{thr}, \Delta\dot{\phi}_{thr}$, the corresponding control module is activated. As the final step, the brake force is regulated by the wheel slip control algorithm. The selection of the wheels to be braked is based on the direction of the lateral acceleration. The desirable brake forces are obtained from the servo controller to be explained (see Section 2.2.2).

2.2.2 SLIDING MODE CONTROL (SMC) STRATEGY FOR ESC

The ESC controller needs servo-control algorithm to overcome the parametric uncertainties and un-modeled dynamics. This sub-section will present a sliding mode control algorithm, which calculates the braking torque necessary to achieve other desired vehicle states and the desired longitudinal slip ratios.

The SMC is applied as the robust servo-control. Before implementation of the controller, the control vehicle model is recomposed. The braking force F_x is defined as the control input as shown in Eq. (2.21). The model is derived from the linear form using Eq.(2.17), which represents the linear vehicle body model with respect to the steering input. The process of the derivation will be shown in the following section. It should be noted that matrix M_2 in Eq. (2.17) and matrix M_{2m} in Eq. (2.2) are respectively defined according to the input such as the tire forces and the steering input

$$\dot{X} = M_1^{-1}M_2X + M_1^{-1}M_3\delta = AX + B_\delta\delta \tag{2.17}$$

where δ is tire steering angle, M_1 is given in (3.8), and M_2 and M_3 are defined as follows

$$M_2 = \begin{bmatrix} \frac{-aC_{\alpha f} + bC_{ar}}{u_x} - mu_x & -\frac{C_{\alpha f} + C_{\alpha r}}{u_x} & Cy_{R\&C\phi} & 0 \\ -m_R h_1 u_x & 0 & -L_\phi + mgh_1 & -L_p \\ -\frac{a^2 C_{\alpha f} + b^2 C_{\alpha r}}{u_x} & \frac{-aC_{\alpha f} + bC_{ar}}{u_x} & Cn_{R\&C\phi} & 0 \\ 0 & 0 & 0 & 1 \end{bmatrix} \tag{2.18}$$

$$M_3 = \begin{bmatrix} C_{\alpha f} & 0 & aC_{\alpha f} & 0 \end{bmatrix}^T \tag{2.19}$$

where $C_{\alpha f}, C_{\alpha r}$ are the cornering stiffness of the front and rear axles, $Cy_{R\&C\phi}, Cn_{R\&C\phi}$ are roll steer coefficients and L_ϕ, L_p are the roll stiffness and damping coefficients. Based on these defined matrices, Eq. (2.17) can be rewritten as

$$M_1 \dot{X} = M_2 X + M_3 \delta = M_{2m} X + M_y F_y^0 \tag{2.20}$$

where F_y^0 is the pure-slip lateral tire force. When F_x is not zero, and when we add additional term to represent model uncertainties. Eq.(2.20) becomes

$$\dot{X} = AX + B_\delta \delta + BF_x + F \tag{2.21}$$

where F is the upper bound of model uncertainties, and the control gain matrix B are derived below. The total tire force is then defined as

$$M_x F_x + M_y F_y \tag{2.22}$$

The truncated Taylor's series gives us the operating point.

$$M_x F_x + M_y F_y = M_x F_x + M_y \left(F_{y0} + \frac{\partial F_y}{\partial F_x} (F_x - F_{x0}) \right) \tag{2.23}$$

$$B = M_1^{-1} \left(M_x + M_y \frac{\partial F_y}{\partial F_x} \right) \tag{2.24}$$

where

$F_{x0,} F_{y0}$: The tire forces at the nominal operating point

$$\frac{\partial F_{y0}}{\partial F_x} = \begin{bmatrix} c_{l1L} & 0 & 0 & 0 \\ 0 & c_{l1R} & 0 & 0 \\ 0 & 0 & c_{l2L} & 0 \\ 0 & 0 & 0 & c_{l2R} \end{bmatrix}, c_{li} = \frac{-F_{xi0} F_{y\max}(\alpha_1, F_{zi})}{\mu F_{zi} \sqrt{(\mu F_{zi})^2 - {F_{xi0}}^2}}$$

We can then obtain the final vehicle model

$$M_1 \dot{X} = M_2 X + M_3 \delta + M_y \frac{\partial F_y}{\partial F_x} F_x + M_x F_x \tag{2.25}$$

The final form of the nominal linear vehicle model is then

$$\dot{X} = f(X,t) + BF_x \equiv AX + B_\delta \delta + BF_x = \hat{f} + BF_x \tag{2.26}$$

where $f(X,t)$ is approximated as $\hat{f}$. The estimation error is assumed to be bounded by F, so that $\left| f(X,t) - \hat{f} \right| \le F$. To achieve the control target in relation to the desired yaw rate, side-slip angle and roll rate, the brake torque at each wheel is designed via the SMC scheme. For sliding mode controls, we first define the switching surface:

$$S = \tilde{X} = X - X_d \tag{2.27}$$

where X_d denotes the desired value of the state vector.

$$X_d = \begin{bmatrix} r_d & v_d & 0 & \dot{\phi}_d \end{bmatrix} \tag{2.28}$$

The sliding surfaces, s^i, define the elements of the sliding surface vector S. In the expression s^i, *i*, superscript, represents N (yaw motion), Y (side slip motion), and L (roll motion).

The average dynamics while in the sliding mode can be approximated as

$$\dot{S} = AX + B_\delta \delta + b_c u - \dot{X}_d = 0 \tag{2.29}$$

If $b_c = \begin{bmatrix} b_c^N & b_c^Y & b_c^L \end{bmatrix}$ is defined as the control gain matrix corresponding to one wheel activating the braking force, the control gain is assumed to be bounded in the range

$$b_{c\min}^i \le b_c^i \le b_{c\max}^i \tag{2.30}$$

The parameters for control gains β^i, b_c^i can be written as

$$\beta^{i-1} \le \frac{\hat{b}_c^i}{b_c^i} \le \beta_i, \quad b_c^i = \sqrt{b_{c\min}^i b_{c\max}^i}, \quad \beta^i = \sqrt{\frac{b_{c\max}^i}{b_{c\min}^i}} \tag{2.31}$$

In order to satisfy Eq.(2.29), the equivalent control input without model error is

$$b_c u_{eq} = -AX - B_\delta \delta + \dot{X}_d \tag{2.32}$$

The yaw/lateral/roll components of the equivalent control input, as denoted by the superscript, are then

$$\begin{aligned} a_{Nr} r + a_{Nv} v + a_{N\phi} \phi + b_{N\delta} \delta &= -b_c^N u_{eq}^N + \dot{r}_d \\ a_{Yr} r + a_{Yv} v + a_{Y\phi} \phi + a_{Y\dot{\phi}} \dot{\phi} + b_{Y\delta} \delta &= -b_c^Y u_{eq}^Y + \dot{v}_d \\ a_{Lr} r + a_{Lv} v + a_{L\phi} \phi + a_{L\dot{\phi}} \dot{\phi} + b_{L\delta} \delta &= -b_c^L u_{eq}^L + \ddot{\phi}_d \end{aligned} \tag{2.33}$$

where the coefficients of .Eq. (2.33) are given as follows

$$a_{Nr} = -\frac{a^2 C_{af} + b^2 C_{ar}}{I_{zz} u_x}, a_{Nv} = \frac{(-aC_{\alpha f} + bC_{\alpha r})}{I_{zz} u_x}, a_{N\phi} = \frac{C_{NRC\phi}}{I_{zz}}$$

$$a_{Yr} = \frac{I_{xx}}{m \cdot D}\left(\frac{(-aC_{\alpha f} + bC_{\alpha r})}{u_x} - mu_x\right) - \frac{h_1^2 m u_x}{D}, a_{Yv} = -\frac{I_{xx}(C_{\alpha f} + C_{\alpha r})}{mu_x D},$$

$$a_{Y\phi} = -\frac{I_{xx} C_{yr\phi}}{m \cdot D} + \frac{h\left(-K_f - K_r - mgh_1\right)}{D}, a_{Y\dot{\phi}} = \frac{h_1\left(-B_f - B_r\right)}{D}$$

$$a_{Lr} = \frac{h_1}{m \cdot D}\left(\frac{(-aC_{\alpha f} + bC_{\alpha r})}{u_x} - mu_x\right) - \frac{hmu_x}{D}, a_{Lv} = -\frac{h_1(C_{\alpha f} + C_{\alpha r})}{u_x D},$$

$$a_{L\phi} = -\frac{h_1 C_{yr\phi}}{m \cdot D} - \frac{h\left(-K_f - K_r - mgh_1\right)}{D}, a_{L\dot{\phi}} = -\frac{\left(-B_f - B_r\right)}{D}$$

$$b_{N\delta} = \frac{aC_{\alpha f}}{I_{zz}}, b_{Y\delta} = -\frac{I_{xx} C_{af}}{m \cdot D}, b_{L\delta} = -\frac{h_1 C_{af}}{D} \; D = mh_1^2 - I_{xx}$$

The overall control law consisting of both the feed-forward terms and the feedback terms is

$$u^i = u_{eq}^i - b_c^{i-1} k^i \cdot sat\left(\frac{s^i}{\psi}\right) \tag{2.34}$$

where ψ is the design parameter to suppress the chattering problem inherent to the sliding control

$$with \;\; k^i \geq \beta^i (F^i + \eta^i) + (\beta^i - 1)\left|u_{eq}^i\right| \tag{2.35}$$

The control inputs obtained in the above will not be applied directly. Instead, they are applied only when they do not result in excessive wheel slip. To realize the wheel slip control, we define a new sliding surface for slip regulation as

$$s^{\lambda} = \lambda - \lambda_d \tag{2.36}$$

And the wheel dynamics are

$$\dot{s}^{\lambda} = \dot{\lambda} - \dot{\lambda}_d = -\frac{\dot{u}_x}{u_x}(\lambda - 1) - \frac{r_w}{J_w u_x}\left(r_w F_x - T_b\right) - \dot{\lambda}_d \tag{2.37}$$

The equivalent brake torque is then

$$u_{eq}^{\lambda} = r_w F_x + \frac{J_w \dot{u}_x}{r_w}(\lambda - 1) \tag{2.38}$$

If the equivalent control inputs in Eq. (2.33) and Eq. (2.38) are applied to Eq. (2.34) and Eq. (2.35), the final control inputs for yaw, lateral, roll motion and wheel slip motion are taken as

$$\begin{aligned}
u_r &= u_{eq}^{N} - b_c^{N-1} k^{N} \cdot sat\left(\frac{r - r_d}{\psi_r}\right) \\
u_v &= u_{eq}^{Y} - b_c^{Y-1} k^{Y} \cdot sat\left(\frac{v - v_d}{\psi_v}\right) \\
u_{RI} &= u_{eq}^{L} - b_c^{L-1} k^{L} \cdot sat\left(\frac{\dot{\phi} - \dot{\phi}_d}{\psi_{\dot{\phi}}}\right) \\
u_{\lambda} &= u_{eq}^{\lambda} - b_c^{\lambda-1} k^{\lambda} \cdot sat\left(\frac{s^{\lambda}}{\psi_s}\right)
\end{aligned} \tag{2.39}$$

where u_r is the yaw control input, u_v is the side slip control input, u_{RI} is the rollover prevention control input, and u_{λ} is the longitudinal slip control input. The obtained braking control inputs are applied according to the priority sequences (wheel slip control, rollover prevention, yaw control, sideslip control), which is superior to CDC control application focusing on providing ride comfort.

The control inputs shown in Eq. (2.39) are derived based on one-wheel braking conditions. If we consider the control inputs of four wheels, the total control inputs are rearranged as follow.

$$BF_x = \begin{bmatrix} b_{c1l}^N & -b_{c1l}^N & b_{c2l}^N & -b_{c2l}^N \\ b_{c1l}^Y & -b_{c1l}^Y & b_{c2l}^Y & -b_{c2l}^Y \\ 0 & 0 & 0 & 0 \\ b_{c1l}^L & -b_{c1l}^L & b_{c2l}^L & -b_{c2l}^L \end{bmatrix} \begin{bmatrix} F_{x1l} \\ F_{x1r} \\ F_{x2l} \\ F_{x2r} \end{bmatrix} \tag{2.40}$$

The new formula can be used for multiple-wheel braking cases. The combined braking forces at the front and rear axles can be more effective than one-wheel braking at the front side in case of the rollover prevention. Then the new control formulation is as follow.

$$\ddot{\phi} = a_{Lr} r + a_{Lv} v + a_{L\phi} \phi + a_{L\dot{\phi}} \dot{\phi} + b_{L\delta} \delta + b_{c1l}^L F_{x1l} + b_{c2l}^L F_{x2l} \tag{2.41}$$

2.2.3 REAR WHEEL STEER (RWS) SYSTEM

The RWS system manipulates the rear steer actively to enhance maneuverability and stability. The objectives of RWS can vary, e.g., reduction of phase difference between lateral acceleration and yaw-rate response at high speeds, or reduction of sideslip angle for better maneuverability at low speeds (Furukawa et al., 1989). Given these two objectives, the reduction of sideslip is selected as the final goal of our RWS system for high-speed vehicle stability.

The RWS can have both feed-forward and feedback controls. In the feed-forward control, the rear wheel has to be adjusted in proportion to the front steering angle for vehicle stability under high speed. In the feedback control, the vehicle state variables are used to compute feedback control inputs (Kimbrough et al., 1988). Despite the usefulness of the feedback control, in this research, feed-forward approaches is adopted because it mainly depends on the stability control responding to unexpected disturbance (Furukawa et al., 1989)

The reduction of sideslip angle through controlling the rear steer can be explained through dynamic analysis using bicycle model as follows.

$$\begin{bmatrix} \dot{v}_y \\ \dot{r} \end{bmatrix} = \begin{bmatrix} \dfrac{-\left(C_{\alpha f}+C_{\alpha r}\right)}{mu_0} & \dfrac{-aC_{\alpha f}+bC_{\alpha r}}{mu_0}-u_0 \\ \dfrac{-aC_{\alpha f}+bC_{\alpha r}}{I_{zz}u_0} & \dfrac{-\left(a^2C_{\alpha f}+b^2C_{\alpha r}\right)}{I_{zz}u_0} \end{bmatrix} \begin{bmatrix} v_y \\ r \end{bmatrix} + \begin{bmatrix} \dfrac{C_{\alpha f}}{m} & \dfrac{C_{\alpha r}}{m} \\ \dfrac{aC_{\alpha f}}{I_{zz}} & \dfrac{-bC_{\alpha r}}{I_{zz}} \end{bmatrix} \begin{bmatrix} \delta_f \\ \delta_r \end{bmatrix} \quad (2.42)$$

At steady-state

$$\begin{aligned} 0 &= \frac{-\left(C_{\alpha f}+C_{\alpha r}\right)}{u_0} v_y + \frac{-aC_{\alpha f}+bC_{\alpha r}-mu_0{}^2}{u_0} r + C_{\alpha f}\delta_f + C_{\alpha r}\delta_r \\ 0 &= \frac{-aC_{\alpha f}+bC_{\alpha r}}{u_0} v_y + \frac{-\left(a^2C_{\alpha f}+b^2C_{\alpha r}\right)}{u_0} r + aC_{\alpha f}\delta_f - bC_{\alpha r}\delta_r \end{aligned} \quad (2.43)$$

Assume $v_y = 0$ and eliminate r, we obtain.

$$K_r = \frac{\delta_r}{\delta_f} = \frac{mu_x^2 a - b(a+b)C_{\alpha r}}{mu_x^2 b + a(a+b)C_{\alpha f}} \cdot \frac{C_{\alpha f}}{C_{\alpha r}} \quad (2.44)$$

The ratio value, K_r between front steer angle, δ_f and rear steering angle, δ_r is a function of longitudinal speed. As the longitudinal speed increases, K_r converges at $aC_{\alpha f} / bC_{\alpha r}$.

Based on Eq. (2.44), the feed-forward compensation strategy for RWS is as shown in Figure 2.9.

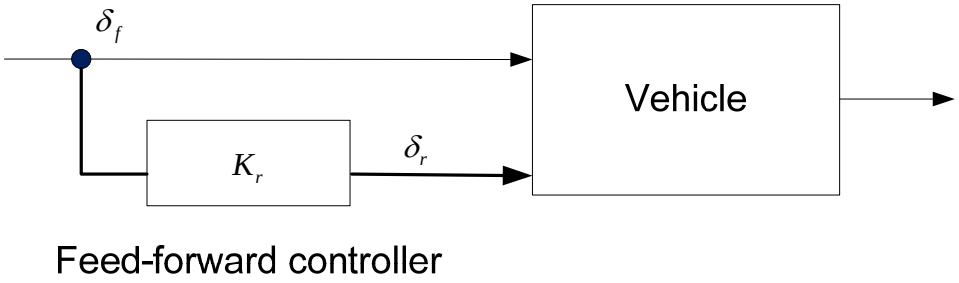

Figure 2.9 Rear wheel steer system design

2.2.4 CONTINUOUS DAMPING CONTROL (CDC)

The CDC system controls sprung mass motion by changing the setting of the variable dampers using a solenoid valve. The control algorithm uses information such as vertical acceleration and velocity, and steering input to manifest the behavior of the vehicle and the intention of the driver. Various active/semi-active suspension control systems have been developed since the 1980's. However, the cost of active suspension is of relatively high so there are few which commercialized the system. In this research, the focus is assumed to be lateral stability control, which aims to stabilize vehicle motion during high speed cornering. The activation of lateral stability control is based on vehicle lateral acceleration, estimated from the bicycle model:

$$\hat{a}_y = \delta \cdot u_x^2 \cdot \left(1 + \left(u_x / u_{ch}\right)^2\right)^{-1} \frac{1}{L} \tag{2.45}$$

This estimated acceleration is a better signal to use than that from an accelerometer because of its predictive nature and because it is less vulnerable to road grade and cross talk disturbances. The quality of the estimation provided by Eq. (2.45) depends on the accuracy of our estimate of characteristic speed, which depends on tire cornering stiffness. The estimated acceleration $\hat{a}_y$ is compared with a threshold value, a_y^{thr} to check the severity of lateral stability threat. If $\hat{a}_y$ is larger than a_y^{thr}, the lateral stability control is activated. Lateral stability control gain, K_{lat} proportional to vehicle speed is calibrated as $K_{\text{lat}} = g_l(u_x)$ and then the desired damping torque calculated as $T_{\text{lat}}^{\text{CDC}} = K_{lat} \cdot \hat{a}_y$ are applied to CDC dampers at the four corners. The overall procedure is described in the flow chart in Figure 2.10.

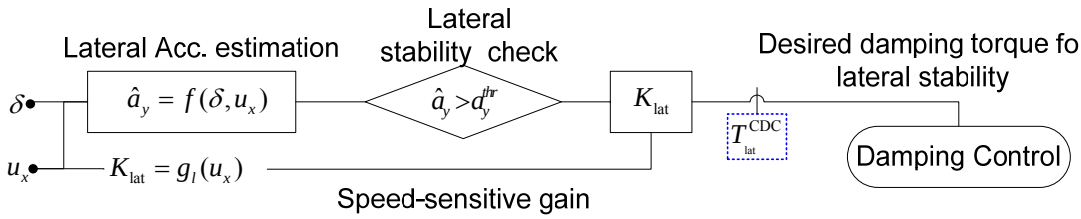

Figure 2.10 CDC lateral stability control flow-chart

Even though the CDC algorithm is developed for lateral stability, we can presume that the lateral stability functionality of the CDC system also contributes to vehicle stability with regard to rollover prevention. The effectiveness of the developed CDC is evaluated through the worst-case scenario evaluation with regard to the rollover prevention function (see Table 4-5).

2.3 SIMULATION RESULTS

The chassis control systems are designed using the Matlab/ SIMULINK program and integrated with the vehicle dynamics software, CarSim. First, the effectiveness of ESC is evaluated under a hard braking maneuver on a split-μ road. The initial vehicle speed is 90 [kph]. Figure 2.11 shows the vehicle lateral velocity, yaw rate and longitudinal velocity, brake pressures, and trajectory distance for both cases (ESC on and off). Under the ESC off condition, "no control", the vehicle loses stability but under the ESC on condition, the vehicle does not.

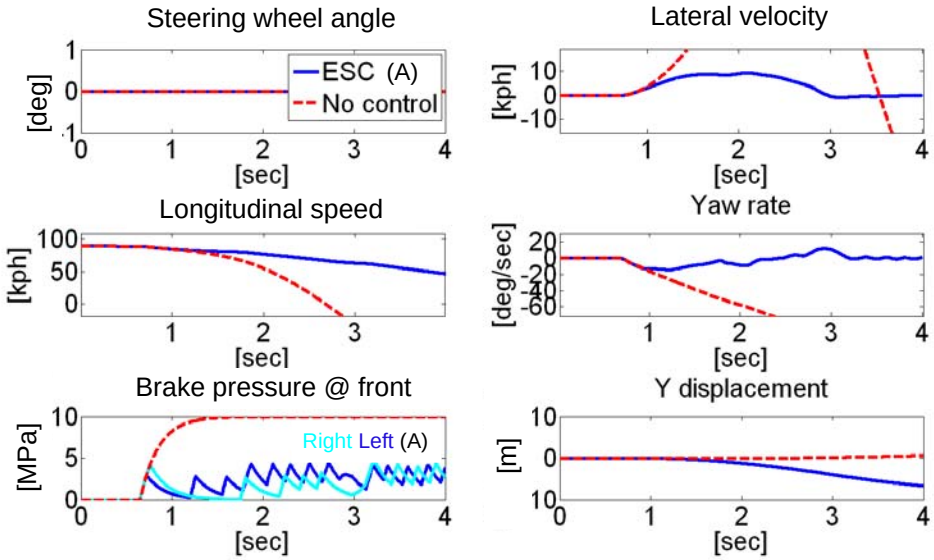

Figure 2.11 ESC-on and ESC-off under split-μ road hard braking

The enhancement of vehicles performance achieved by ESC, RWS and CDC system is investigated through the NHTSA sine-with-dwell test. Those control systems

stabilize vehicles via differing mechanisms of brake force, rear wheel steer and damping force. However, if the vehicle does not have any control system, it loses stability (see Figure 2.12, Figure 2.13, Figure 2.14 and Figure 2.15).

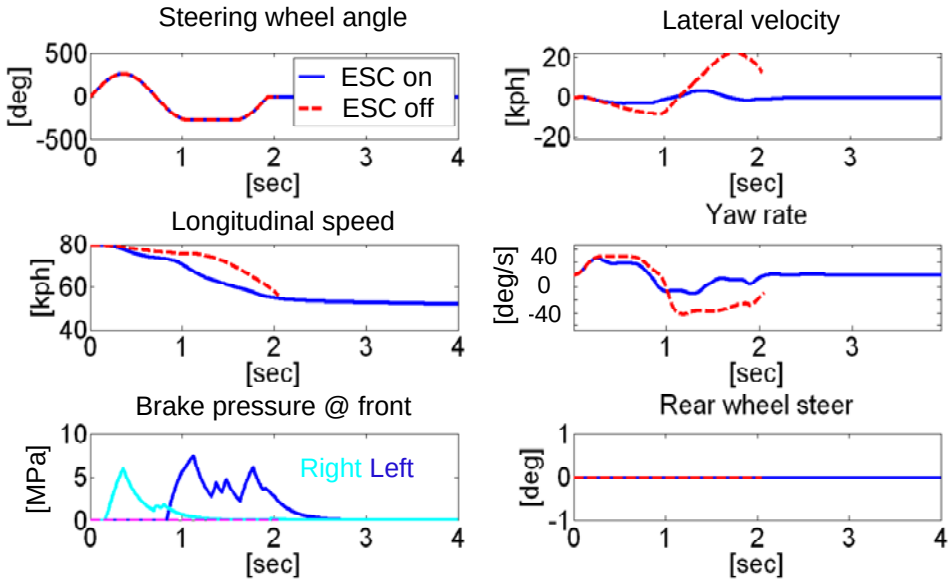

Figure 2.12 ESC-on and ESC-off under the sine-with-dwell tests @ μ=0.9 (Rollover under the ESC-off)

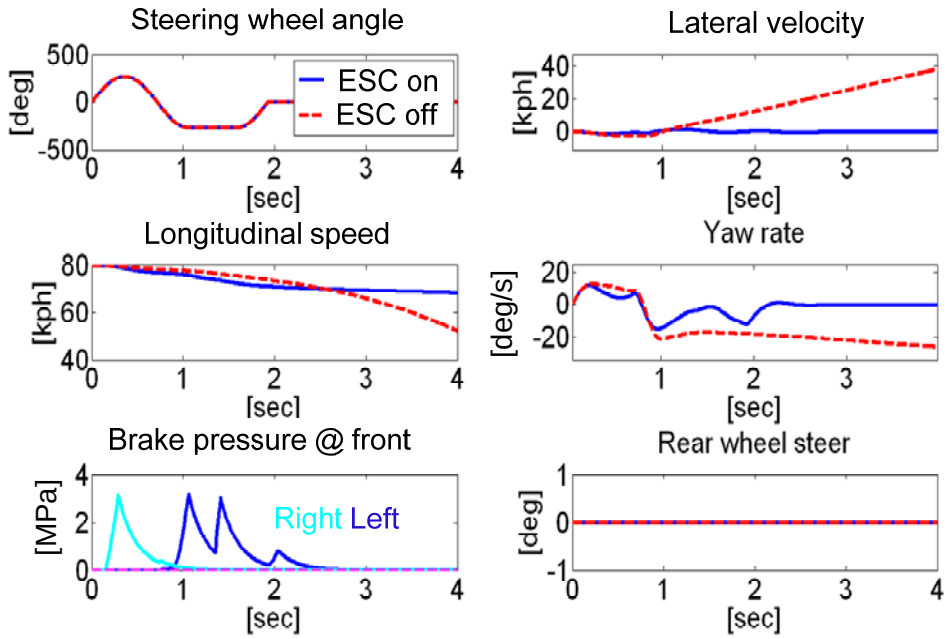

Figure 2.13 ESC-on and ESC-off on a slippery road under the sine-with-dwell tests @ μ=0.4 (spin-out with ESC-off)

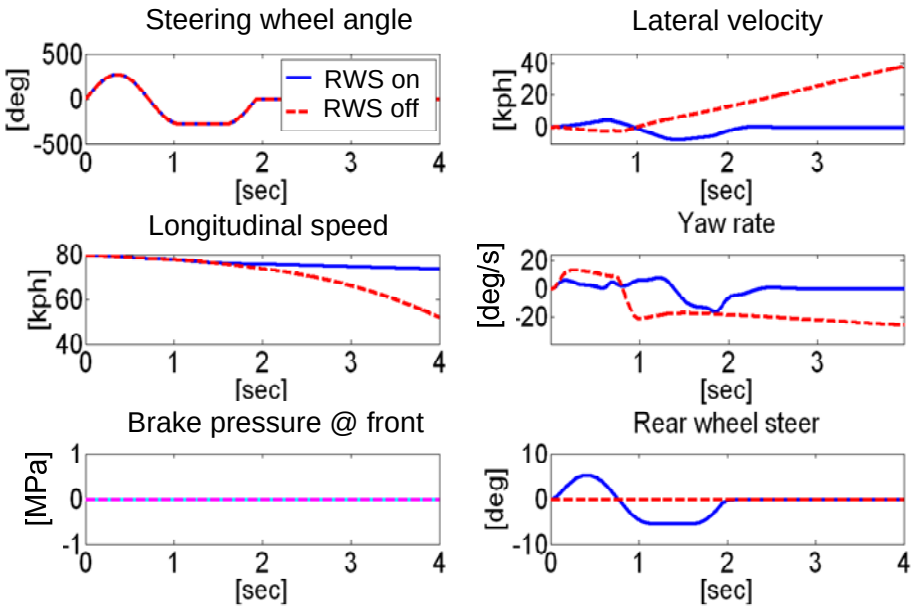

Figure 2.14 RWS on and RWS off on slippery road under the sine-with-dwell tests @ μ=0.4 (spin-out with RWS off)

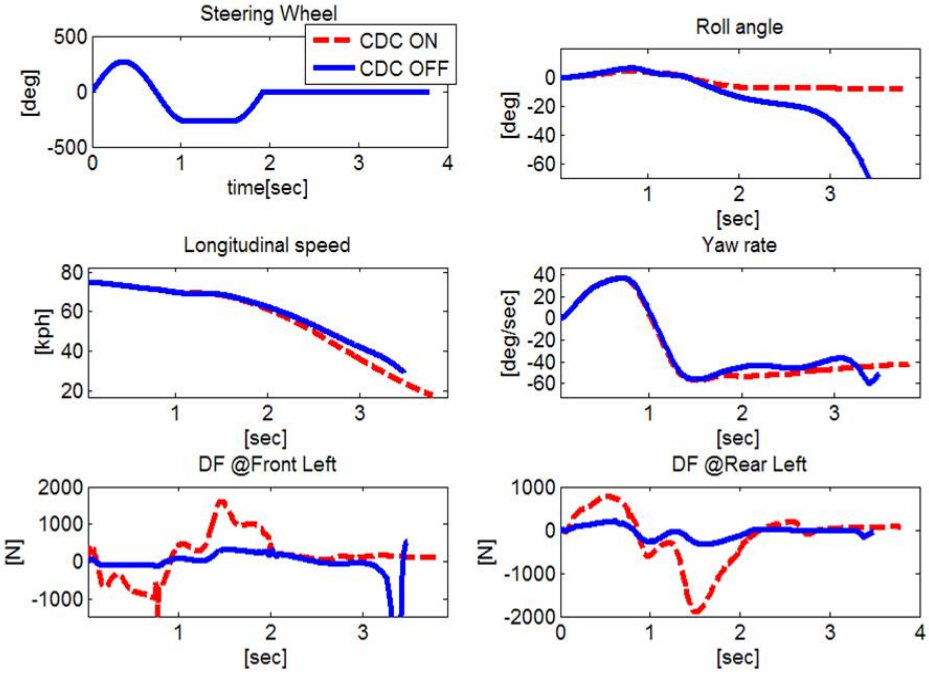

Figure 2.15 CDC-on and CDC-off under the sine-with-dwell tests @ μ=0.9 (Rollover under the CDC off)

The same simulation is attempted using another SUV model in order to check the effectiveness of combination of both ESC and RWS in different vehicles. In this case,

the ESC and the RWS individually achieve the stabilization of the vehicle (see Figure 2.16) but it can be seen that uncoordinated activation of ESC and RWS can result in unsatisfactory results in comparison with stand-alone activation of ESC (see Figure 2.17). This simple example demonstrates the necessity for coordinated chassis control systems. It should be noted that not all uncoordinated combinations of ESC and RWS necessarily degrade the vehicle performance compared with individual systems; this example is set up to show the possible problem of un-coordination.

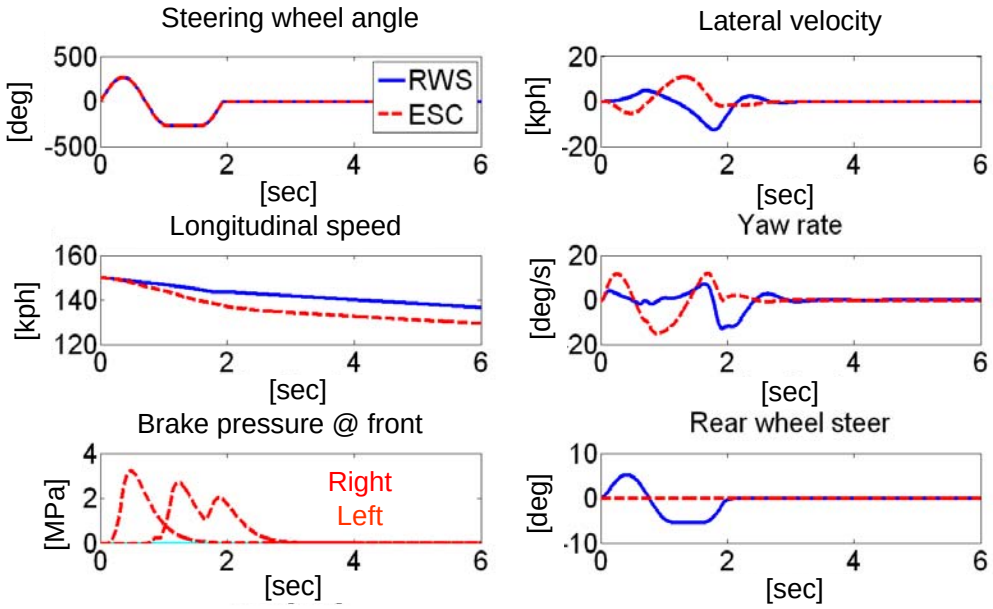

Figure 2.16 Performance with both ESC and RWS under 0.7[Hz] sine-with-dwell test @ $\mu = 0.4$ and u_x=150[kph]

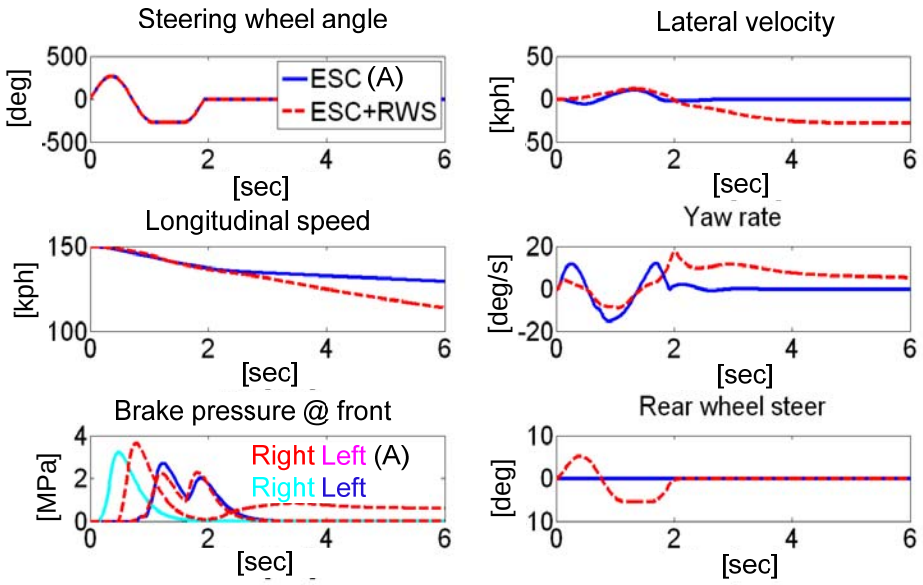

Figure 2.17 Uncoordinated system (ESC+RWS) and ESC under 0.7[Hz] sine-with-dwell test @ $\mu = 0.4$ and u_x=150[kph]

2.4 SUMMARY

A nonlinear 3-DOF vehicle model is developed, and the verification procedure shows it to be a good approximation of a sport utility vehicle. This nonlinear model captures the lateral-yaw-roll motions of the vehicle with difference less than 10 [%] from the CarSim model. Its simplicity and accuracy make it suitable for application to the sliding mode control design of the ESC.

The ICC system developed and studied in this research includes an electronic stability control (ESC) system, a rear wheel steer (RWS) system and a continuous damping control (CDC) system. The RWS and the CDC in this study serve as "place holder" algorithms. In other words, they were developed to approximate mature systems for intended production. The ESC algorithm, designed via the SMC scheme, includes a rollover prevention strategy as well as lateral/yaw motion control.

The ESC and the RWS systems demonstrate their effectiveness in achieving enhanced vehicle stability by their performance in the NHTSA sine-with-dwell tests.

Two SUV vehicle models are used to investigate performances of developed control algorithms. The preliminary simulation results are introduced in this chapter

One significant finding derived from the simulation results is that while two independently designed chassis control systems improve vehicle performance when they work alone, the combined system does not consistently produce satisfactory results when the systems are not coordinated. This simple example shows the importance of the coordination in the development of ICC.

CHAPTER 3

DEVELOPMENT OF INTEGRATED CHASSIS CONTROL SYSTEMS

3.1 LITERATURE REVIEW OF INTEGRATED CHASSIS CONTROL

The objectives of integrated chassis control (ICC) systems are to (i) improve safety and comfort, (ii) simplify the control design (Gordon et al., 2003), (iii) reduce system costs, and (iv) enhance system reliability (Wang and Nagai, 1999; Chang, 2007). Many automotive companies (Hac and Bodie, 2002; Koehn et al., 2006) are actively working on development of ICC systems. Independent design of stand-alone control systems is no longer suitable with the advent of a steadily increasing number of deployed chassis control systems. It cannot resolve the functional overlap of sub-systems actuations combined with increasing design complexity and control authority of chassis control systems (Webers and Busch, 2003). The recent literatures will be reviewed in order to identify problems and examine solutions for ICC development.

Our literature review is based on the categorization of control architectures for integrated control systems as centralized or decentralized control architecture. The centralized ICC is mainly based on a top-down pattern (Mokhiamar and Abe, 2005; A Hac, 2006), in which desired forces or optimal forces are hierarchically allocated via optimization schemes, and the decentralized ICC is based on ad-hoc switching rules (Webers and Busch, 2003) for coordinating or integrating individual sub control systems. The development of ICC systems will be discussed in detail in the next sub-section.

3.1.1 CENTRALIZED INTEGRATION APPROACHES

The centralized ICC approach is a good option when all control inputs can be simultaneously manipulated, i.e., a central supervisory controller is allowed full authority over all the actuators. Some recent centralized ICC systems have been designed through actuator apportionment by solving optimization problems. They can be implemented with multi-layers through modularization (Chang, 2007; Falcone, 2007 b). Many automakers and suppliers have developed centralized integration schemes for chassis control systems (Webers and Busch, 2003; Koehn et al., 2006).

The centralized ICC systems consist of a supervisory controller and sub-chassis control system in charge of servo-controls of the respective actuator, as shown in Figure 3.1. In the supervisory controller, the desired intermediate command such as optimal longitudinal slip ratio and tire slip angle can be calculated on the basis of the current vehicle states, X_0. The desired commands are communicated so that the sub-chassis control systems can realize the commands using actuators such as brakes and steering. These centralized integration schemes frequently deploy control reference models and optimization schemes to calculate the desired control commands (Wang and Nagai, 1999; Hac and Bodie, 2002). Various control models and optimization methods suitable for the models were applied depending on their requirement for computation efficiency and accuracy.

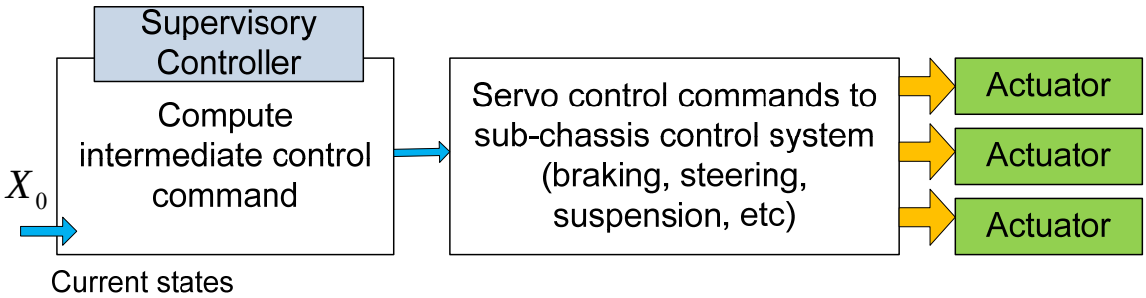

Figure 3.1 Common architecture of centralized integrated chassis control strategy

Such centralized ICC systems mainly include steering systems, braking systems and in rare cases, suspension systems. This is because both steering and braking systems are relatively effective in influencing the vehicle dynamics (Furukawa and Abe, 1997). For mitigating the consequences of potential brake actuator failure in vehicles, integrated brake-by wire and steer-by-wire systems have been studied; in these systems, the control algorithm is based on rules derived from vehicle dynamics (Hac and Bodie, 2002). An integrated control system of active front steer (AFS) and direct yaw moment control was designed by model-matching control techniques that make the performance of the actual vehicle model follow that of an ideal vehicle model (Nagai et al., 2002). Some recent active safety systems were on the basis of model predictive control (MPC) schemes (Borrelli et al., 2005; Chang, 2007; Falcone et al., 2007). In these studies, controllers are hierarchically designed in modules. In individual control layers, desired vehicle motions and corresponding desired intermediate control commands such as optimal slip ratios are calculated, and servo controllers track the desired intermediate control commands. The linear time-varying MPC scheme is deployed to calculate the desired intermediate control command for the actuator apportionment.

There are critical obstacles to the realization of the centralized ICC systems. A disadvantage of the online optimization-based centralized ICC is the relatively high computational effort needed to solve the optimization problem in real-time. Furthermore, the centralized approach is not practical in today's business practice, in which independent design of stand-alone control systems is still the most common practice (Webers and Busch, 2003). This means that centralized ICC faces difficulties unless it can clarify the roles of auto-makers and suppliers (Koehn et al., 2006).

3.1.2 DECENTRALIZED INTEGRATION APPROACHES

The decentralized integration approaches to be developed in this research aim to coordinate the control commands of the sub-control systems, which were separately designed for their individual objectives. To see how such a coordination design has been applied in other areas, a brief review of the literature involving various engineering aspects of decentralized control is conducted.

A major application of vehicle coordination control is the motion control in unmanned vehicles including aerial, underwater and on road (Saberi et al., 2004). All these systems are mainly based on pre-defined decentralized approaches, in which pure subsumption architecture and rule-based ad-hoc approaches are used to switch among or coordinate the actions of sub-control systems. Behavior-based programming, a modified form of the subsumption architecture has been widely applied in autonomous vehicles by integrating the behaviors for survival and navigation (Brooks, 1990; Brooks, 1991). A well-known drawback of the behavior-based approaches is that they are difficult to analyze rigorously. Therefore, it is hard to guarantee the performance of the control systems.

The rule-based approaches that are widely deployed in industrial applications are mainly based on the engineer's intuition and prior knowledge (Hac and Bodie, 2002). This approach is not reusable and the procedures must be repeated when the target vehicle is changed. Similarly, artificial neural networks and fuzzy rule-based coordination suffer the same re-usability problem (Yoshimura and Emoto, 2003; Karbalaei et al., 2007).

For a decentralized approach, controllers based on a switching scheme have been attempted. They can be verified by framing models and controllers in the context of hybrid automata (Girard, 2005). Systems that include both discrete and continuous dynamics are usually referred to as hybrid systems in the literature (Frazzoli, 2001). In these systems, while the control layers that interact directly with the plant operate on a

continuous state space, higher control layers operate on a discrete state space as logical decision-making agents.

Diagonal decoupling for multivariable dynamic system have been studied through the relative gain array (RGA) analysis (Skogestad and Postlethwaite, 2005). To realize this approach, two design problems, input-output pairing and interaction minimization, are solved. RGA analysis and development of decoupling compensators are deployed through the use of the steady state response matrix. However, because of the strong interactions among vehicle dynamics, the design of such decoupling compensators is usually not appropriate. For example, chassis control elements such as steering and braking systems cannot manipulate the vehicle dynamics independently, because the yaw rate and lateral velocity are strongly coupled. RGA analysis of ICC system (AFS+ESC, RWS+ESC) will be studied in section 3.2.1.

3.2 DECENTRALIZED DESIGN OF ICC

A proposed decentralized approach is for the integration of sub-control systems that are already designed. First, a diagonal decoupling control is investigated as the representative decentralized control. The diagonal decoupling control is a fully decentralized approach, in which individual controllers are independently in charge of corresponding outputs. The decoupled approach works well only when the inputs/outputs of the dynamic system are equal in number and can be readily decoupled. Therefore, a relative gain array analysis of the ICC system is conducted to assess the suitability of diagonal decoupling control.

The coordinator in a decentralized ICC design approach modifies the sub-system control commands. The number of system inputs/outputs does not need to be the same. The decentralized ICC consists of a lower layer and a higher layer. At the lower layer, the control modules of the sub-systems generate servo-level control commands. At the

higher layer, a coordinator (to be designed) intercepts and manipulates the sub-system control commands, as shown in Figure 3.2. The primary aim of the coordinator is to avoid conflict and eliminate redundancies among the controllers without the need to access information internal to the sub-systems.

The proposed coordination strategy is based on the assumption that activation of individual sub-control systems such as braking and steering systems generates sufficient actuation to meet the performance requirements. Therefore, amplification of the control commands is not necessary. The proposed coordinator is designed to coordinate sub control commands to satisfy the virtual control command. The coordination is implemented through a hybrid approach--an offline model predictive control (MPC) and an online fixed-point (FP) control allocation method. These two methods were selected to achieve a balance between real-time computation load and flexibility in implementation. The design of the above coordinator will be amplified and discussed in the following subsections.

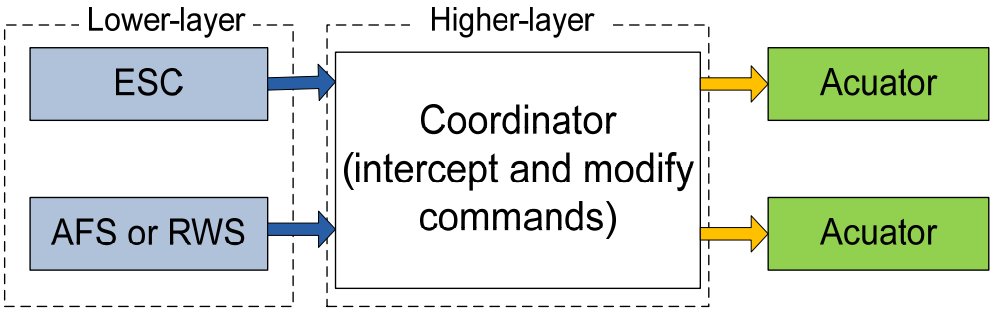

Figure 3.2 An example of decentralized ICC strategy with two individual chassis control functions designed by two suppliers.

3.2.1 ANALYSIS FOR DECOUPLING DECENTRALIZED ICC CONTROL

A relative gain array analysis is used to assess the ease of decoupling of multi-input-multi-output control problems (Skogestad and Postlethwaite, 2005). RGA provides a measure of interactions between input-output pairs (Xiong et al., 2006). Research on

the diagonal decoupling control for ICC systems was attempted by applying a linear vehicle model (Kitajima and Peng, 2000). This study is merely a first step and an analysis of the feasibility of this approach is necessary. Therefore, the feasibility of the diagonal decoupling control for ICC design can be investigated. The following shows the process of deriving the RGA of a two-input two-output control problem. Assuming the steady-state relation of the dynamic systems is

$$y_1 = K_{11}u_1 + K_{12}u_2 \text{ and } y_2 = K_{21}u_1 + K_{22}u_2 \tag{3.1}$$

where K_{ij} represents the steady state gains of the plant transfer function matrix. The RGA is then calculated as

$$\Lambda = \mathbf{K} * (\mathbf{K}^T)^{-1} \tag{3.2}$$

where the `*' operator denotes an element by element multiplication. In our 2x2 example,

$$\Lambda = \frac{1}{K_{11}K_{22} - K_{12}K_{21}} \begin{bmatrix} K_{11}K_{22} & -K_{12}K_{21} \\ -K_{12}K_{21} & K_{11}K_{22} \end{bmatrix} \tag{3.3}$$

Defining

$$\Lambda \equiv \begin{bmatrix} \lambda_{11} & \lambda_{12} \\ \lambda_{21} & \lambda_{22} \end{bmatrix} \tag{3.4}$$

Then we have $\lambda_{11} + \lambda_{12} = 1, \lambda_{12} = \lambda_{21}, \lambda_{11} = \lambda_{22}$. If the diagonal terms are close to 1, the system can be more easily decoupled with the main pairing $y_1 - u_1$ and $y_2 - u_2$. If λ_{ii} are much larger than 1, then the off-diagonal elements of the RGA are negative, which means that the resulting interactions will take controlled outputs in a direction away from what the control is trying to achieve(please see Appendix C for detailed explanation).

The feasibility of decoupling the input-output pairs is illustrated below using a simplified two-DOF vehicle model. In this model, it is assumed that both steering and differential braking are available in two configurations: AFS+ESC and RWS+ESC. In the matrix form, the state space model is

$$\dot{X} = A_{2X2}X + B_{2X2i}U_{ICCi} \tag{3.5}$$

where $X = \begin{bmatrix} v & r \end{bmatrix}^T$, $U_{\mathrm{ICCf}} = \begin{bmatrix} \delta_f & M_{ESC} \end{bmatrix}^T$, $U_{\mathrm{ICCr}} = \begin{bmatrix} \delta_r & M_{ESC} \end{bmatrix}^T$, $i = f, r$, and

$$A_{2\mathrm{X2}} = \begin{bmatrix} -\dfrac{C_{\alpha f} + C_{\alpha r}}{u_x m} & \dfrac{-aC_{\alpha f} + bC_{ar}}{u_x m} - mu_x \\ \dfrac{-aC_{\alpha f} + bC_{ar}}{u_x I_{zz}} & -\dfrac{a^2 C_{\alpha f} + b^2 C_{\alpha r}}{u_x I_{zz}} \end{bmatrix} \tag{3.6}$$

$$B_{2\mathrm{X2f}} = \begin{bmatrix} \dfrac{C_{\alpha f}}{m} & 0 \\ \dfrac{aC_{\alpha f}}{I_{zz}} & \dfrac{1}{I_{zz}} \end{bmatrix} \text{ and } B_{2\mathrm{X2r}} = \begin{bmatrix} \dfrac{C_{\alpha r}}{m} & 0 \\ \dfrac{-bC_{\alpha r}}{I_{zz}} & \dfrac{1}{I_{zz}} \end{bmatrix} \tag{3.7}$$

The DC gain matrices, $\mathbf{K}_i$ are obtained under the assumption of constant inputs

$$\mathbf{K}_f = -A_{2\mathrm{X2}}{}^{-1} B_{2\mathrm{X2f}} \qquad \mathbf{K}_r = -A_{2\mathrm{X2}}{}^{-1} B_{2\mathrm{X2r}} \tag{3.8}$$

The diagonal decoupling control is explained using the two DOF vehicle models. The system configuration for the decoupling diagonal control in the 2x2 MIMO system is shown in Figure 3.3. Through the decoupling compensator, input-output pairings are composed for independent interaction between individual pairings as shown in Eq. (3.9).

$$\mathbf{G_{des}} = \mathbf{G}\mathbf{G}_c^* = \begin{bmatrix} K_{d11} & 0 \\ 0 & K_{d22} \end{bmatrix} = \begin{bmatrix} K_{11} & K_{12} \\ K_{21} & K_{22} \end{bmatrix} \begin{bmatrix} K_{c11}^* & K_{c12}^* \\ K_{c21}^* & K_{c22}^* \end{bmatrix} \tag{3.9}$$

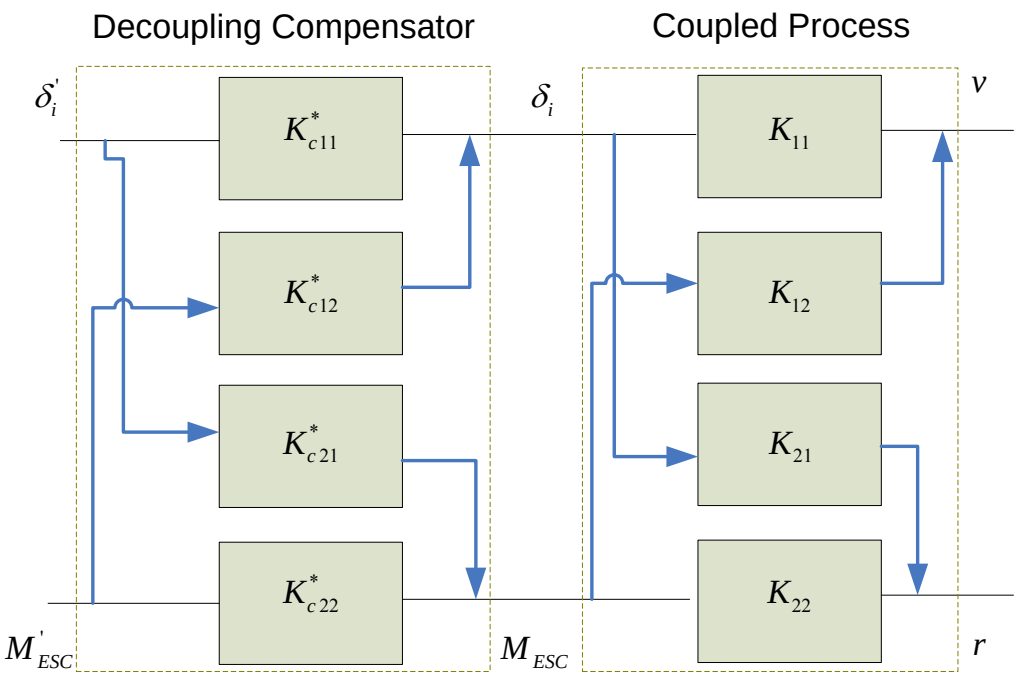

Figure 3.3 Decoupling control configuration for the 2 DOF vehicle models

The form of the decoupling diagonal control of the two DOF vehicle model is derived as shown in Eq. (3.10). We can identify whether our ICC systems are suitable for this decoupling approaches or not through the following RGA analysis.

$$\begin{bmatrix} v \\ r \end{bmatrix} = \begin{bmatrix} K_{d11} & 0 \\ 0 & K_{d22} \end{bmatrix} \begin{bmatrix} \delta_i' \\ M_{ESC}' \end{bmatrix} \tag{3.10}$$

Table 3-1 Parameters of two DOF vehicle

m	vehicle sprung mass	1650 [kg]
g	gravitational constant	9.81 [m/s^2]
I_{zz}	yaw moment of inertia	3000 [kg-m^2]
a	distance of c.g. to front axle	1.47 [m]
b	distance of c.g. to rear axle	1.53 [m]
$C_{\alpha f}$	front axle cornering stiffness	0.4*1800*57.3 [N-m/rad]
$C_{\alpha r}$	rear axle cornering stiffness	0.4*1600*57.3 [N-m/rad]

The RGA analysis of the two DOF vehicle model is performed by applying DC gain matrix with the vehicle parameters shown in Table 3-1. In the analysis results (see Table 3-2), the magnitude of the diagonal elements are not much larger than those of the off-diagonal elements. It means that the ICC system exhibits strong interactions and is difficult to decouple. In other words, neither the AFS-ESC case nor the RWS-ESC case is suitable for diagonal decentralized control approach. Therefore, a new coordination strategy is demanded not relying on the decoupling control strategy.

Table 3-2 Relative gain array of the two DOF vehicle model

	AFS and ESC		
$u_x[m/\sec]$	20	30	40
Steady-state matrix	$\begin{bmatrix} 51.1 & 1.0 \\ -6.6 & -0.1 \end{bmatrix}$	$\begin{bmatrix} 173 & 3.2 \\ -9.3 & -0.2 \end{bmatrix}$	$\begin{bmatrix} 388 & 7.0 \\ -12. & -0.2 \end{bmatrix}$
RGA	$\begin{bmatrix} -4.6 & 5.6 \\ 5.6 & -4.6 \end{bmatrix}$	$\begin{bmatrix} -10. & 11. \\ 11. & -10. \end{bmatrix}$	$\begin{bmatrix} -17. & 18. \\ 18. & -17. \end{bmatrix}$
	RWS and ESC		
Steady-state matrix	$\begin{bmatrix} -72. & 1.07 \\ 6.67 & -0.11 \end{bmatrix}$	$\begin{bmatrix} -204. & 3.2 \\ 9.3 & -0.2 \end{bmatrix}$	$\begin{bmatrix} -429 & 7.0 \\ 11. & -0.2 \end{bmatrix}$
RGA	$\begin{bmatrix} 7.3 & -6.3 \\ -6.3 & 7.3 \end{bmatrix}$	$\begin{bmatrix} 14 & -13 \\ -13 & 14 \end{bmatrix}$	$\begin{bmatrix} 22. & -21. \\ -21. & 22. \end{bmatrix}$

For the analysis of decoupling ICC control, the bode plots are presented in Figure 3.4. The relative magnitudes of the normalized transfer functions on the diagonal are almost same as the off-diagonal entries, indicating that there is severe dynamic coupling. Based on the bode plots, both combinations of ICCs (AFS+ESC and RWS+ESC) are not suitable for decoupling decentralized approaches. Therefore, a new coordination strategy is required.

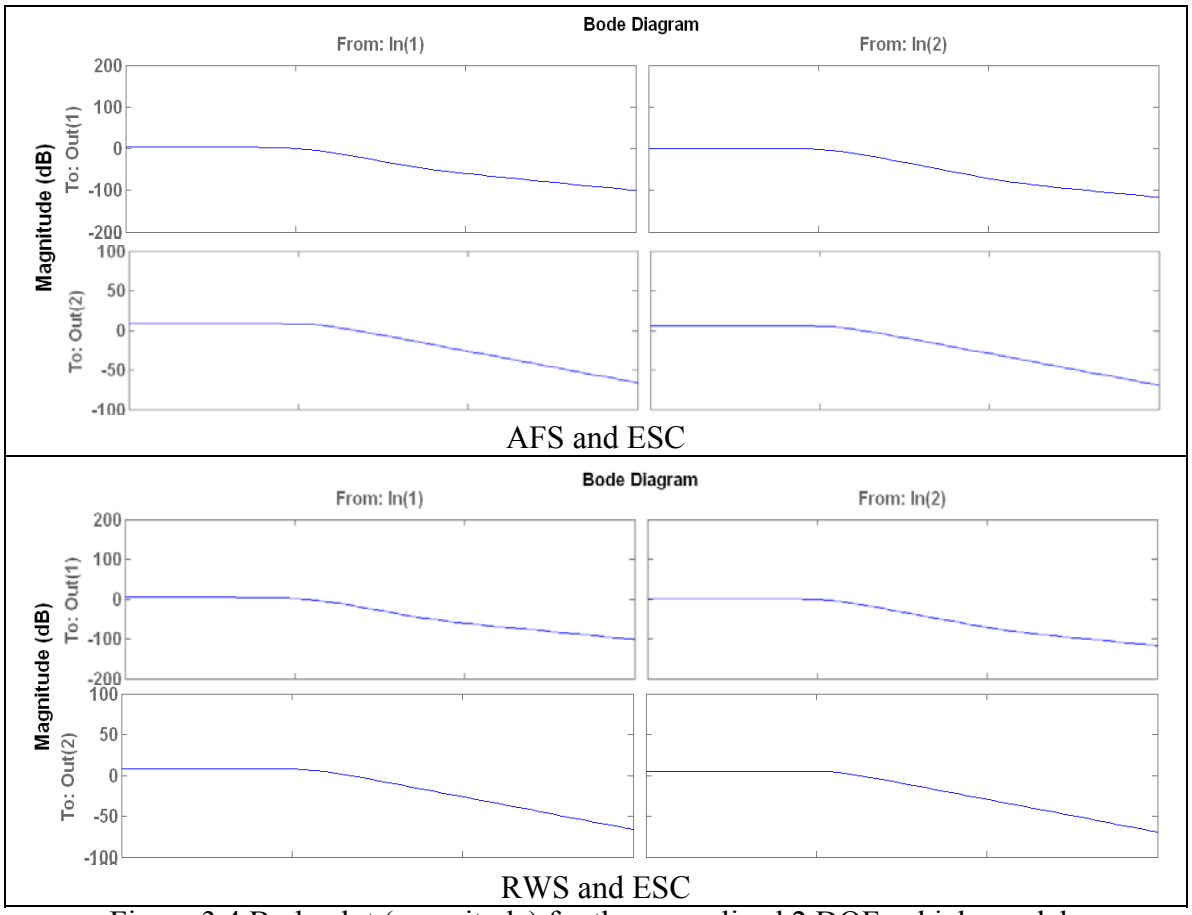

Figure 3.4 Bode plot (magnitude) for the normalized 2 DOF vehicle models

3.2.2 COORDINATION STRATEGY

Our decentralized ICC design begins with the assumption that the sub-control algorithms are encapsulated, and our design procedure must be realized without internal information about the sub-control algorithms. Under these conditions, the coordination approach of adjusting control commands generated from the sub-control systems is proposed. A coordination strategy is defined as setting an upper bound of the sub-control commands from sub-control systems.

The tire force diagram shown in Figure 3.5 shows how conflict and redundancy between two sub-systems are reduced. The actual forces generated from u_{ESC} and u_{RWS} are assumed to be F_{ESC} and F_{RWS}. F^{e}_{RWS} and F^{e}_{RWS} are effective tire forces that correspond to projected magnitudes of F_{ESC} and F_{RWS}. It is assumed that the forces from

the sub-systems are simply added together (a simplification to illustrate the basic concept).

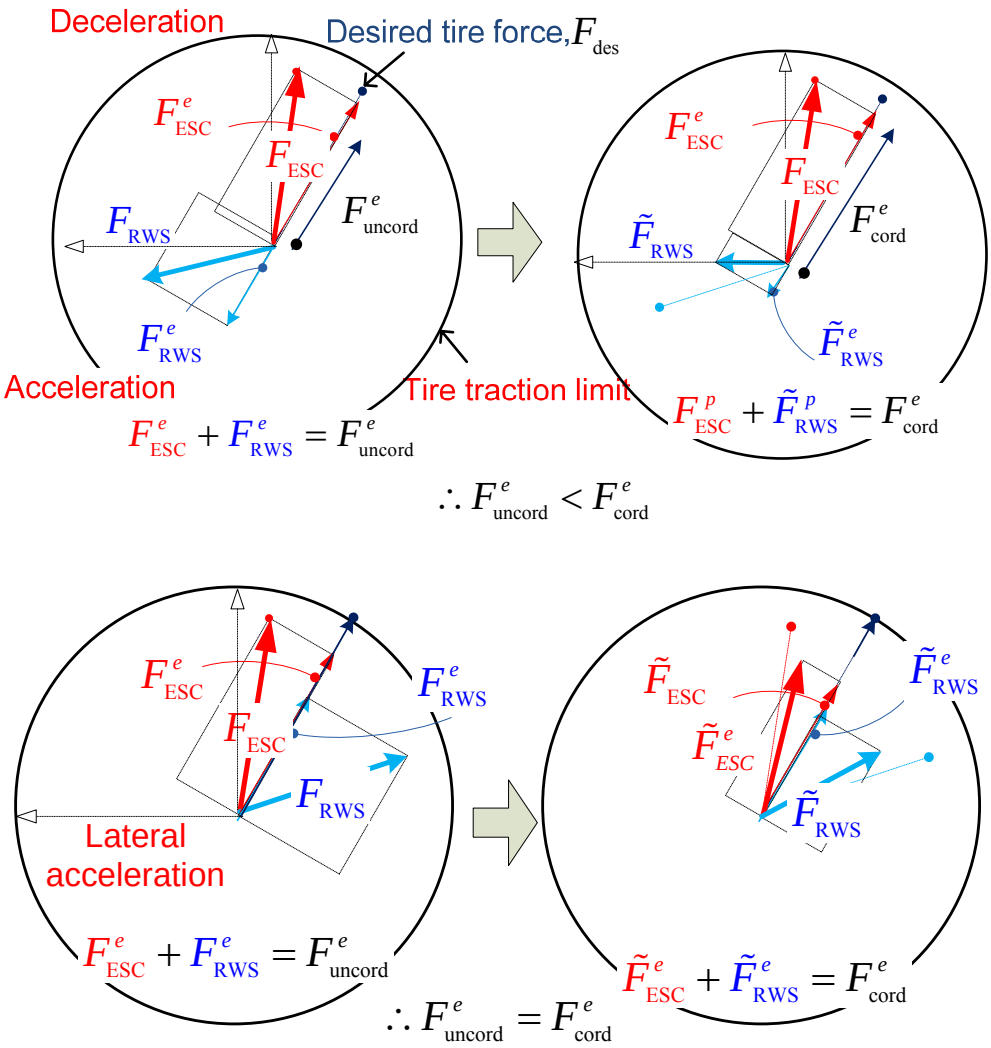

Figure 3.5 Tire force coordination principle

In case of conflict between controls, the effectiveness of uncoordinated tire forces, F^e_{uncord}, can become smaller than it would be if only one sub-control system were activated. A higher effectiveness, F^e_{cord}, can be preserved to most nearly reach the optimal tire force, F_{des}, through reducing the magnitude of one of the control actions. In case of redundancy, we can see that F^e_{uncord} may become saturated. A down-scaling modification

can eliminate redundancy while maintaining the effectiveness of control, F_{cord}. This saturation modification can be defined as the coordination strategy for sub-control command coordination. Furthermore, the coordination strategy approach has another important characteristic; the commands from the subsystems are scaled only down, not up to prevent over-actuation of subsystem in the sense of liability issue.

It is difficult to perform a rigorous analysis to justify the coordination strategy approach without information of the sub-control algorithms. In the following, the simplified analyses on Liner Quadratic (LQ) regulator for the AFS-ESC and RWS-ESC system are conducted. The vehicle model is the two DOF vehicle model shown in Eq. (3.5) and Eq.(3.6), i.e.,

$$\dot{X} = A_{2X2} X + B_{2X2i} U_{\text{ICCi}} \tag{3.11}$$

In an LQ problem, one aims to find the steady state solution of $U_{\text{ICCi}} = -L_{\text{ICCi}} X$ that minimizes a cost function

$$\min J = \int_0^\infty \left(X^T Q X + U_{\text{ICCi}}{}^T R U_{\text{ICCi}} \right) dt \tag{3.12}$$

The optimal feedback gains are respectively computed by applying the lqr(.) in Matlab with different control matrices; $B_{AFS} = B_{2X2f}(:,1)$, $B_{RWS} = B_{2X2r}(:,1)$ and $B_{\text{ESC}} = B_{2X2i}(:,2)$. Table 3-3 shows the optimal feedback gains, L_{ICCi} of the LQ problem for both AFS-ESC and RWS-ESC cases with the optimal feedback gains; $L_{\text{AFS}}, L_{\text{RWS}}$ and L_{ESC} for the respective individual subsystems; AFS, RWS and ESC. The gains of the two ICC cases are smaller in comparison to the cases when only one sub-system is used. This simple example demonstrates one reason why the control signals from the sub-systems is saturated, not up. Another (more hand-waving) reason is for legal/liability considerations.

Table 3-3 Results of optimal feedback gain (where ICCf: AFS+ESC and ICCr: RWS+ESC)

$u_x[m/\sec]$		25	30	35	40
R	Q	$L_{\mathrm{ICCf}}(1,:)/L_{\mathrm{AFS}}$			
$\begin{bmatrix} 5e3 & 0 \\ 0 & 1 \end{bmatrix}$	$\begin{bmatrix} 1 & 0 \\ 0 & 1 \end{bmatrix}$	$[0.76 \quad 0.69]$	$[0.7 \quad 0.61]$	$[0.67 \quad 0.57]$	$[0.64 \quad 0.54]$
		$L_{\mathrm{ICCf}}(2,:)/L_{\mathrm{ESC}}$			
		$[0.93 \quad 0.89]$	$[0.90 \quad 0.84]$	$[0.88 \quad 0.80]$	$[0.87 \quad 0.79]$
		$L_{\mathrm{ICCr}}(1,:)/L_{\mathrm{RWS}}$			
		$[0.86 \quad 0.77]$	$[0.81 \quad 0.70]$	$[0.78 \quad 0.66]$	$[0.76 \quad 0.63]$
		$L_{\mathrm{ICCr}}(2,:)/L_{\mathrm{ESC}}$			
		$[0.84 \quad 0.78]$	$[0.80 \quad 0.73]$	$[0.78 \quad 0.70]$	$[0.77 \quad 0.69]$

3.2.3 HYBRID APPROACH: OFFLINE VIRTUAL CONTROL COMPUTATION AND ONLINE CONTROL ALLOCATION

Incorporating heavy-computation control functions in embedded hardware can be costly. Real-time approaches via hardware architecture with high computation capability pose critical problem under the current vehicle implementation from the point of view of cost. Furthermore, considerable cost increases due to the requirement for an additional controller make the problem of expense even more critical in the decentralized ICC. Under the circumstance, approach that does not require significant online computations should be pursued. In general, we can substitute an offline approach for some replaceable real time computation to lessen the computational power requirement. The offline approach applying pre-computed results to reduce real-time computation needs was explored (Storkaas, 2002) for a commercial ESC system. This approach, however, has limited flexibility for dealing with plant variations and furthermore additional memory to achieve these flexibilities causes cost to increase. This implementation

problem leads to a compromise approach that can realize simultaneously flexibility and reduction of computational loads for the decentralized ICC design.

A hybrid approach is proposed to achieve decentralized coordination. The hybrid approach consists of an online module for control allocation and an offline module to compute the virtual control commands. The hybrid approach reduces the computational loads through the offline module and achieves adaptability for activation of sub-control systems through the online module.

In the design of the hybrid approach, the virtual control commands can be computed without knowing the composition of the sub-systems. The virtual control demands are determined considering the tire capability based on the vehicle dynamics. Computing the virtual commands is based on the model predictive control (MPC) approach because (i) it considers the vehicle performance over a horizon; and (ii) the limitations imposed by the tire capacity can be incorporated. The output from the MPC optimization process is stored in the form of a look-up table. The optimal virtual control commands from the lookup table then need to be realized by the control commands from the chassis sub-systems. Typically, the number of actual control inputs is larger than the number of virtual control commands. Therefore, a control allocation (CA) process (typically under-determinant) is used in the online module, which in many cases solves optimization problems. Through this online CA procedure, we can realize an adaptable control strategy under different combinations and different activations of the sub-control systems.

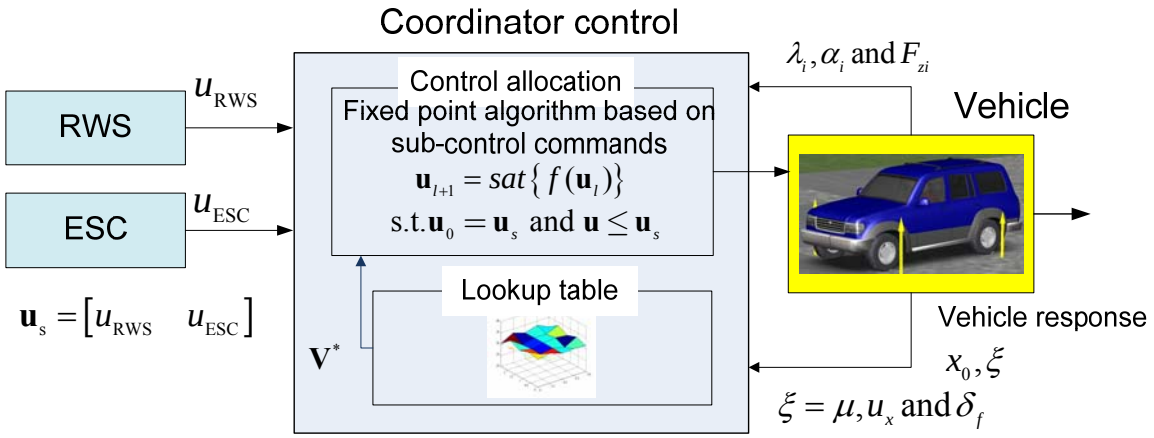

Figure 3.6 The proposed ICC configuration

Figure 3.6 shows the proposed ICC configuration. In the lookup table, vehicle states, x_0, road friction, μ, vehicle speed, u_x and driver steering commands, δ_f are used as input variables to obtain a virtual control command set, $\mathbf{V}^*$. In the online control allocation module, a sub-control command set, $\mathbf{u}_s = [u_{RWS} \quad u_{ESC}]$ serves as upper bounds of the optimization problem and as the initial guess, $\mathbf{u}_0$ for the fixed-point iterations. Tire model parameters are used for formulation of the CA problem. Subsequently, the optimal control inputs are computed using the fixed-point iteration method. The design of these two modules is explained in detail in the following sub-sections.

3.2.4 OFFLINE MODEL PREDICTIVE CONTROL (MPC)

MPC, which is also referred to as receding horizon control, is based on iterative and finite horizon optimization of the predicted output in a plant model. The general principle of MPC is illustrated in Figure 3.7. In the MPC, the future responses of the plant, $y(k)$, due to a sequence of manipulated inputs, $u(k)$, over the prediction horizon, P, are predicted. The manipulated inputs to make predictive responses to follow the desired outputs are computed by minimizing a cost function. Only the control signal at the first time step is applied and this process is repeated for each time step. The amplitude and rate can be limited by imposing constraints.

The MPC approach has the following advantages (Maciejowski, 2002): (i) MPC can handle multivariable controls such as multiple-input-multiple-output (MIMO) control, (ii) MPC can accommodate the actuator limit or the output limit through constraints, (iii) MPC approaches can combine feedback control and feed-forward control: The feedback control is achieved through measured/estimated states and outputs, and the feed-forward control is achieved through the responses prediction of the system. The MPC method is successfully applied to compute the optimal control commands on the basis of a quadratic programming formulation (Bemporad et al., 2003), and this QP based MPC is applied in automotive control systems (Falcone et al., 2007; Falcone, 2007 b).

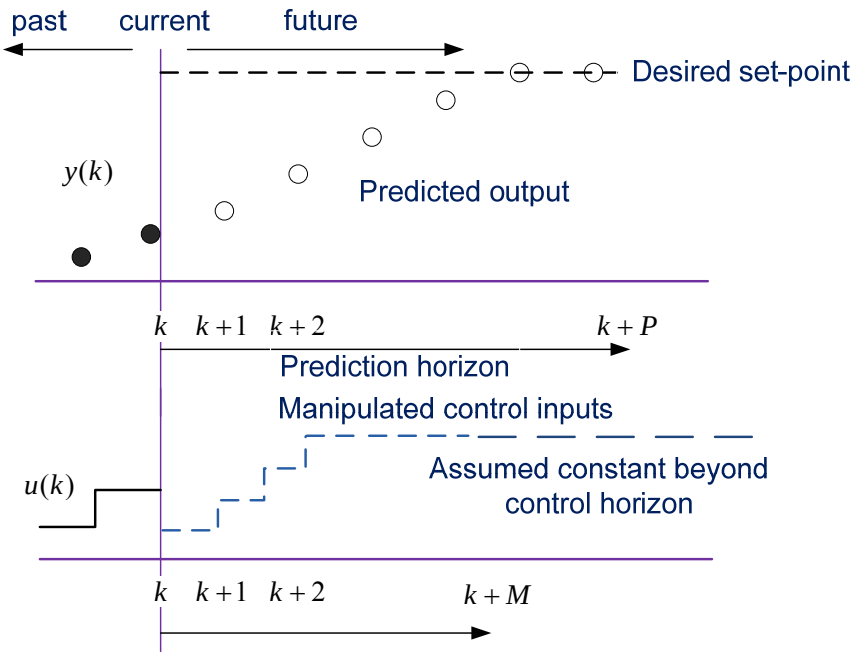

Figure 3.7 Principle of the model predictive control (MPC).

Despite the benefits noted above, it is not easy to implement MPC in on-board systems because MPC demands high computationally efficient hardware. Real-time MPC for ground vehicles has been implemented using hardware with computing power

equal to or higher than that of the desktop PC. The offline approach provides an alternative way of implementing MPC with hardware system with a modest computing power. This error in online optimization can be resolved through pre-computation via the offline approaches.

The MPC design starts from the derivation of the difference equation-based predictive model in order to formulate a linear quadratic optimization problem. In our MPC design, by defining virtual control commands F_y : lateral force and M_z : yaw moment, the two DOF vehicle model can be rewritten as

$$\dot{X} = A_c X + B_c V \tag{3.13}$$

$$\begin{bmatrix} \dot{v}_y \\ \dot{r} \end{bmatrix} = \begin{bmatrix} 0 & -u_x \\ 0 & 0 \end{bmatrix} \begin{bmatrix} v_y \\ r \end{bmatrix} + \begin{bmatrix} 1/m & 0 \\ 0 & 1/I_{zz} \end{bmatrix} \begin{bmatrix} F_y \\ M_z \end{bmatrix} \tag{3.14}$$

This continuous-time state-space system is discretized (Bemporad et al., 2003) as follows

$$X_{j+1|j} = AX_j + BV_j \tag{3.15}$$

where T_s is the sampling time and linearization is based on the previous successful studies (Chang, 2007; Zhou, 2008)

$$A = (I + T_s A_c), \;\; B = T_s B_c \tag{3.16}$$

The predicted state in the discrete form can be expressed as follows:

$$\begin{bmatrix} X_{j+1|j} \\ X_{j+2|j} \\ X_{j+3|j} \\ \cdots \\ X_{j+n||j} \end{bmatrix} = \begin{bmatrix} A \\ A^2 \\ A^3 \\ \cdots \\ A^n \end{bmatrix} X_j + \begin{bmatrix} B & 0 & 0 & 0 & 0 \\ AB & B & 0 & 0 & 0 \\ A^2B & AB & B & 0 & 0 \\ \cdots & \cdots & \cdots & \cdots & \cdots \\ A^{n-1}B & A^{n-2}B & \cdots & AB & B \end{bmatrix} \begin{bmatrix} V_j \\ V_{j+1} \\ V_{j+2} \\ \cdots \\ V_{j+n-1} \end{bmatrix} \tag{3.17}$$

If we define

$$\mathbf{X}_j \equiv \begin{bmatrix} X_{j+1|j}; & X_{j+2|j}; & X_{j+3|j}; & \ldots & X_{j+n|j} \end{bmatrix} \text{ and } \mathbf{V}_j \equiv \begin{bmatrix} V_j; & V_{j+1}; & V_{j+2}; & \ldots & V_{j+n-1} \end{bmatrix} \tag{3.18}$$

Eq. (3.17) can be rewritten in a compact matrix form, i.e.,

$$\mathbf{X}_j = \mathbf{G}X_j + \mathbf{F}_1 \mathbf{V}_{j-1} \tag{3.19}$$

Defining the weighting parameters $Q_{ei} = \begin{bmatrix} Q_{ev_y} & 0 \\ 0 & Q_{er} \end{bmatrix}$ and $Q_{ui} = \begin{bmatrix} Q_{uF_y} & 0 \\ 0 & Q_{uM_z} \end{bmatrix}$, the cost function to balance tracking performance for vehicle stability is defined in the following mathematical form

$$J = \sum_{i=1}^{n} e_{j+i|j}^T Q_{ei} e_{j+i|j} + \sum_{i=1}^{n} V_{j+i}^T Q_{ui} V_{j+i} \tag{3.20}$$

where $e_{j+i|j} = X_{j+i|j} - X_d$, $X_d = \begin{bmatrix} r_d & v_{yd} \end{bmatrix}$, $r_d = f(\delta_f, \xi)$ and $v_{yd} = 0$.

The MPC problem is to minimize J in Eq. (3.20), which can be solved by casting it into a Quadratic Programming (QP) problem with constraints that has the following general form:

$$\min_{\mathbf{V}} J = \frac{1}{2}(\mathbf{X}_d - \mathbf{G}X_j - \mathbf{F}_1\mathbf{V})^T \mathbf{Q}_e (\mathbf{X}_d - \mathbf{G}X_j - \mathbf{F}_1\mathbf{V}) + \frac{1}{2}\mathbf{V}^T\mathbf{Q}_u\mathbf{V} \tag{3.21}$$

$$\mathbf{A}_{\text{cnstr}}\,\mathbf{V} \le \mathbf{b}_{\text{cnstr}} \tag{3.22}$$

Amplitude limits are applied as constraint condition by taking into account of road-friction as follow

$$\begin{bmatrix} \mathbf{I}_{N\times N} \\ -\mathbf{I}_{N\times N} \end{bmatrix} \mathbf{V} \le \begin{bmatrix} I_{N\times 1} V_{\max} \\ -I_{N\times 1} V_{\min} \end{bmatrix} \tag{3.23}$$

where

$$\begin{aligned} &I_{n\times 1} = \begin{bmatrix} I & I & \dots & I \end{bmatrix}^T \\ &V_{\max} = \begin{bmatrix} F_{y\max} & M_{z\max} \end{bmatrix} \text{ and } V_{\min} = \begin{bmatrix} F_{y\min} & M_{z\min} \end{bmatrix} \\ &F_{y\max} = \mu mg \text{ and } M_{z\max} = \mu \frac{mg}{2} T_w \end{aligned} \tag{3.24}$$

Rate limits are applied as constraints as follow

$$\begin{bmatrix} \Delta\mathbf{I}_{n\times n} \\ -\Delta\mathbf{I}_{n\times n} \end{bmatrix} \mathbf{V} \le \begin{bmatrix} I_{n\times 1}\Delta V_{\max} + E_{n\times 1}\Delta V_{\max} \\ -I_{n\times 1}\Delta V_{\min} - E_{n\times 1} V_{\min} \end{bmatrix} \tag{3.25}$$

where

$$\Delta \mathbf{I}_{n\times n} = \begin{bmatrix} I & 0 & 0 & \dots & 0 \\ I & -I & 0 & \dots & 0 \\ 0 & I & -I & 0 & \dots \\ \vdots & \vdots & \vdots & \vdots & \ddots \\ 0 & \dots & \dots & I & -I \end{bmatrix} \text{ and } E_{n\times 1} = \begin{bmatrix} I & 0 & \dots & 0 \end{bmatrix}^T$$

$$\Delta V_{\min} = \begin{bmatrix} \Delta F_{y\min} & \Delta M_{z\min} \end{bmatrix} \text{ and } \Delta V_{\max} = \begin{bmatrix} \Delta F_{y\max} & \Delta M_{z\max} \end{bmatrix}$$

The matrices for constraints in Eq. (3.22) are defined as follow

$$\mathbf{A}_{\text{cnstr}} = \begin{bmatrix} \mathbf{I}_{n\times n} \\ -\mathbf{I}_{n\times n} \\ \Delta\mathbf{I}_{n\times n} \\ -\Delta\mathbf{I}_{n\times n} \end{bmatrix} \text{ and } \mathbf{b}_{\text{cnstr}} = \begin{bmatrix} I_{n\times 1} V_{\max} \\ -I_{n\times 1} V_{\min} \\ I_{n\times 1}\Delta V_{\max} + E_{n\times 1} V_{\max} \\ -I_{n\times 1}\Delta V_{\min} - E_{n\times 1} V_{\min} \end{bmatrix} \tag{3.26}$$

The MPC cost function can be defined according to the desired objectives such as yaw-rate compensation, slip reduction, etc. The problem is solved repeatedly under all grid points selected for the vehicle states, road friction coefficient, vehicle forward speed, and steering angle (see Table 3-4) with MPC parameters. In our example, the total number of independent variables of the lookup table is 5. Once the MPC solution is found, the first step of the obtained control sequence: $V^* = \begin{bmatrix} 1 & \dots & 0 \end{bmatrix} \mathbf{V}$ is stored in a lookup table (5 inputs and 2 outputs, F_y and M_z). Selection of prediction horizon should be based on a trade-off between computational load and ensuring control performance. However, the larger number of the prediction horizon does not necessarily guarantee better vehicle motion prediction because this MPC is based on the linearization at operating points (e.g. fixed longitudinal velocity). The predictive horizon is selected to be 0.3[sec] for capturing appropriately the change of vehicle motions. We consider a response time of vehicle motions resulting from the activation of tire forces and external moments. The minimizing of sampling time of MPC has trade-off between computational burden and proper simulation of the vehicle motion, similar to that of the prediction horizon. The sampling time is selected as value 0.02 [sec] based on the previous successful studies (Chang, 2007; Zhou, 2008).

Table 3-4 Definition of states and input grids and other MPC parameters

	Symbol [units]	Grid
Driver demand	δ_f [deg]	[-100 -75 -50 -25 0 25 50 75 100]
Vehicle states and parameters	u_x [m/sec]	[20 25 30 35]
	r [deg/sec]	[-30 -25 -20 -15 0 15 20 25 30]
	v_y [m/sec]:	[-17 -14 -11 -8.5 0 8.5 11 14 17]
	μ	[0.3 0.45 0.6 0.75 0.9]
MPC sampling time (s)	T_s	0.02
Prediction horizon	n	15
Tracking error weight	Q_{ev_y}/Q_{er}	3e7/5e5
Control input weight	Q_{uF_y}/Q_{uM_z}	1/0.5

The grid sizes of the states are important because they are directly related to the accuracy of lookup table interpolation and the memory size. Fine grids demand a large size memory but produce more accurate optimization results; coarse grids on the other hand, reduce the size of the required memory and thus reduce costs. The accuracy of their results, however, may deteriorate. The selection of grid points of the states therefore is based on a trade-off between simulation accuracy and memory size (see Table 3-5). To check accuracy of the offline lookup table, percentage error is defined in Eq. (3.27) between the virtual control commands obtained from lookup table and online MPC results from 100 randomly selected vehicle states, lateral velocity and yaw rate.

$$e_{\tilde{F}_Y^*} = \left(F_Y^{*\text{off}} - F_Y^{*\text{on}}\right)/F_Y^{*\text{on}} \quad e_{\tilde{M}_z^*} = \left(M_z^{*\text{off}} - M_z^{*\text{on}}\right)/M_z^{*\text{on}} \tag{3.27}$$

Table 3-5 Errors between interpolated lookup tables and online calculations with varying grid sizes

	5 grids	7 grids	9 grids
$m_{err\left(F_y^*\right)} \pm \sigma_{err\left(F_y^*\right)}$ [%]	2.6 $\pm$ 4.2	2.8 $\pm$ 3.2	2.5 $\pm$ 2.2
$m_{err\left(M_z^*\right)} \pm \sigma_{err\left(M_z^*\right)}$ [%]	2.5 $\pm$ 3.7	2.4 $\pm$ 2.8	2.1 $\pm$ 1.8

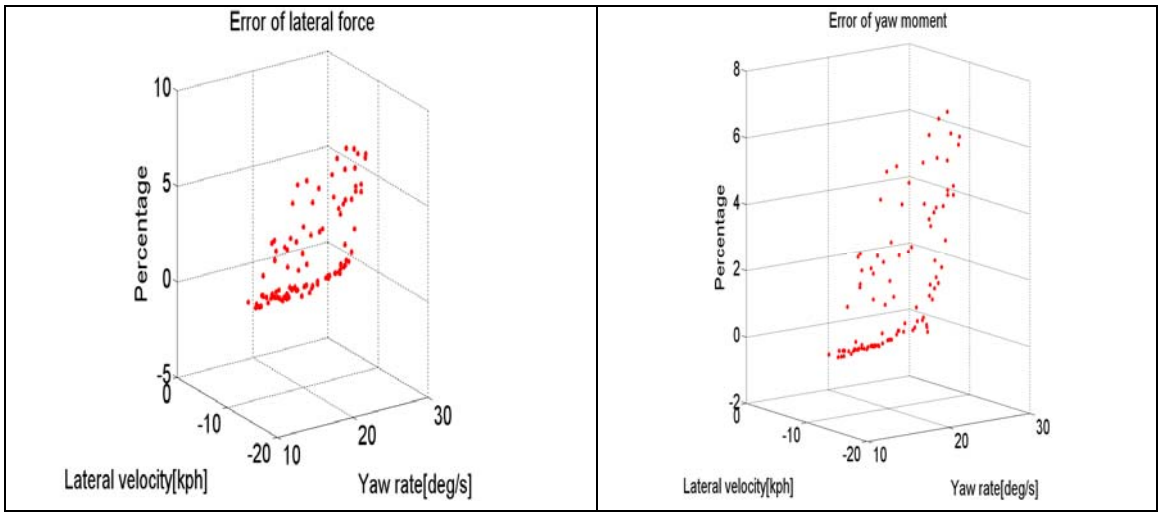

Figure 3.8 Errors between interpolated lookup tables and online calculation: $m_{err\left(F_y^*\right)} \pm \sigma_{err\left(F_y^*\right)}$=2.5 $\pm$ 2.2 [%] and $m_{err\left(M_z^*\right)} \pm \sigma_{err\left(M_z^*\right)}$=2.1 $\pm$ 1.8 [%]

The mean values, $m_{err\left(F_y^*\right)}$ and $m_{err\left(M_z^*\right)}$ and, the standard deviations, $\sigma_{F_y^*}$ and $\sigma_{M_z^*}$ of the on/offline error are calculated with regard to the virtual control commands, F_y^* and M_z^* as shown in Figure 3.8.

3.2.5 CONTROL ALLOCATION VIA FIXED POINT ITERATION ALGORITHM

Control allocation approaches are employed to optimally allocate the virtual control command among control inputs/effectors by solving the systems of linear equations with constraints. In our online CA module, the desired virtual control commands are realized by applying sub-control inputs for real-time reconfiguration and actuator management. In other words, this CA approach creates sub-control inputs from changeable sub-systems to generate virtual control command effectively under the condition of actuator-failures and different system combinations. The CA approaches have been actively implemented to realize desired control commands via redundant actuators, as shown in several studies (Davidson, 2001; Oppenheimer et al., 2006).

The selection of optimization schemes is critical for real-time implementation of CA computing. Several research to find computationally efficient CA algorithms for aircraft (Burken et al., 2001) and ground vehicles (Wang, 2007) has been reported.

In our study, the CA approach is employed so that sub control inputs such as braking torque and steering inputs are allocated to achieve the virtual control commands (desired lateral force and yaw moment). The saturated sub control commands replace the original sub-control inputs through the online coordination procedure.

A simple, globally convergent fixed point (FP) iteration algorithm is applied because of its computation efficiency and effectiveness, to be demonstrated in 3.2.7. Therefore, this algorithm is suitable for on-board systems that have the modest computation ability. The FP iteration algorithm and the accelerated FP algorithm have been successfully applied to a coordinated ground vehicle control problem. In this study, quadratic programming (QP) optimization problem including inequalities constraints is applied to solve the CA problem (Wang, 2007).

The concept of the FP iteration method is based on the contraction-mapping theorem: a contraction mapping in a complete metric space has exactly one fixed point (for detailed explanation of terminologies see Appendix D). The overall explanation of fixed-point iteration application in the online module of the coordinator is explained in this section.

The main goal of the QP problem is to find sub control inputs ($\mathbf{u}$) to track the optimal virtual control commands ($\bar{\mathbf{V}}$) obtained from the lookup table. In the meantime, it is desirable to use smallest possible inputs, $\mathbf{u}$. The optimization cost function for the QP problem based CA is defined as follows

$$\begin{aligned} &\min_{\mathbf{u}} J = \frac{1}{2}(1-\varepsilon)\left(B_{\mathbf{u}}\mathbf{u}-\bar{\mathbf{V}}\right)^T W_V \left(B_{\mathbf{u}}\mathbf{u}-\bar{\mathbf{V}}\right) + \varepsilon\frac{1}{2}\mathbf{u}^T W_{\mathbf{u}}\mathbf{u} \\ &C_{\mathbf{u}}\mathbf{u} \le d_{\mathbf{u}} \end{aligned} \tag{3.28}$$

where $0 \le \varepsilon \le 1$, and W_V and $W_{\mathbf{u}}$ are the weighting matrices for the virtual control commands, and the control inputs. $C_{\mathbf{u}}$ and $d_{\mathbf{u}}$ are for the inequalities constraints. Constraints are defined by taking into account limits of actuators as Eq. (3.29).

$$\underline{u}_i \le u_i \le \overline{u}_i \quad \text{where } i = 1,...l \tag{3.29}$$

$$\mathbf{C}_{\mathbf{u}} = \begin{bmatrix} 1 & 0 & 0 & 0 & 0 \\ -1 & 0 & 0 & 0 & 0 \\ 0 & 1 & 0 & 0 & 0 \\ 0 & -1 & 0 & 0 & 0 \\ 0 & 0 & \ddots & \vdots & \vdots \\ 0 & 0 & \dots & 0 & 1 \\ 0 & 0 & \dots & 0 & -1 \end{bmatrix}, d_{\mathbf{u}} = \begin{bmatrix} \overline{u}_1 \\ -\underline{u}_1 \\ \overline{u}_2 \\ -\underline{u}_2 \\ \vdots \\ \overline{u}_m \\ -\underline{u}_m \end{bmatrix} \tag{3.30}$$

The optimal solution *u** of the problem with a convex const function defined above needs to satisfy the Karush-Kuhn-Tucker (KKT) conditions below (Fletcher, 1989).

$$\begin{aligned} &\left((1-\varepsilon) B_{\mathbf{u}}^T W_V B_{\mathbf{u}} + \varepsilon W_{\mathbf{u}}\right)\mathbf{u} - (1-\varepsilon) B_{\mathbf{u}}^T W_V \overline{\mathbf{V}} + C_{\mathbf{u}}{}^T \boldsymbol{\lambda} = 0 \\ &\boldsymbol{\lambda}^T \left(C_{\mathbf{u}}\mathbf{u} - d_{\mathbf{u}}\right) = 0 \\ &\boldsymbol{\lambda} = \begin{bmatrix} \overline{\lambda}_1 & \underline{\lambda}_1 & \dots & \overline{\lambda}_m & \underline{\lambda}_m \end{bmatrix} \qquad \overline{\lambda}_i \ge 0,\ \underline{\lambda}_i \ge 0,\ \ i = 1,...,m \end{aligned} \tag{3.31}$$

Define a saturation function

$$sat\left(\xi, \underline{u}, \overline{u}\right) = \begin{cases} \overline{u}, & \xi \ge \overline{u} \\ \xi & \underline{u} \le \xi \le \overline{u} \\ \underline{u} & \underline{u} \le \xi \end{cases} \tag{3.32}$$

The FP computation algorithm for the QP problem is then developed based on the follow theorem (Lu, 1996; Wang, 2006)

Theorem: Assume that matrix $\mathbf{P} \equiv \left((1-\varepsilon) B_{\mathbf{u}}^T W_V B_{\mathbf{u}} + \varepsilon W_{\mathbf{u}}\right)$ is nonsingular.

(1) The unique optimal control $\mathbf{u}^*$ to problem in Eq. (3.31) is the unique solution of the fixed-point equation in $\mathbf{u}$

$$\mathbf{u} = sat\left\{ \frac{(1-\varepsilon) B_{\mathbf{u}}^T W_V \overline{\mathbf{V}}}{\|\mathbf{P}\|_f} + \left(I - \frac{\left((1-\varepsilon) B_{\mathbf{u}}^T W_V B_{\mathbf{u}} + \varepsilon W_{\mathbf{u}}\right)}{\|\mathbf{P}\|_f} \right) \mathbf{u} \right\} \triangleq \rho(\mathbf{u}) \tag{3.33}$$

where all the arguments have been suppressed for clarity, I is an identity matrix, and $\|\mathbf{P}\|_f = \left[\sum_{i=1}^{m}\sum_{j=1}^{m} p_{ij}^2\right]^{1/2}$

(2) The fixed-point iteration sequence $\{u^l\}$ generated by

$$\mathbf{u}^l = \rho\left(\mathbf{u}^{l-1}\right),\ l = 1,2,...,\forall \mathbf{u}^0 \in R^m \tag{3.34}$$

converges to $\mathbf{u}^*$

Proof: For part (1), we exploit the special structure of the $C_{\mathbf{u}}$ matrix and realize that the $\overline{\lambda}_i$ and $\underline{\lambda}_i$ for any $1 \le i \le m$, cannot be nonzero (positive) simultaneously by Eq.(3.31). Rewrite Eq. (3.31) as follow

$$\left((1-\varepsilon)B_{\mathbf{u}}^T W_V B_{\mathbf{u}} + \varepsilon W_{\mathbf{u}}\right)\mathbf{u} - (1-\varepsilon)B_{\mathbf{u}}^T W_V \overline{\mathbf{V}} = -C_{\mathbf{u}}{}^T \boldsymbol{\lambda} \tag{3.35}$$

We can prove Eq. (3.36) by taking into account three cases in Eq. (3.37).

$$\mathbf{u} = sat\left\{\mathbf{u} + \frac{C_{\mathbf{u}}{}^T \boldsymbol{\lambda}}{\|\mathbf{P}\|_f}\right\} \tag{3.36}$$

$$\begin{aligned} &1)\ \underline{u}_i \le u_i \le \overline{u}_i \quad &&=> \overline{\lambda}_i = \underline{\lambda}_i = 0 \\ &2)\ u_i \ge \overline{u}_i \quad &&=> \overline{\lambda}_i = 0 \left(\because u_i \ne \underline{u}_i\right) \\ &3)\ u_i \le \underline{u}_i \quad &&=> \underline{\lambda}_i = 0 \left(\because u_{ii} \ne \overline{u}\right) \end{aligned} \tag{3.37}$$

In case u_i exists in case 1), Lagrange multipliers are zero $\left(\underline{\lambda}_i = \overline{\lambda}_i = 0\right)$ to satisfy 2nd condition in Eq. (3.31). We categorize case 2) and 3) using Eq. (3.36) as follows.

$$\frac{C_{\mathbf{u}}{}^T \boldsymbol{\lambda}}{\|\mathbf{P}\|_f} + \mathbf{u} = \begin{bmatrix} 0 \\ \vdots \\ \dfrac{1\cdot\overline{\lambda}_i}{\|\mathbf{P}\|_f} + \overline{u}_i \\ \vdots \\ 0 \end{bmatrix} or \begin{bmatrix} 0 \\ \vdots \\ \dfrac{-1\cdot\underline{\lambda}_i}{\|\mathbf{P}\|_f} + \underline{u}_i \\ \vdots \\ 0 \end{bmatrix} \tag{3.38}$$

Since $\frac{1}{\|\mathbf{P}\|_f} > 0$ and $\overline{\lambda}_i \ge 0, \underline{\lambda}_i \ge 0$, one can see that $\overline{u}_i + \frac{1}{\|\mathbf{P}\|_f}\underline{\lambda}_i \ge \overline{u}_i$ and $-\frac{1}{\|\mathbf{P}\|_f}\overline{\lambda}_i + \underline{u}_i \le \underline{u}_i$. As shown in case 1) of Eq. (3.37), Eq. (3.36) is true under case 2) and 3) in Eq. (3.37).

Therefore, we have

$$\mathbf{u} = sat\left\{\mathbf{u} - \frac{1}{\|\mathbf{P}\|_f}\left[\left((1-\varepsilon)B_{\mathbf{u}}^T W_V B_{\mathbf{u}} + \varepsilon W_{\mathbf{u}}\right)\mathbf{u} - (1-\varepsilon)B_{\mathbf{u}}^T W_V \bar{\mathbf{V}}\right]\right\} = sat\left\{\mathbf{u} + \frac{C_{\mathbf{u}}{}^T \boldsymbol{\lambda}}{\|\mathbf{P}\|_f}\right\} \tag{3.39}$$

Any $\mathbf{u}$ that satisfies the necessary condition Eq. (3.31) also satisfies Eq. (3.33) for any $\|\mathbf{P}\|_f > 0$. When $\mathbf{P} > 0$, there is a unique optimal solution $\mathbf{u}^*$ that satisfies Eq. (3.31).

The fixed-point iteration to seek an optimal solution is as follow

$$\mathbf{u}_{l+1} = sat\left[\left\{I - \frac{\left((1-\varepsilon)B_{\mathbf{u}}^T W_V B_{\mathbf{u}} + \varepsilon W_{\mathbf{u}}\right)}{\|\mathbf{P}\|_f}\right\}\mathbf{u}_l + \frac{(1-\varepsilon)B_{\mathbf{u}}^T W_{\mathbf{u}} \bar{\mathbf{V}}}{\|\mathbf{P}\|_f}\right] \tag{3.40}$$

Eq. (3.40) is simplified by applying the definition $\mathbf{P} \equiv \left((1-\varepsilon)B_{\mathbf{u}}^T W_V B_{\mathbf{u}} + \varepsilon W_{\mathbf{u}}\right)$ as follows.

$$\mathbf{u}_{l+1} = sat\left[\left\{I - \eta_{\mathbf{P}}\mathbf{P}\right\}\mathbf{u}_l + \eta_{\mathbf{P}}(1-\varepsilon)B_{\mathbf{u}}^T \bar{\mathbf{V}}\right] \tag{3.41}$$

where $\eta_{\mathbf{P}} = 1/\|\mathbf{P}\|_F$

Furthermore, the fixed-point iteration $\mathbf{u}_{l+1} = \rho[\mathbf{u}_l],\ l = 1, 2, ...,\ \forall \mathbf{u}_l^{(0)} \in R^m$ converges to the unique solution of the QP problem for any initial guess $\mathbf{u}_l^{(0)}$.

To show contraction characteristics of $\rho(\mathbf{u})$, we define a new function as $\omega(\mathbf{u}) \equiv \mathbf{u} - \eta_{\mathbf{P}}\left(\mathbf{P}\mathbf{u} - (1-\varepsilon)B^T \bar{\mathbf{V}}\right)$

From the definition of the mapping $sat(\cdot)$, we have that for any $\mathbf{u}^i$ and $\mathbf{u}^j \in R^m$,

$$\begin{aligned} &\left\|sat(\mathbf{u}^i) - sat(\mathbf{u}^j)\right\| \le \left\|\omega(\mathbf{u}^i) - \omega(\mathbf{u}^j)\right\| = \left\|(I - \eta_{\mathbf{P}}\mathbf{P})(\mathbf{u}^i - \mathbf{u}^j)\right\| \\ &\le \left\|(I - \eta_{\mathbf{P}}\mathbf{P})\right\|\left\|(\mathbf{u}^i - \mathbf{u}^j)\right\| = \alpha\left\|(\mathbf{u}^i - \mathbf{u}^j)\right\| \end{aligned} \tag{3.42}$$

where $\|\ \|$ is the L_2 norm. Since $\eta_{\mathbf{P}} = 1/\|\mathbf{P}\|_F > 0$, the matrix $I - \eta_{\mathbf{P}}\mathbf{P}$ is positive definite and then

$$\begin{aligned} \alpha &= \left\|I - \eta_{\mathrm{p}}\mathbf{P}\right\| \\ \lambda_{\max}\left[I - \eta_{\mathrm{p}}\mathbf{P}\right] &= 1 - \eta_{\mathrm{p}}\mu_1 \end{aligned} \tag{3.43}$$

where $\lambda_{\max}(\cdot)$ denotes the largest eigenvalue of the matrix. μ_1 is the smallest eigenvalue of the matrix $\mathbf{P}$. We have $0 < \alpha < 1$. Therefore, $sat(\mathbf{u})$ is a global contraction mapping

in $\mathbf{R}^m$. Finally, the fixed-point equation has a unique solution and the fixed-point sequence converges to a solution in the form, $sat(\mathbf{u}^*) = \mathbf{u}^*$ (Wang, 2006).

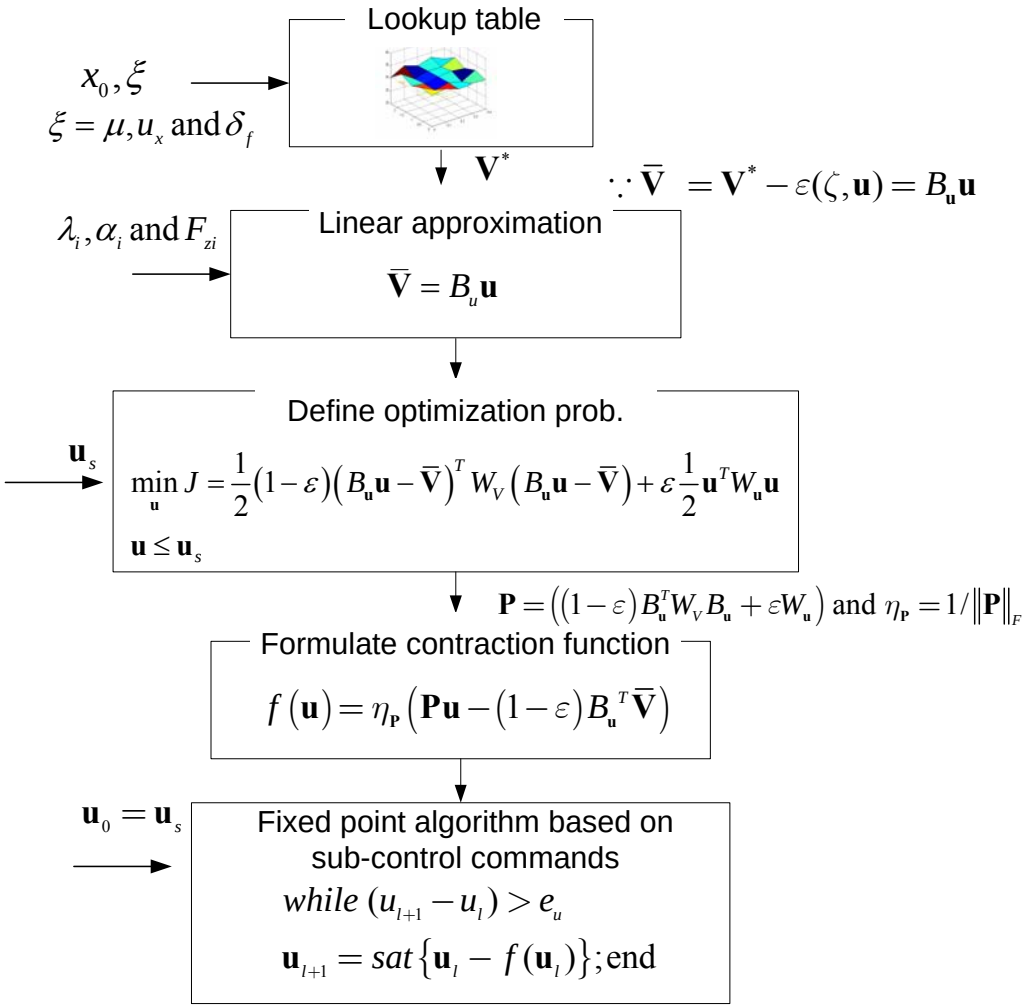

Figure 3.9 Flow chart of online coordination process

Figure 3.9 shows a flow chart to explain the overall procedure of the online control allocation for ICC. We begin with the current states, x_0 and environmental parameter, ξ. Virtual control commands, $\mathbf{V}^*$, which are the desired lateral force, F_y^* and the desired yaw moment, M_z^* are obtained by means of interpolation from the lookup table. Nonlinear relation between control inputs, $\mathbf{u}$ such as brake torques at each wheel, T_b and steering angle input, δ and the obtained virtual control commands, $\mathbf{V}^*$ are used for a new linear approximation, $\bar{\mathbf{V}} = B_u\mathbf{u}$ to formulate control allocation problem.

In this linear approximation approach, a tire model is used in conjunction with two DOF vehicle and wheel dynamics model, which is to be explained in Section 3.2.6. The CA problem is re-casted as an optimization problem with inequality constraints, in which sub-control commands, $\mathbf{u}_s$ are upper bounds for the CA problem. We define a new parameter, $\mathbf{P} = (1-\varepsilon) B_{\mathbf{u}}^T W_V B_{\mathbf{u}} + \varepsilon W_{\mathbf{u}}$ in order to transform the equation for solving the constrained optimization problem to a contraction function. Subsequently, it is possible to compute iteratively the optimal control input using the fixed-point iteration method until given convergence criteria, e_u is satisfied. Control commands form the sub-control systems are used as initial guess, $\mathbf{u}_0$ for the iterations.

The FP iteration method is a gradient searching scheme. Therefore, the convergence rate of the FP algorithm depends heavily on the initial guess and thus selection of good initial guess is critical to effective searching for optimal solution. In our application, the sub-system control commands are applied as initial points for the FP iteration method. This is based on the assumption that sub-control commands are close to the optimal solutions. Search starting from sub-control commands can guarantees equal or better performance than the performance of uncoordinated control systems. The gradient search characteristic of the FP method is suitable for the online CA, where the optimization approach uses the candidates for good initial point. This can lead to reduction of the online computation load.

3.2.6 LINEAR APPROXIMATION FOR CONTROL ALLOCATION PROBLEM

The virtual commands, V* in a control allocation problems are in reality nonlinear functions, $\mathbf{V}^* = g(\zeta, \mathbf{u})$ of the control inputs, u and parameter, ζ. However, control allocation algorithms use the assumption that a linear relationship exists between the virtual control command and the control inputs. A linearization approach to deal with the nonlinearity is proposed for improving the performance of control allocation system (Doman and Oppenheimer, 2002). Figure 3.10 shows a one-dimensional representation

of linearization of nonlinear function at sampling time, k. Accuracy of the linear approximation of the relationship between virtual control and control element vector is based on a sufficiently small sampling time. The local slope and an intercept term are used to adjust virtual control command as follows

$$\begin{aligned} \mathbf{V}_{k-1}^{*} &\approx B_{\mathbf{u}(k-1)}\mathbf{u}_{k-1} + \varepsilon(\zeta, \mathbf{u}_{k-1}) \\ \bar{\mathbf{V}}_{k-1} &= \mathbf{V}_{k-1}^{*} - \varepsilon(\zeta, \mathbf{u}_{k-1}) = B_{\mathbf{u}(k-1)}\mathbf{u}_{k-1} \end{aligned} \tag{3.44}$$

In a discrete-time implementation, one would use the following

$$\bar{\mathbf{V}}_{k} \equiv \mathbf{V}_{k}^{*} - \varepsilon(\zeta, \mathbf{u}_{k-1}) = B_{\mathbf{u}(k-1)}\mathbf{u}_{k} \tag{3.45}$$

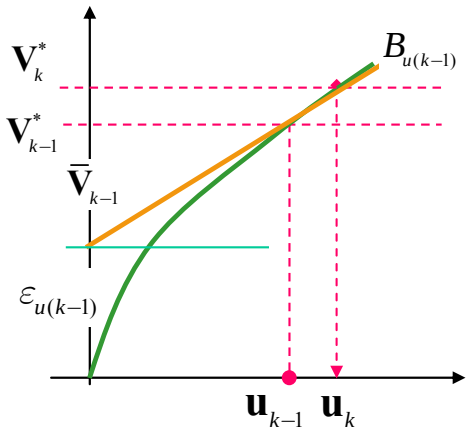

Figure 3.10 One dimensional example of linearization for nonlinear control allocation problem.

In this CA problem, the control inputs include braking torque, T_b and rear steer, δ_r. The control effective matrix $\mathbf{B}_{\mathbf{u}(k-1)}$ is calculated and updated with estimated tire force using tire longitudinal slip ratio, λ, lateral slip angle α, vertical load, F_z and road friction, μ. The wheel dynamics are

$$r_w \cdot F_x = J\dot{\omega} + T_b \tag{3.46}$$

where a linear tire force model is used with $C_\lambda = \hat{F}_x(\lambda, \alpha, F_z, \mu)/\lambda$ and $\lambda = \left(u_x - r_w\omega\right)/u_x$.

Applying $\lambda = 1 - r_w\omega/u_x = 1 - c_\omega\omega$. , then Eq. (3.46) can be rewritten as

$$r_w \cdot C_\lambda\lambda = -\frac{J}{c_\omega}\dot{\lambda} + T_b \tag{3.47}$$

and finally,

$$r_w \cdot F_x = -\frac{J}{c_\omega}\frac{\dot{F}_x}{C_\lambda} + T_b \tag{3.48}$$

A discrete model can be derived by applying Euler approximation to Eq. (3.48) and the estimated longitudinal force for the next sampling step, $\hat{F}_x(k+1)$ is calculated from

$$\hat{F}_x(k+1) = \varepsilon_{F_x} + \frac{T_b(k)}{\eta_{Fx}} \tag{3.49}$$

where $\eta_{Fx} = \dfrac{J}{c_\omega T_s C_\lambda}$ and $\varepsilon_{Fxi} = \left(1 - \dfrac{r_w}{\eta_{F_x}}\right)\hat{F}_{xi}(k)$

Similarly, the estimated lateral force, is calculated from side slip angle of tire, α. The tire side slip angle is also computed from the rear steering angle, δ_r, and vehicle parameters, *b* and states as follow

$$\alpha(k) = \delta_r(k) - \tan^{-1}\left(\frac{v_y - rb}{u_x}\right) \tag{3.50}$$

The side slip angle is then applied to calculate the estimated lateral force at the next sampling step

$$\hat{F}_y(k+1) = C_\alpha(k)\cdot\left(-\delta_r(k) + \varepsilon_\alpha\right) \tag{3.51}$$

where $C_\alpha = \hat{F}_y(\lambda, \alpha, F_z, \mu)/\alpha$ and $\varepsilon_\alpha = \tan^{-1}\left(\dfrac{v_y - rb}{u_x}\right)$

The virtual control commands relate to tire forces through the relations

$$F_y = \sum_{i=1}^{4} F_{yi} \tag{3.52}$$

$$M_z = t_{wf}(F_{x1} - F_{x2}) + t_{wr}(F_{x3} - F_{x4}) + a(F_{y1} + F_{y2}) - b(F_{y3} + F_{y4}) \tag{3.53}$$

where t_{wf} and t_{wr} are the track width at the front and rear axle, respectively.

The control allocation problem in the ICC online coordination is then to minimize $\left\|\bar{\mathbf{V}} - \mathbf{B_u u}\right\|$ by applying braking to selected wheels and steering steer angle. In case single wheel braking, T_{b1} and rear wheel steer, δ_r are used, we can have the CA problem as shown in Eq (3.54).

$$\bar{\mathbf{V}} = \begin{bmatrix} F_y^* - \hat{F}_{y1} - \hat{F}_{y2} + 2C_\alpha \varepsilon_\alpha \\ M_z^* - a\left(\hat{F}_{y1} + \hat{F}_{y2}\right) - 2bC_\alpha \varepsilon_\alpha - t_w \varepsilon_{F_x} \end{bmatrix}$$
$$\mathbf{B}_\mathbf{u} = \begin{bmatrix} 0 & 2C_\alpha \\ t_w / \eta_{F_x} & -2bC_\alpha \end{bmatrix}, \mathbf{u} = \begin{bmatrix} T_{b1} \\ -\delta_r \end{bmatrix} \tag{3.54}$$

CA problems based on two different combinations of control inputs; four wheel braking with rear wheel steer and one wheel braking with front wheel steer are shown in Table 3-6.

Table 3-6 Control allocation problems for ICC coordination

Four wheel braking & rear wheel steer	$\bar{\mathbf{V}} = \begin{bmatrix} F_y^* - \hat{F}_{y1} - \hat{F}_{y2} + 2C_\alpha \varepsilon_\alpha \\ M_z^* - t_w\left(\varepsilon_{F_{x1}} + \varepsilon_{F_{x3}}\right) + t_w\left(\varepsilon_{F_{x2}} + \varepsilon_{F_{x4}}\right) - a\left(\hat{F}_{y1} + \hat{F}_{y2}\right) + 2bC_\alpha \varepsilon_\alpha \end{bmatrix}$ $\mathbf{B}_\mathbf{u} = \begin{bmatrix} 0 & 0 & 0 & 0 & 2C_\alpha \\ t_w / \eta_{F_{x1}} & t_w / \eta_{F_{x3}} & -t_w / \eta_{F_{x2}} & -t_w / \eta_{F_{x4}} & -2bC_\alpha \end{bmatrix}$ $\mathbf{u} = \begin{bmatrix} T_{b1} & T_{b2} & T_{b3} & T_{b4} & -\delta_r \end{bmatrix}^T$
One wheel braking & front wheel steer	$\bar{\mathbf{V}} = \begin{bmatrix} F_y^* - \hat{F}_{y3} - \hat{F}_{y4} + 2C_\alpha \varepsilon_\alpha \\ M_z^* + b\left(\hat{F}_{y3} + \hat{F}_{y4}\right) - 2aC_\alpha \varepsilon_\alpha - t_w \varepsilon_{F_{x1}} \end{bmatrix}$ $\mathbf{B}_\mathbf{u} = \begin{bmatrix} 0 & 2C_\alpha \\ t_w / \eta_{F_{x1}} & 2aC_\alpha \end{bmatrix}, \mathbf{u} = \begin{bmatrix} T_{b1} \\ -\delta_f \end{bmatrix}$

3.2.7 COMPUTATIONAL EFFICIENCY OF FIXED POINT ITERATION METHOD

In the literature, the fixed-point algorithm has been compared against several QP algorithms (Lu, 1996). In this research, independent verification is conducted to study the computation efficiency and effectiveness. A simple QP example is defined as follows

$$\min_{\mathbf{u}} J = \frac{1}{2}(1-\varepsilon)\left(B_\mathbf{u}\mathbf{u} - V^*\right)^T W_V \left(B_\mathbf{u}\mathbf{u} - V^*\right) + \varepsilon \frac{1}{2}\mathbf{u}^T W_\mathbf{u} \mathbf{u}$$
$$s.t.\ C_\mathbf{u}\mathbf{u} \le d_\mathbf{u} \tag{3.55}$$

$$\text{where } \varepsilon = 0.0, B_{\mathbf{u}} = \begin{bmatrix} 1.5 & 0.5 \end{bmatrix}, V^* = 1, W_V = 1, W_{\mathbf{u}} = \begin{bmatrix} 1 & 0 \\ 0 & 1 \end{bmatrix}$$

$$C_{\mathbf{u}} = \begin{bmatrix} 1 & 0 \\ -1 & 0 \\ 0 & 1 \\ 0 & -1 \end{bmatrix}, d_{\mathbf{u}} = \begin{bmatrix} 1 \\ 0 \\ 1 \\ 0 \end{bmatrix} \text{and} \, u_0 = \begin{bmatrix} 1 + rand(1) \\ 0.9 + rand(1) \end{bmatrix}$$

Random initial points for CA problem are sampled to test the robust performance of the fixed-point iteration method. Simulation results in

Figure 3.11 show that elapsed time of the FP algorithm is typically 35 times faster than that of Matlab QP solver (quadprog()) based on the active-set method. Even though the convergence error of FP is higher than that of Matlab solver, FP algorithms satisfy the convergence tolerance, T_J=5% of final value --which can be tightened by the designer (see Figure 3.12).

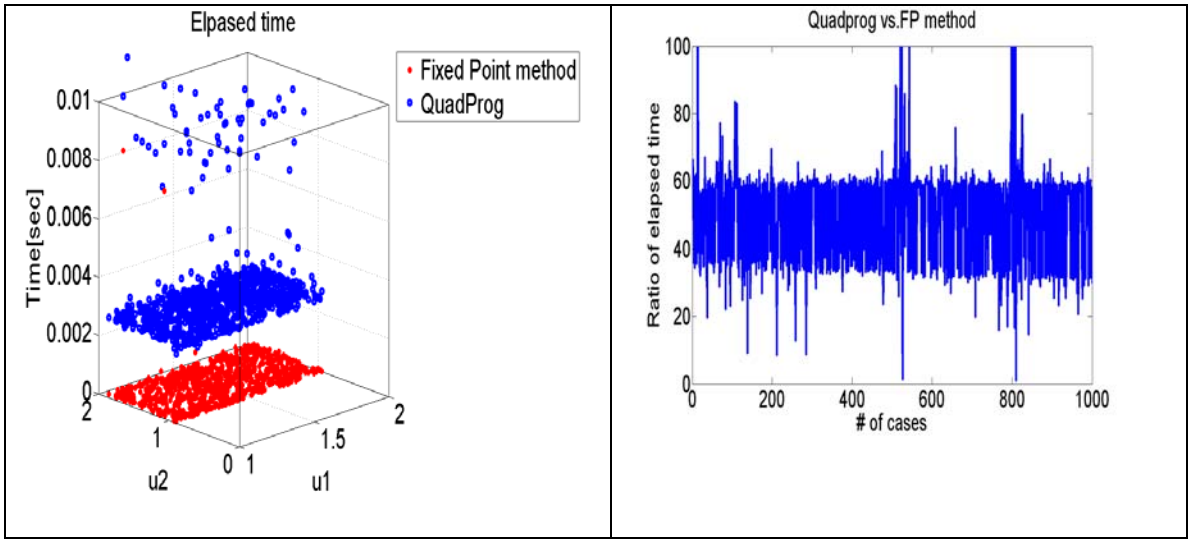

Figure 3.11 Comparison of elapsed time between two optimization methods

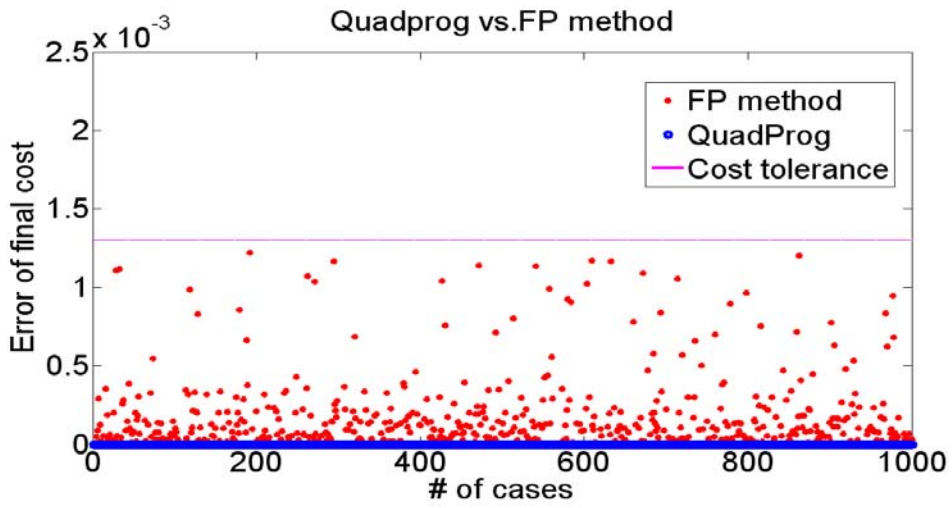

Figure 3.12 Comparison of convergence error between two optimization methods

3.3 SIMULATION RESULTS

The vehicle responses with ICC (RWS and ESC) are compared with responses of vehicles with uncoordinated systems. The ESC is designed on the basis of a sliding mode control scheme considering yaw, side slip and roll control of the vehicle dynamics, explained in Section 2.2.2. The RWS is based on a feed-forward compensation approach focusing on stability under high-speed condition (see Section 2.2.3). Both control system algorithms demonstrate stable performances under NHTSA sine-with-dwell test conditions, as shown in Figure 3.13 It is apparent that both RWS and ESC contribute positively to stabilization of vehicle motion whether they are installed together or individually, whereas uncontrolled vehicle loses stability under that maneuver (see Figure 3.14).

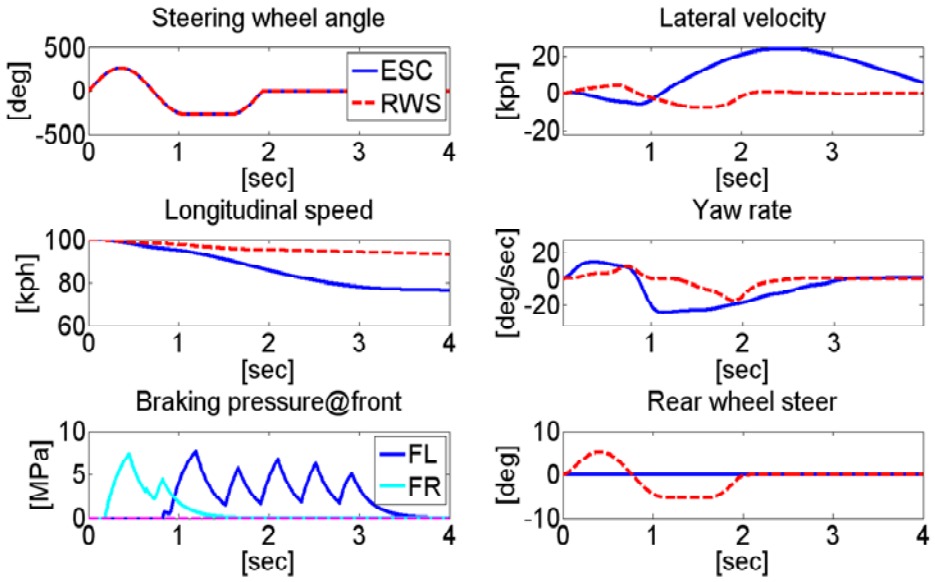

Figure 3.13 0.7[Hz] Sine-with-dwell tests of RWS and ESC @ 100[kph] and μ=0.4
($\max\left|r^{\mathrm{ESC}}\right|$:19[deg/s], $\max\left|r^{\mathrm{RWS}}\right|$:18[deg/s])

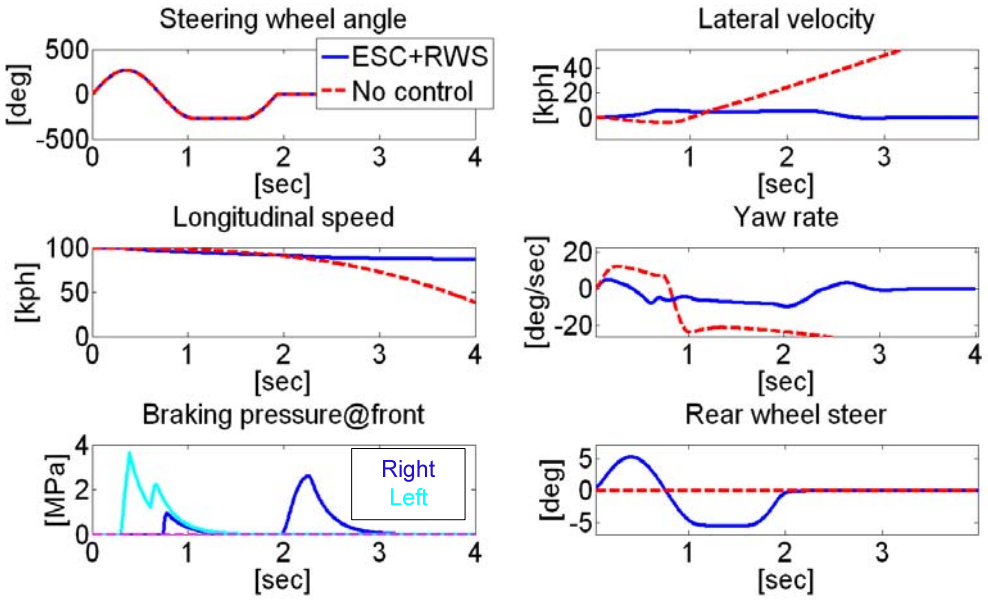

Figure 3.14 Sine-with-dwell tests of uncoordinated ESC plus RWS and no control system @ 100[kph] and μ=0.4

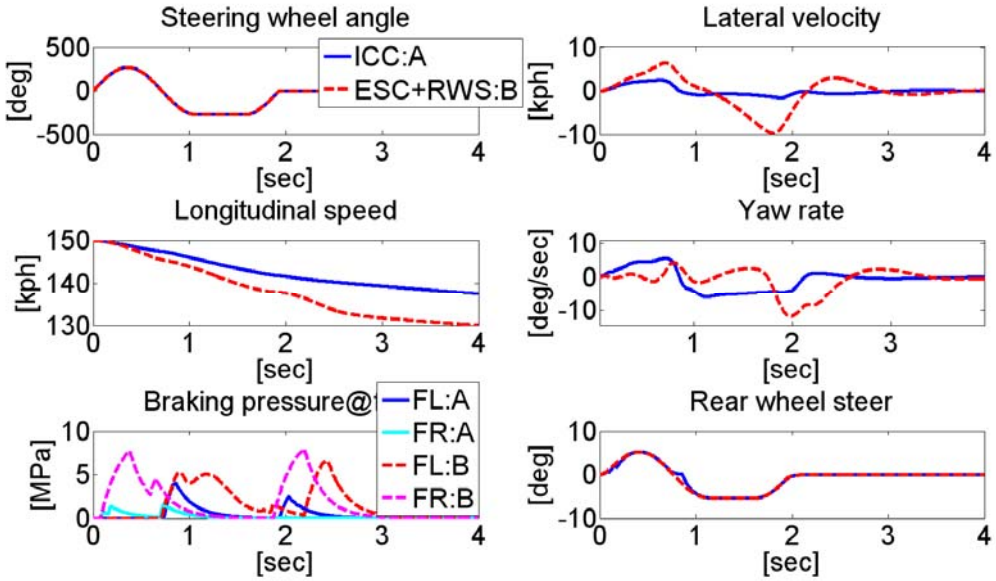

Figure 3.15 Tests of ICC and uncoordinated ESC plus RWS ;0.7[Hz] sine-with-dwell test @ μ=0.4 ($\max\left|r^{\text{cord}}\right|$ =4[deg/s], $\max\left|r^{\text{uncord}}\right|$ =9.9[deg/s])

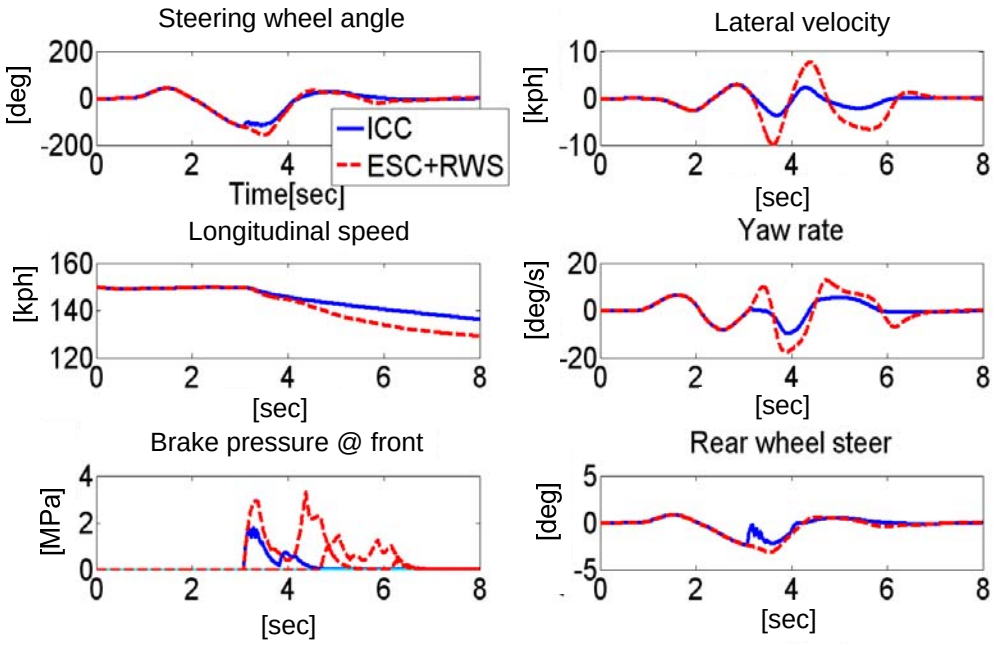

Figure 3.16 Closed-loop double lane change test@ μ=0.4 ($\max\left|r^{\text{cord}}\right|$ =12[deg/s], $\max\left|r^{\text{uncord}}\right|$ =18[deg/s])

As shown in Figure 3.15, the vehicle response with ICC shows better performance than the vehicle with uncoordinated ESC plus RWS. When ESC and RWS are both installed but uncoordinated, the vehicle performance is inconsistent; it may be better than cases with only a single chassis control system even though an uncoordinated system makes the vehicle unstable, as shown in Figure 2.17 (p 38).

Figure 3.16 shows that ICC achieves better performance than uncoordinated case under a closed-loop simulation using a human driver model. It is noteworthy that the final control actions from ESC and RWS are reduced through coordination. Comparison of the maximum yaw rates of the ICC case and the ESC case shows that the peak value of the ICC system ($\max\left|r^{\text{cord}}\right|$ =8[deg/s]) is 40% smaller than that of the ESC-system ($\max\left|r^{\text{ESC}}\right|$:15[deg/s]). More importantly, this improved performance is achieved with reduced braking.

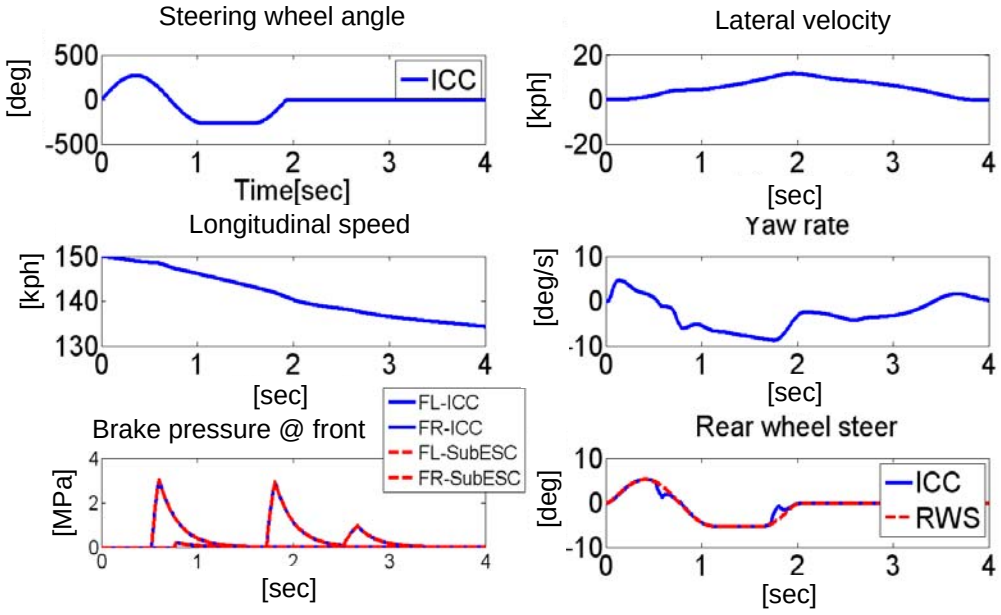

Figure 3.17 Comparison between original control inputs and modified control inputs in the coordinator of ICC

In Figure 3.17, we can see how sub-system control inputs are modified by the online control module. ESC commands are maintained while RWS commands are reduced.

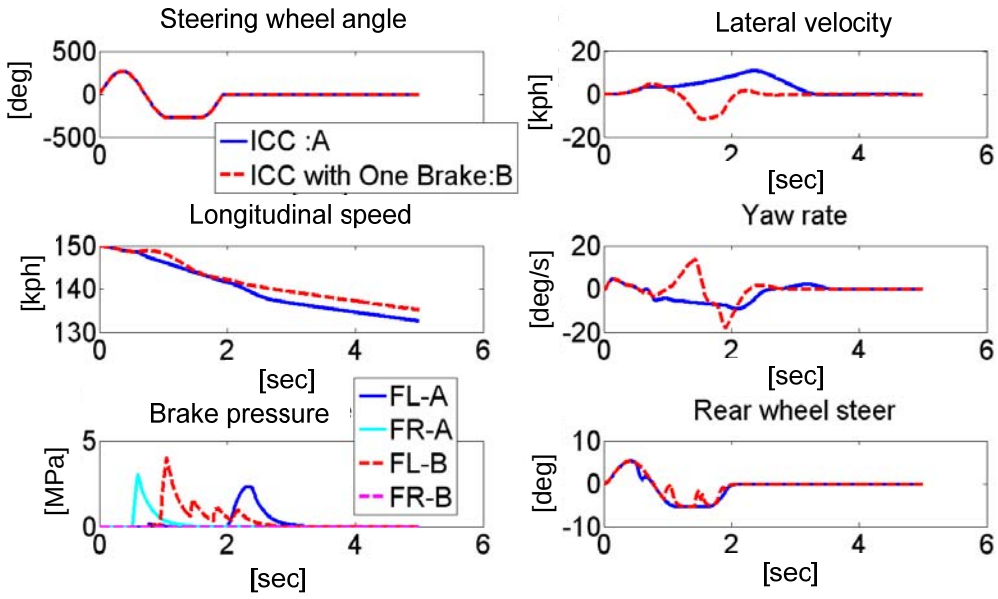

Figure 3.18 Comparison between ICC with ICC (FR brake actuator failed) under sine-with-dwell tests @ 150[kph] and μ=0.4 ($\max|r|$ =10[deg/s], $\max|r^{fail}|$ =18[deg/s])

Figure 3.18 shows that the coordinator is able to deal with the situation when one brake actuator fails. Through online control allocation, only one-wheel brake and rear wheel steering are needed to stabilize the vehicle. The performance in the actuator failure case is inferior to that of the ICC case without actuator failure, showing that the maximum yaw rate in the actuator failure case ($\max|r^{fail}|$ =18 [deg/s]) is 80 % larger than that of the original system ($\max|r|$: 10 [deg/s]).

The offline MPC approach is based on fixed model parameters including mass and states such as longitudinal speed and friction. Therefore, we must investigate the robustness of the ICC coordination control under model-plant mismatch. The following robustness studies show how the controller deals with road friction error and mass change. Under the added mass conditions (see Figure 3.19) and road-friction error (see

Figure 3.20), the proposed ICC system exhibits robust performance even though little difference between the yaw rate responses of the two cases (ICC and ICC including parameter uncertainty) does exist.

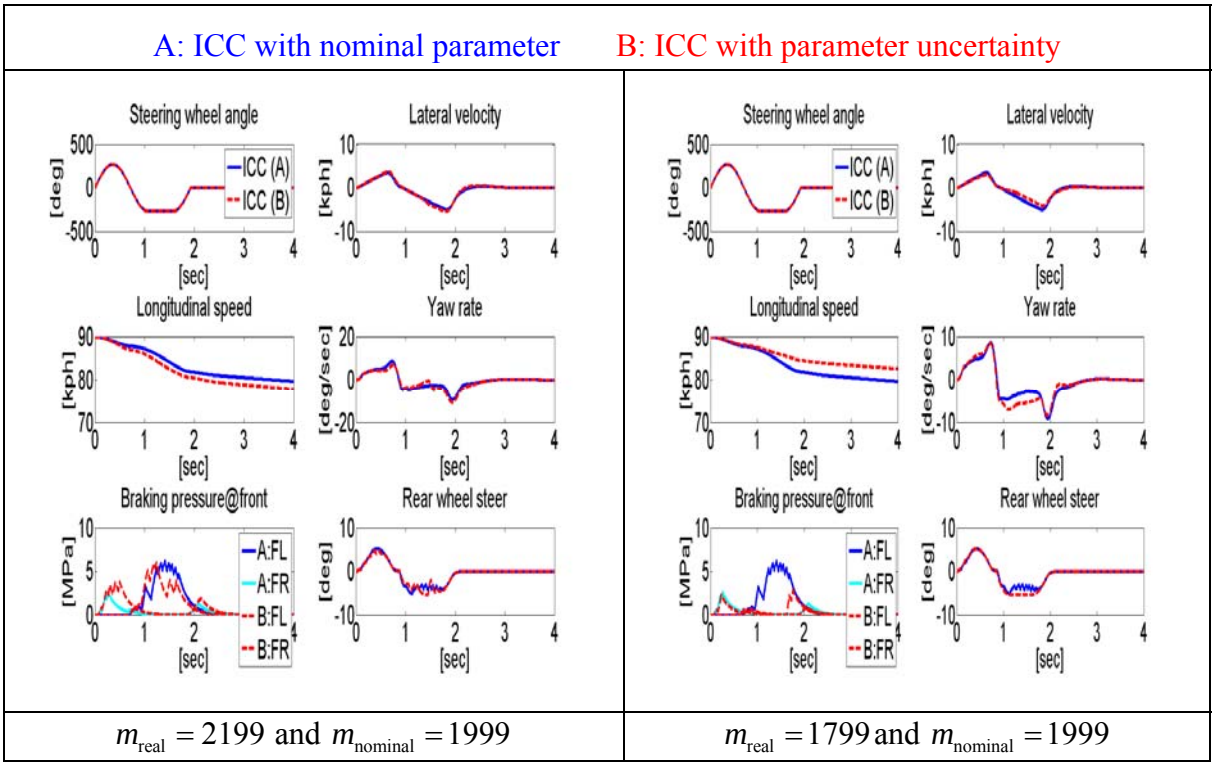

Figure 3.19 Responses of the proposed ICC under mass uncertainty conditions

A: ICC with nominal parameter	B: ICC with parameter uncertainty
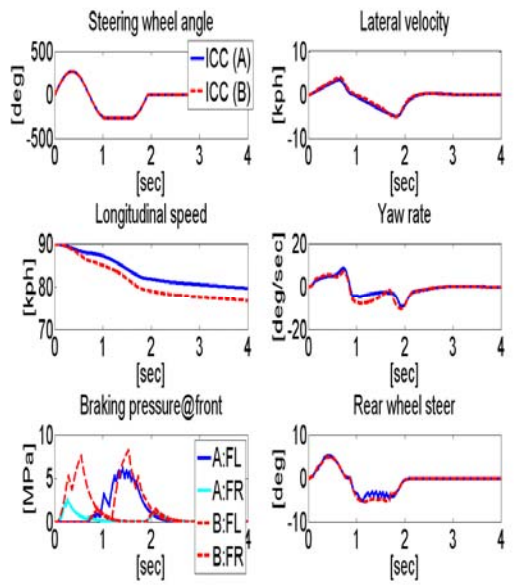	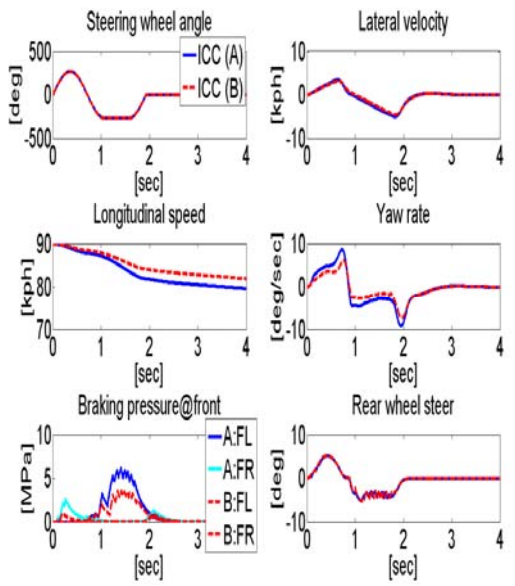
$\mu_{real} = 0.3$ and $\mu_{nominal} = 0.4$	$\mu_{real} = 0.5$ and $\mu_{nominal} = 0.4$

Figure 3.20 Responses of the proposed ICC under friction uncertainty conditions

ICC responses can be adjusted through modification of the weighting matrices in the online CA. Figure 3.21 show that an increase of weighting factor for the lateral velocity minimization improves the performance of ICC with minimal braking intervention. The online approach of coordinator has flexibility in the ICC systems because it permits adjustment to the weighting factors.

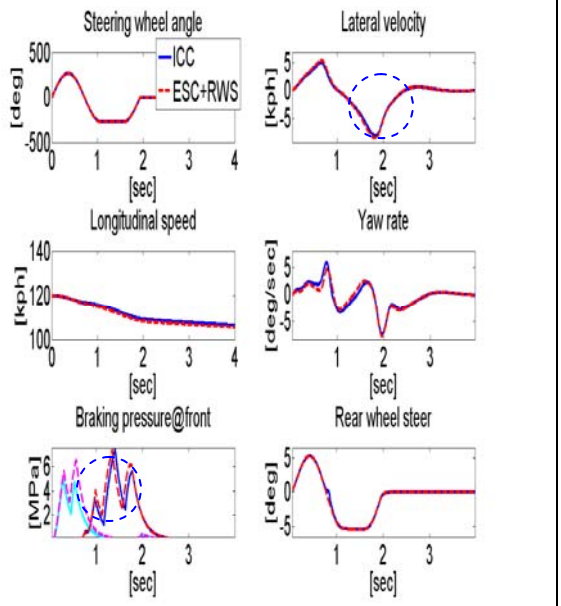

$$W_V = \begin{bmatrix} 0.1 & 0 \\ 0 & 1 \end{bmatrix}$$

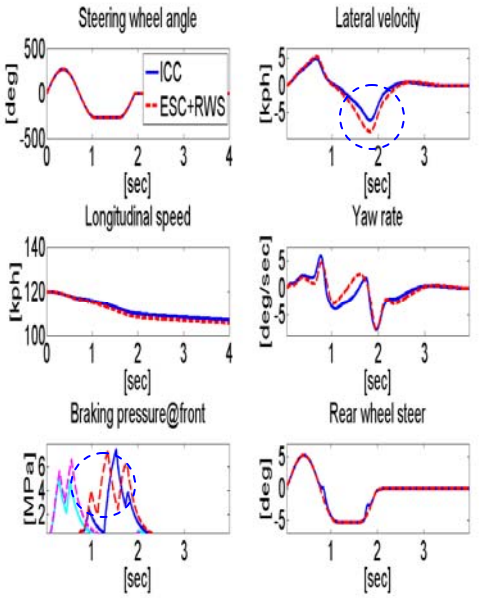

$$W_V = \begin{bmatrix} 1 & 0 \\ 0 & 1 \end{bmatrix}$$

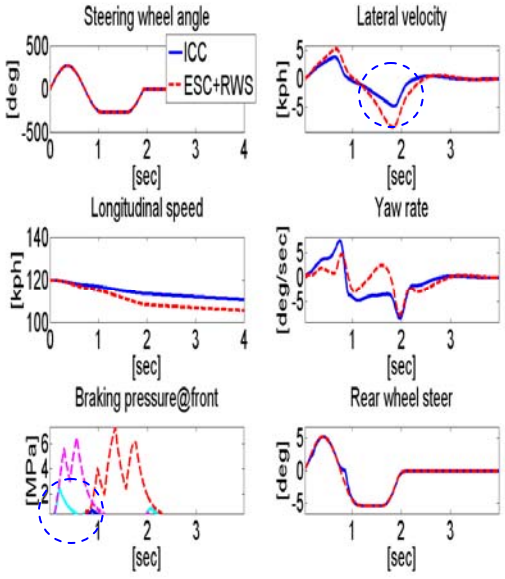

$$W_V = \begin{bmatrix} 2 & 0 \\ 0 & 1 \end{bmatrix}$$

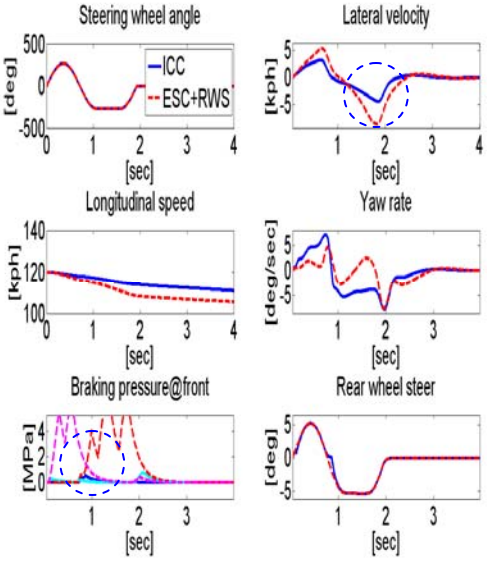

$$W_V = \begin{bmatrix} 5 & 0 \\ 0 & 1 \end{bmatrix}$$

Figure 3.21 ICC responses according to different weighting matrices of CA scheme

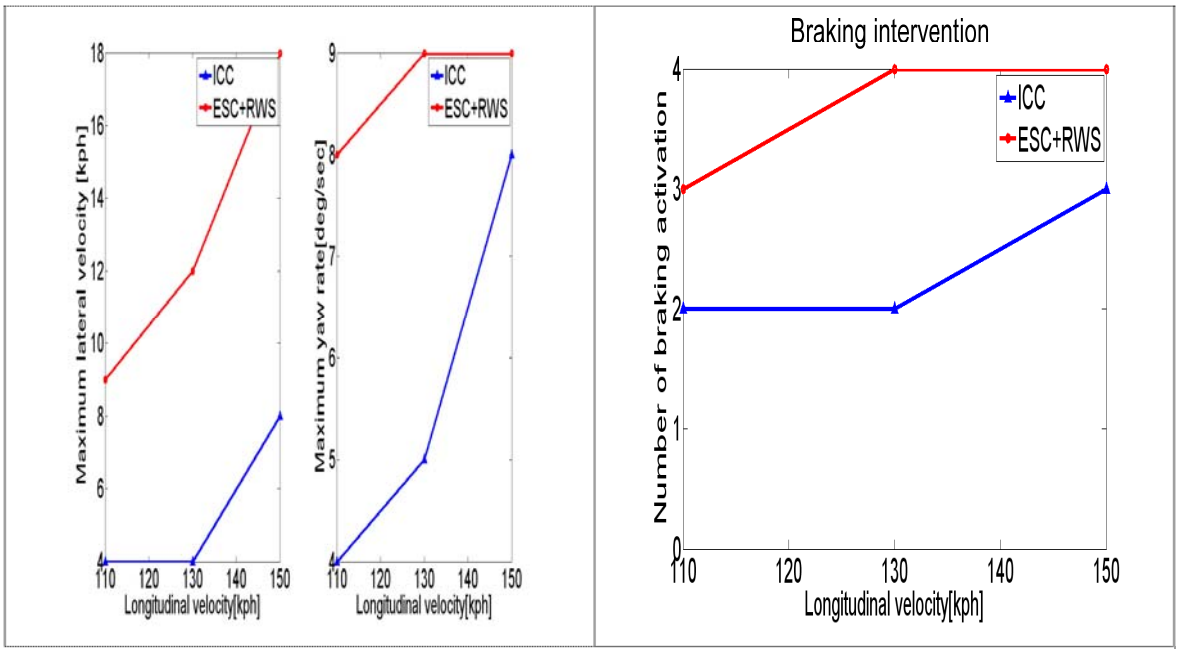

Figure 3.22 Comparison between ICC and uncoordinated ESC and RWS: 0.7[Hz] sine-with-dwell test @ μ=0.4 under different longitudinal speeds.

Figure 3.22 shows that the maximum values of yaw rate and lateral velocity of the proposed ICC are always smaller than those of the uncoordinated system while the number of braking intervention is lower. The low number of the braking interventions means that discomfort delivered to the driver can be minimized and the vehicle can maintain the speed intended by the driver. The results in Figure 3.22 show that the proposed coordinator can enhance the vehicle performance in the various speed ranges by eliminating redundancy due to uncoordinated actuator operation. Through various simulation results shown above, the effectiveness and robustness of the coordination for decentralized ICC design are investigated.

3.4 SUMMARY

To develop a new ICC system, the benefits and limitations of various integrated chassis control systems presented are identified in the current literature. Additionally, these ICC systems can be categorized as centralized and decentralized approaches to

determine the feasibility of implementation under the current business practice. Based on the literature, the decoupling control can be a potentially suitable decentralized approach according to system characteristics. A relative gain array analysis is conducted to investigate the feasibility of decoupling control of ICC systems. Our results showed that a decoupling control design is not suitable for ICC system. Therefore, a new decentralized design of ICC should coordinate control commands from the sub-control systems.

For the most effective coordination of sub-control command and avoidance of over control, the coordination strategy of saturating sub-control commands is proposed. This strategy is explained in terms of the tire ellipse, and its feasibility is demonstrated through a linear quadratic regulator example.

This research focused on a coordinator that would be computationally efficient enough for practical implementation. A hybrid approach combining offline model predictive control (MPC) and a fixed-point iteration based online control allocation (CA) is used. The MPC method is applied to compute the optimal virtual control commands, and the CA is employed for real-time reconfiguration and actuator management.

The effectiveness of the offline MPC is verified by comparing results with those obtained from online MPC applications. The computation efficiency and effectiveness of online CA based on a fixed-point iteration method assessed through a comparison with the representative optimization method, quadprog(), in a simple CA example. In the online CA process, sub-control commands are used as initial point and as upper bounds of the CA optimization scheme.

A linearization of the nonlinear relationship between control demands (steering input and braking torque) and virtual control commands is proposed for enhancing the performance of the CA approach. A linear approximation for the different combinations among four braking torque commands with front or rear steering inputs is analyzed.

The effectiveness of the decentralized ICC is verified through the CarSim simulations. The simulation results show that the coordinator achieves improved stability while using reduced control inputs. Under representative uncertainties, such as increased vehicle weight and varied road friction, the ICC demonstrates diminished performance but maintains vehicle stability even under the challenging maneuvers such as NHTSA tests. It is also demonstrated that when we have actuator failures, the online CA approach uses the remaining actuators and is still able to maintain a high level of performance.

CHAPTER 4

EVALUATION OF INTEGRATED CHASSIS CONTROL SYSTEMS

4.1 CONVENTIONAL EVALUATION METHODS OF CHASSIS CONTROL SYSTEMS

Electronic Stability Control (ESC), one of the most promising systems for enhancing safety systems, is used in ICC. Agencies/companies have developed methods to evaluate its performance. An effort to develop a way to objectively assess the effectiveness of ESC on the test track was recently undertaken by the National Highway Traffic Administration (NHTSA), which has developed and executed numerous official vehicle tests (Forkenbrock et al., 2005). Automotive companies have also developed new evaluation methods to explore levels of performance in handling stability and responsiveness achieved by ESC (Bedner et al., 2007). These ESC evaluation studies can provide useful information for ICC evaluation research. ESC evaluation researches are investigated as follows.

The objective of NHTSA's initial approach (Forkenbrock et al., 2005) is to isolate a small number of maneuvers capable of demonstrating the effectiveness of ESC. Using five vehicles equipped with ESC, NHTSA applied three groups of tests. They found that a quantitative description of spinout is necessary as the termination criterion to evaluate the ESC's performance. In a recent ESC study by NHTSA (NHTSA, 2007a), 0.7[Hz] sine-with-dwell tests are proposed. These tests primarily assessed ESC effectiveness in mitigating vehicle over-steer. The over-steering and under-steering concepts are illustrated in Figure 4.1, which shows vehicle handling and ESC intervention. The criteria of the tests are based on lateral stability and responsiveness (see Figure 4.2, Eq. (4.1) and (4.2)). The stability is measured on the basis of how quickly the vehicle stops

yawing after the steering angle is returned to zero. The quantitative stability criteria require that the vehicle yaw rate decrease to no more than 35 percent of the peak value after one second and that it continue to drop to no more than 20 percent after 1.75 seconds, as shown in Eq. (4.1). Since a vehicle that simply responds minimally to steering commands could meet the stability criteria, a minimum responsiveness criterion is imposed to the same test. Eq. (4.2) states that all passenger cars reached the proposed limit of 1.83 [m] after 1.07 [sec] while vehicles larger than 3,500 [kg] have a different limit, 1.52 [m].

The NHTSA acknowledges that the sine-with-dwell tests are not adequate as an objective performance test for the under-steer mitigation or rollover prevention. Therefore NHTSA has continued to develop better standard tests for ESC (NHTSA, 2007b).

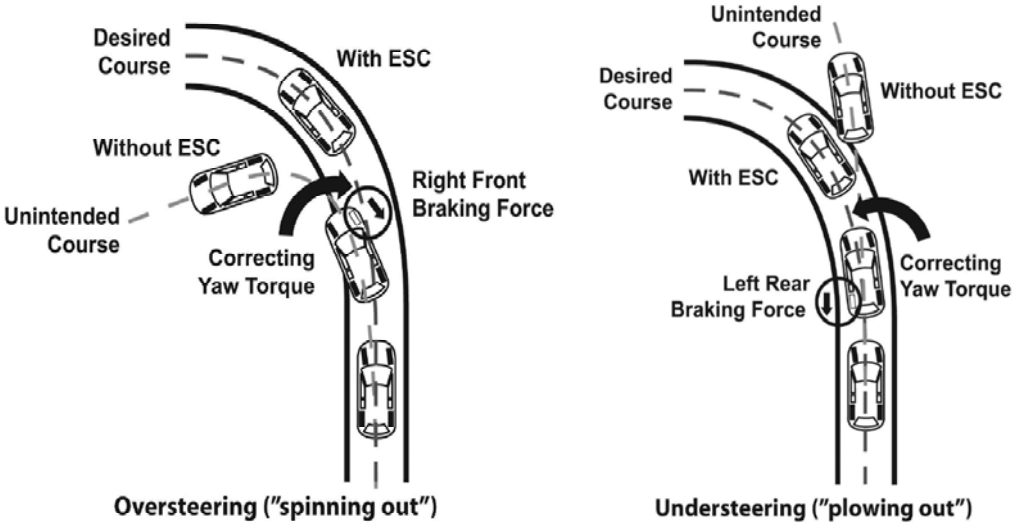

Figure 4.1 ESC intervention for over-steering and under-steering (NHTSA, 2007b)

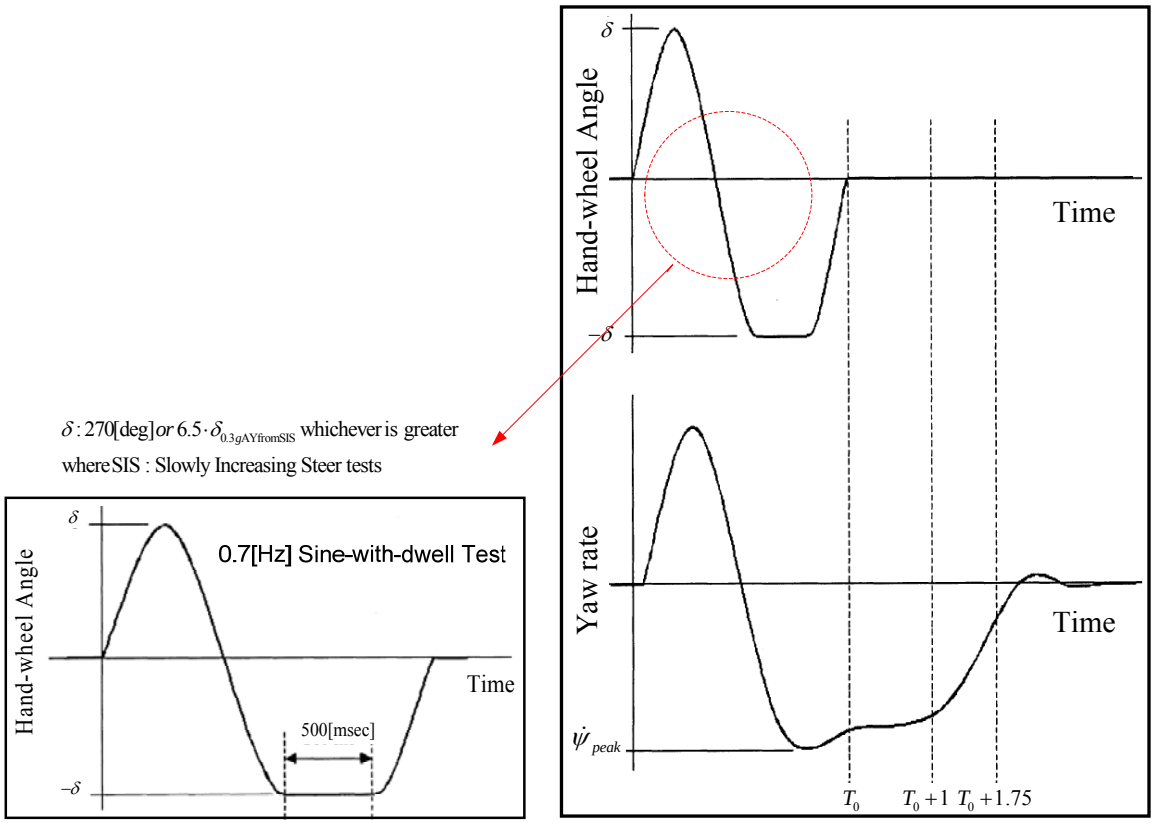

Figure 4.2 Sine-with-dwell maneuver and steering wheel position and yaw velocity information used to assess lateral stability (NHTSA, 2007b)

Lateral stability criteria

$$\begin{cases} \dfrac{\dot{\psi}_{(t_0+1.00)}}{\dot{\psi}_{peak}} \times 100 \le 35\% \quad \text{(criterion \#1), and} \\ \dfrac{\dot{\psi}_{(t_0+1.75)}}{\dot{\psi}_{peak}} \times 100 \le 20\% \quad \text{(criterion \#2)} \end{cases}$$

where (4.1)

t_0 : the time to complete the steering input, $\dot{\psi}$: the first local peak yaw rate

Responsiveness criteria

$$\textit{Lateral displacement } y_d = \iint a_{yCG}\, dt$$

$$y_d(t_{res}) \ge 1.83 \text{ m (6 feet) } @\text{GVWR} \le 3{,}500\text{kg (7,716 lb)}$$

$$y_d(t_{res}) \ge 1.52 \text{ m (5 feet) } @\text{GVWR} \ge 3{,}500 \text{ kg (7,716 lb)} \quad (4.2)$$

where

a_{yCG} : lateral acceleration at the vehicle center of gravity *and* $t_{res} = 1.07$[sec]

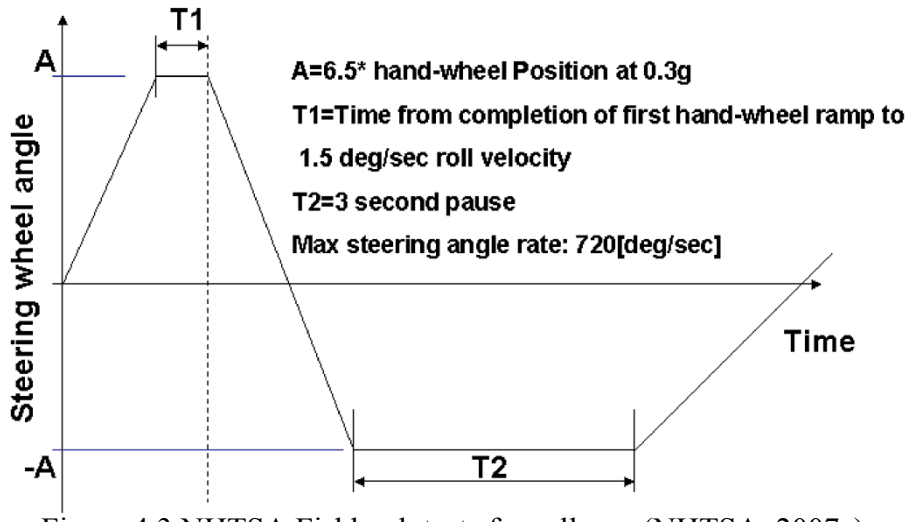

Figure 4.3 NHTSA Fishhook tests for rollover (NHTSA, 2007a)

NHTSA started to move away from one-size-fits-all tests toward customized tests in recent years. As an example, Figure 4.3 shows the fishhook test maneuver defined by NHTSA for rollover propensity test of the vehicle. The hand-wheel steering magnitude 'A', and dwell time 'T1' are selected based on vehicle response and thus are different for each vehicle. This customization is necessary to ensure the test is somewhat normalized. However, vehicles with low steering ratio or high performance tires are not penalized inadvertently. More customization is necessary, to accommodate on the effects of newly developed smart control systems.

One major supplier, Delphi Corporation, performed a study of advanced chassis control systems and their stability-relevant performance (Bedner et al., 2007). It explores the trade-off between yaw rate, sideslip, and roll motion of a vehicle, and their relationships to handling stability and handling responsiveness. This trade-off exists because the stability and responsiveness are opposing phenomena that must be balanced, as shown in the NHTSA studies. Fast response in the transient requires higher control actions, which may be detrimental for stability. J-turn maneuver on slippery roads is used to investigate vehicle-level effects under different tuning modes (mode A: ESC off, mode B: balanced yaw rate & side slip control, mode C: aggressive yaw rate control,

mode D: tight side slip control) of Delphi's own ESC. Researchers identified measurable variables to quantify stability and responsiveness, and the appropriate level of ESC tuning. Vehicle path (or turn radius), yaw rate, and lateral acceleration are indicators of responsiveness, while orientation (or sideslip angle) and roll angle are indicators of stability.

Despite these efforts, we still face a major hurdle: experimental evaluations are, by nature, expensive, time-consuming and not easily repeatable because of the large number of uncontrolled variables and parameters such as tire wear, road friction and driver variation.

4.2 WORST-CASE SCENARIO EVALUATION (WCSE)

The worst-case scenario evaluation (WCSE) process is a possible alternative to the current experiment-based evaluation process for future vehicles that may or may not be equipped with active safety devices. The simulation-based WCSE eliminates the effect of human uncertainties due to various drivers' styles and experiences. The WCSE method identifies weaknesses of a vehicle and safety systems through extensive numerical search. In addition, it allows a wide variety of scenarios, including those that are not feasible or too costly in field tests. Through extensive numerical searches, WCSE challenges the vehicle with a large set of demanding maneuvers and can be a valuable tool in the development of active safety systems. As the one for evaluation by the WCSE here rollover prevention of chassis control systems is selected because its importance has been emphasized as a major vehicle safety performance and actively investigated among various functionalities of chassis control systems (NHTSA, 2007a).

For the WCSE procedure, the following processes must be undertaken as shown in Figure 4.4. (i) Development of a proper simulation model for the vehicle. The first requirement of the vehicle models are accuracy under extreme maneuvers and at the same

time easy integration with ICC and possibly other software. (ii) Development of the chassis control system models. In this research, two chassis control systems; a differential braking function, ESC and a suspension function, CDC are used. This choice is based on the observed relatively high effectiveness of rollover prevention. (iii) Generation of initial point for effective local searching (iv) Selection of a numerical method for WCSE. Two numerical methods, Mesh Adaptive Direct Searching (MADS) and Sequential Quadratic Programming (SQP) are selected.

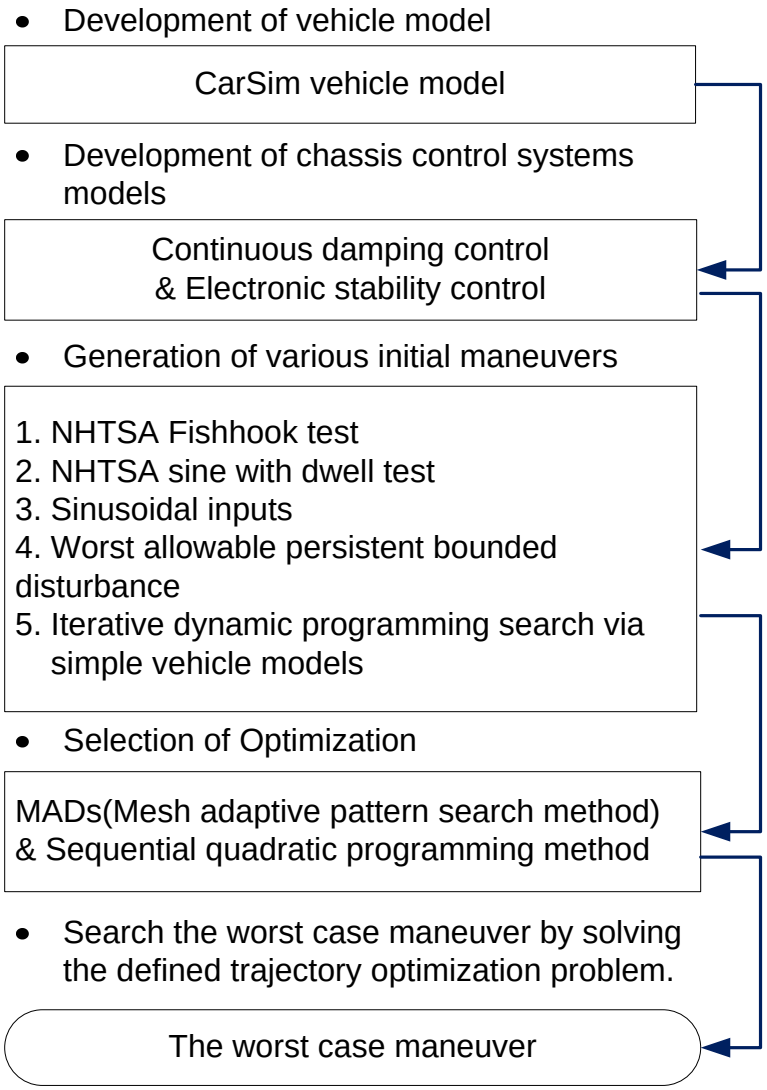

Figure 4.4 Diagram of the worst-case scenario evaluation method

4.3 IMPLEMENTATION OF WCSE

4.3.1 FORMULATION OF THE PROBLEM

The WCSE is formulated as a trajectory optimization problem, which searches for the driver maneuvers that maximize a cost function, e.g., the 2-norm of vehicle roll angle throughout the optimization horizon. The numerical schemes of WCSE must be able to accommodate: (i) nonlinearity with complex numerical subroutines (e.g., CarSim, Adams, etc.); (ii) equality and/or inequality constraints; and (iii) non-accumulated form of the performance index (e.g. infinity norm).

The WCSE problem is set up as follows. The time horizon is discretized into grid points

$$t_0 = \tau_1 \le \ldots \le \tau_{N-1} \le \tau_N = t_f \tag{4.3}$$

where t_0 : intial time t_f : final time.

The disturbances (steering wheel angles) at these discrete time point set, $\mathbf{w}_{sw}$, are design variables to be solved in the optimization problem; the actual disturbance is smoothed through interpolation (see Figure 4.5)

$$\mathbf{w}_{sw} = [w_{sw}^1, w_{sw}^2, \ldots, w_{sw}^{N-1}, w_{sw}^N] \tag{4.4}$$

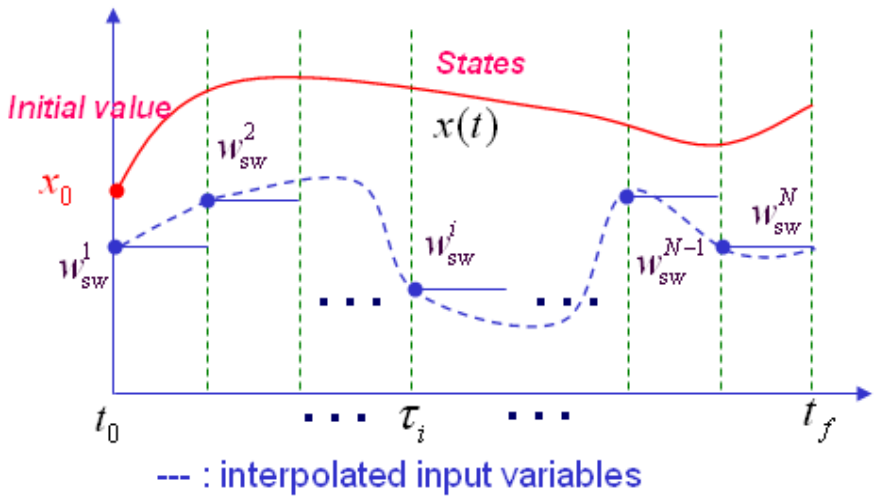

Figure 4.5 Trajectory optimization problem for WCSE

The disturbances have constraints because there are limits for the steering angle and the steering rate that the human driver is able to maneuver during the specific time step. The maximum peak values of this hand wheel magnitude and rate are based on the specification of the NHTSA standard tests (NHTSA, 2007b). The constraints are expressed as follows.

$$-\Delta w_{\max} \le w_{\mathrm{sw}}^{k+1} - w_{\mathrm{sw}}^{k} \le \Delta w_{\max} \tag{4.5}$$

$$-w_{\max} \le w_{\mathrm{sw}}^{k} \le w_{\max} \tag{4.6}$$

where $w_{\max}$:maximum magnitude and $\Delta w_{\max}$: maximum rate under the given time step

The proceeding equations (4.5) and (4.6) can be transformed to a constraint matrix form for the optimization methods as follow.

$$\begin{bmatrix} w_{\mathrm{sw}}^{1} & 0 & 0 & \ldots & 0 \\ 0 & w_{\mathrm{sw}}^{2} & 0 & \ldots & 0 \\ 0 & 0 & w_{\mathrm{sw}}^{3} & \ldots & 0 \\ \ldots & \ldots & \ldots & .. & \ldots \\ 0 & \ldots & 0 & 0 & w_{\mathrm{sw}}^{N} \\ -w_{\mathrm{sw}}^{1} & 0 & 0 & \ldots & 0 \\ 0 & -w_{\mathrm{sw}}^{2} & 0 & \ldots & 0 \\ 0 & 0 & -w_{\mathrm{sw}}^{3} & \ldots & 0 \\ \ldots & \ldots & \ldots & \ldots & \ldots \\ \ldots & \ldots & \ldots & 0 & -w_{\mathrm{sw}}^{N} \end{bmatrix} \le \begin{bmatrix} w_{\max} \\ w_{\max} \\ . \\ . \\ w_{\max} \\ . \\ . \\ . \\ w_{\max} \end{bmatrix} \& \begin{bmatrix} w_{sw}^{1} & -w_{sw}^{2} & 0 & \ldots & 0 \\ 0 & w_{sw}^{2} & -w_{sw}^{3} & \ldots & 0 \\ 0 & 0 & w_{sw}^{3} & \ldots & 0 \\ \ldots & \ldots & \ldots & .. & \ldots \\ 0 & \ldots & 0 & w_{sw}^{N-1} & -w_{sw}^{N} \\ -w_{sw}^{1} & w_{sw}^{2} & 0 & \ldots & 0 \\ 0 & -w_{sw}^{2} & w_{sw}^{3} & \ldots & 0 \\ 0 & 0 & -w_{sw}^{2} & \ldots & 0 \\ \ldots & \ldots & \ldots & \ldots & \ldots \\ \ldots & \ldots & \ldots & 0 & w_{sw}^{N} \end{bmatrix} \le \begin{bmatrix} \Delta w_{\max} \\ . \\ . \\ . \\ \Delta w_{\max} \\ \Delta w_{\max} \\ . \\ . \\ . \\ \Delta w_{\max} \end{bmatrix} \tag{4.7}$$

4.3.2 PROGRAM CONFIGURATION

The WCSE program is designed using Matlab/SIMULNK integrated with the CarSim software. As shown in Figure 4.6, constraints and initial conditions are applied to the optimization problem searching for the optimal steering disturbances. The

optimization solver written with Matlab code is hooked up to the CarSim software, which calculates cost functions. These procedures are executed iteratively.

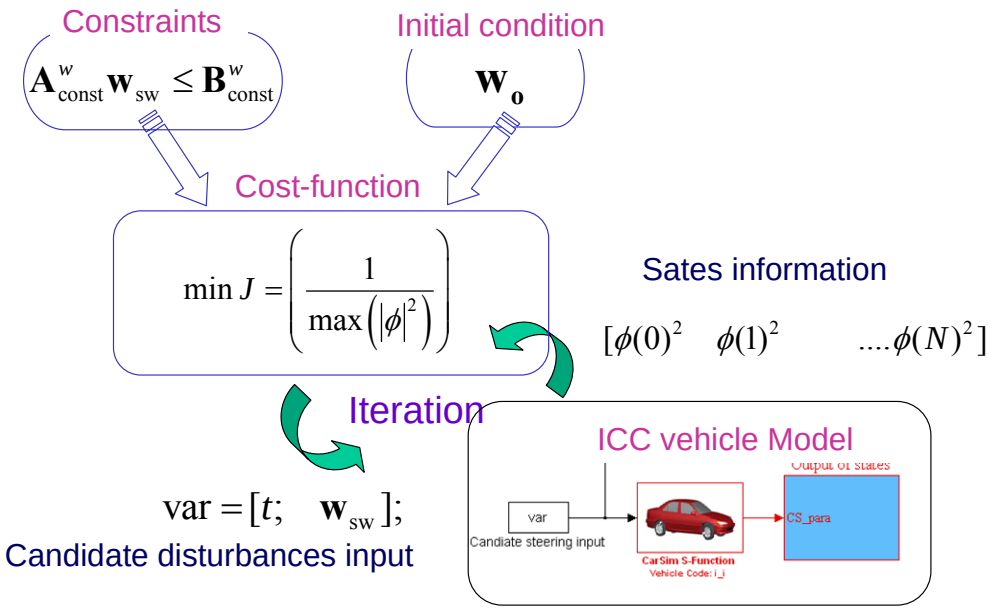

Figure 4.6 WCSE program configuration

4.3.3 NUMERICAL METHODS FOR SOLVING THE WCSE PROBLEM

Selection of the optimization methods is critical because WCSE is applied to nonlinear dynamic model with high computation load. Various optimization methods are actively applied in engineering problems. The computational efficiency and convergence of these methods are evaluated via a linear quadratic (LQ) example as shown in Eq.(4.8)

$$\begin{aligned} &\min J = x_N^2 + \sum_{k=1}^{N-1} x_k^2 + u_k^2 \\ &\text{s.t} \\ &x_{k+1} = 0.8x_k + 0.92u_k, y_k = x_k \\ &x \in [0,1], u \in [-0.6,0] \end{aligned} \tag{4.8}$$

Sequential quadratic programming (SQP) method and mesh adaptive direct searching (MADS) find optimal costs with acceptable computing time as shown in Table 4-1.

Table 4-1 LQ control results among optimization methods

Optimization Method	Program	Optimal cost , J	Grid points	Elapsed time
Dynamic Programming (DP)	Home-grown Code	1.4185	9, 9	1.898
Iterative DP (IDP)	Home-grown Code	1.4301	5,5	0.717
Direct search	Matlab	1.3504	NA	30.
Simaneal	Matlab	1.64	NA	7.
MADS	**Home-grown code**	**1.3467**	**NA**	**2.6**
SQP	**Matlab**	**1.3466**	**NA**	**0.363**

However, the DP method, which ensures global optimality, is not practical for high-dimension dynamic systems due to the curse of dimensionality (Bellman and Kalaba, 1966). It should be noted that IDP and DP are not compatible because the state initialization process for generating the transition cost table is not available using the built-in vehicle dynamics software, CarSim. Simplified models (e.g. 8 DOF model or 3 DOF model) based on a reduced number of states can be applied to solve state initialization problem and reduce the computational load resulting from the high dimensionality. However, there is a serious problem: the simplified model cannot properly represent the vehicle motion under extreme dynamic conditions such as rollover.

Based on the above considerations regarding convergence and computational speed, the SQP and MADS methods are selected. The SQP method is a local search method but is very efficient even for high-dimensional problem due to its rich development history (Buskensa, 2000). The MADS algorithm is a generalization of the

class of Generalized Pattern Search (GPS) algorithm, a derivative-free method (Audet, 2006). Because both are local search methods, global optimality cannot be guaranteed. Therefore, they must be used with multiple initial points, which is illustrated in an example below.

An example searching history of the MADS method is shown in Figure 4.7. It can be seen that the solution may be stuck at a certain local minimum for extended number of iterations before it suddenly breaks loose and finds a better optimum point. This is typical of local search methods, which demonstrate the necessities of allowing large numbers of iterations.

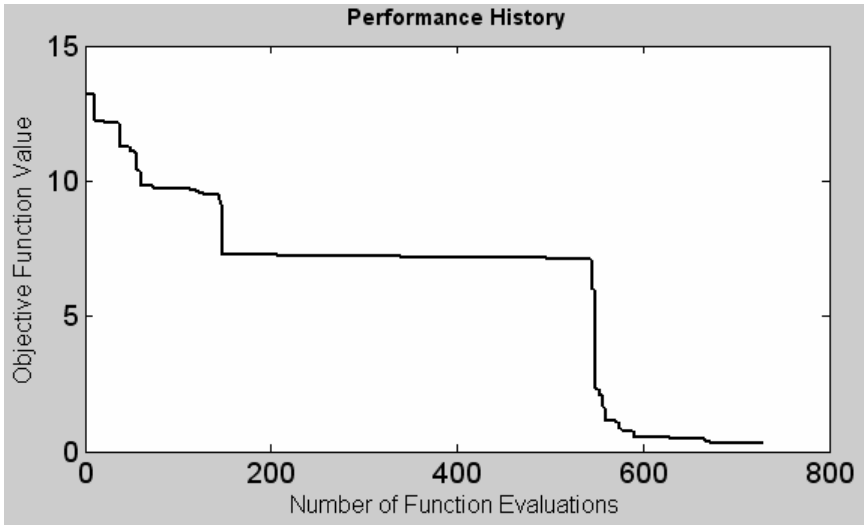

Figure 4.7 An example MADS searching history $J = 2000/\left|\phi_{\max}\right|^2$

Despite the fact that both SQP and MADS are local-search methods, they can find local optimum that is quite different from the same initial guess if a large number of iterations is allowed. One such example is illustrated in Figure 4.8. In this example, the cost function to be minimized is selected to be $J = 2000/\left|\phi_{\max}\right|^2$. From the same initial condition, the worst-case maneuvers obtained via SQP and MADS methods can both cause rollover. Detailed evaluation results are shown in Table 4-2. Two optimal solutions are the values corresponding rollover despite the fact that the steering angle and

vehicle roll motions are different. This indicates that they converge to different local minima, both of which are of interest in understanding the performance of the vehicle ICC system. It should be noted that CarSim results in a specific value of roll angle under the condition where dynamic simulation is stopped even though the final roll angles are shown differently.

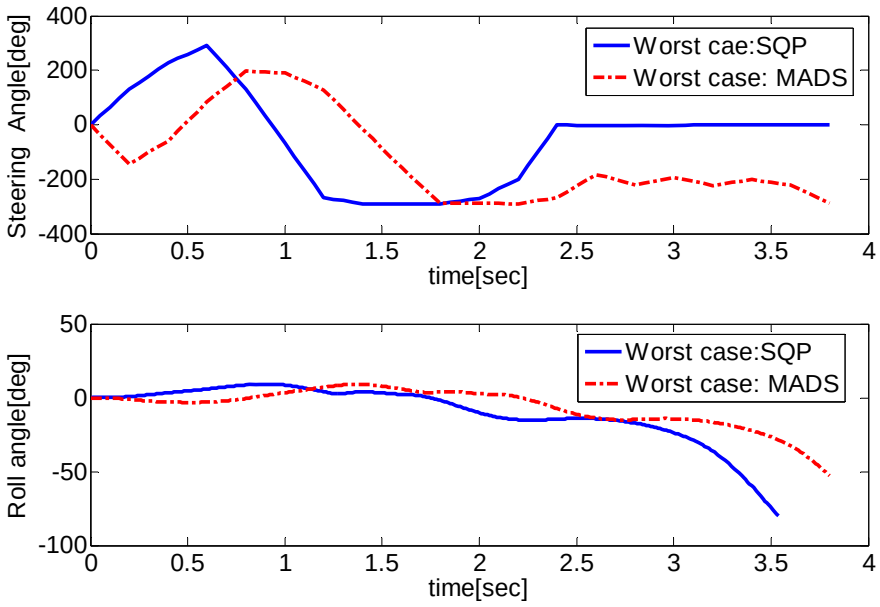

Figure 4.8 The worst case results from SQP & MADS $u_x = 82[\text{kph}], \mu = 0.9$

Table 4-2 WCSE search results

	Iteration #	# of evaluation Function	Convergence Tolerance	Final Cost function
SQP	74	2019	0.001	0.31
MADS	349	729	0.001	0.31

The effectiveness of the obtained worst-case maneuver (from SQP) is compared against a standard rollover test, the NHTSA Fishhook test (see Figure 4.3). The vehicle rolls over under the WCSE but not under the standard fishhook test. What is even more interesting is that we are able to achieve rollover even when the initial vehicle speed is 10 [kph] lower than in the fishhook test (see Figure 4.9).

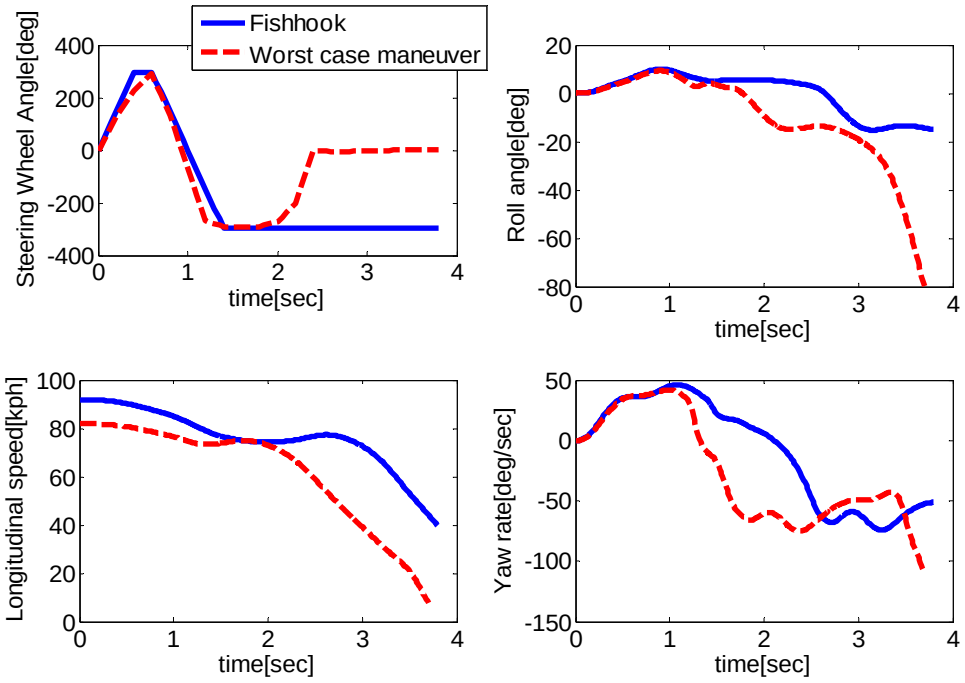

Figure 4.9 Comparison between standard fishhook and the worst-case maneuver

4.3.4 GENERATION OF INITIAL CONDITIONS

Initial point generation is critical for the WCSE process. Since both numerical methods (SQP and MADS) search locally, initial points that are rich and close to local minimum are critical for reaching an array of local optima that truly reflect the safety performance. We can observe the limited performance of the local searching in the result generated from null initial points in Figure 4.10.

A common practice in generating initial points for local search methods such as SQP is the use of pseudo-random points. The idea is to cover the high dimensionality of the disturbance inputs in a systematical way to ensure richness. Some of the initial points used in our WCSE program will be generated in this pseudo-random fashion. However, we put more emphasis on another method, which is to leverage existing standard tests, engineering practice and controls theory.

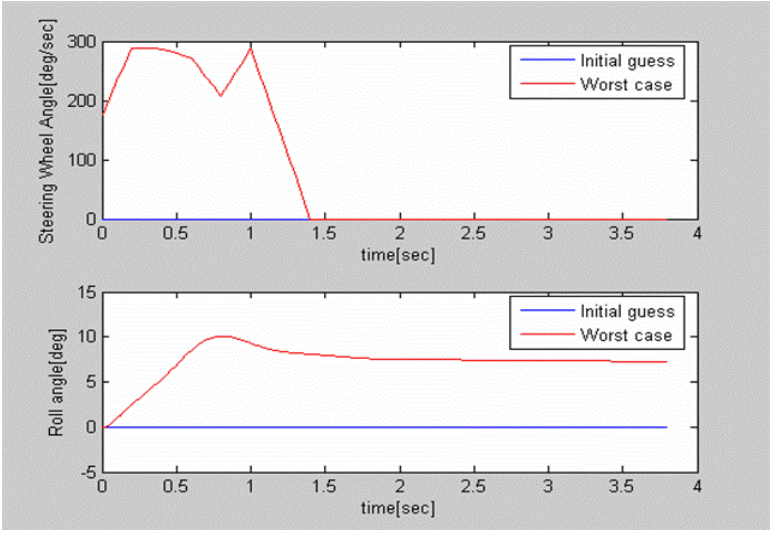

Figure 4.10 Searching result for the worst steering disturbance input, which starts from null initial steering input under the same simulation condition in Figure 4.8

The worst allowable persistent bounded disturbance (WAPBD) provides useful insight for disturbance input generation (Jayasuriya, 1995). The basic concept of WAPBD is the generation of worst-case input via impulse response of a linear time invariant (LTI) system.

The procedure is depicted in Figure 4.11. First, $g(t)$, the impulse response due to steering input, is obtained. The response is trimmed at 3% steady-state error and the time span, T is determined. The worst persistent disturbance, $w_0(t,T)$ for $t \in [0,\mathrm{T}]$, is then obtained from $w_0(t,T) = \mathrm{sign}\{g(T-t)\}$. Assuming that the maximum steering value is $\delta_{\max}$, then a good initial point for the WCSE search is $\delta_{\max} \cdot sign\{g(T-t)\}$. Constraint of the rate limit should be applied to calculate the final signals; in this calculation, the maximum the range of steering rates the human driver can generate must be taken into consideration. The effectiveness of WAPDB method can be identified through rollover propensity WCSE in two types of SUV as shown in Table 4-3.

$g(t)$

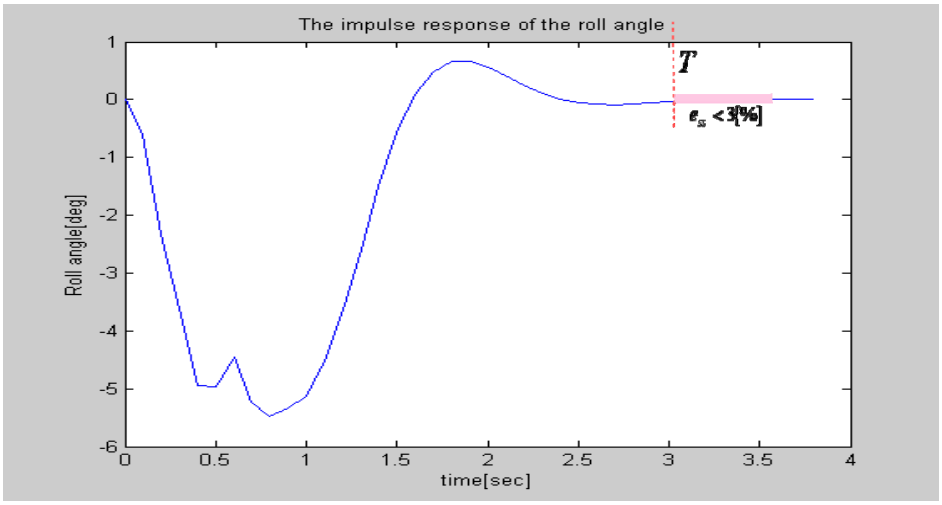

$w_0(t,T) = g(T-t)$

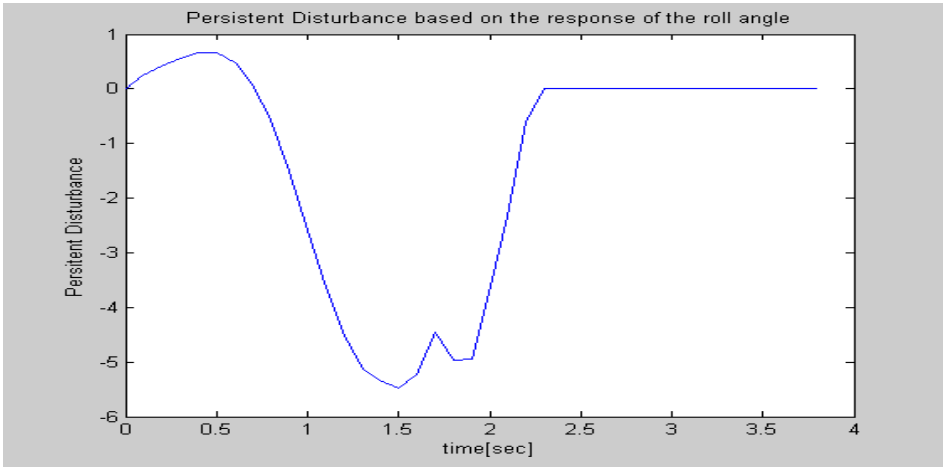

$\delta_{\max} \cdot sign\{g(T-t)\}$ [deg]

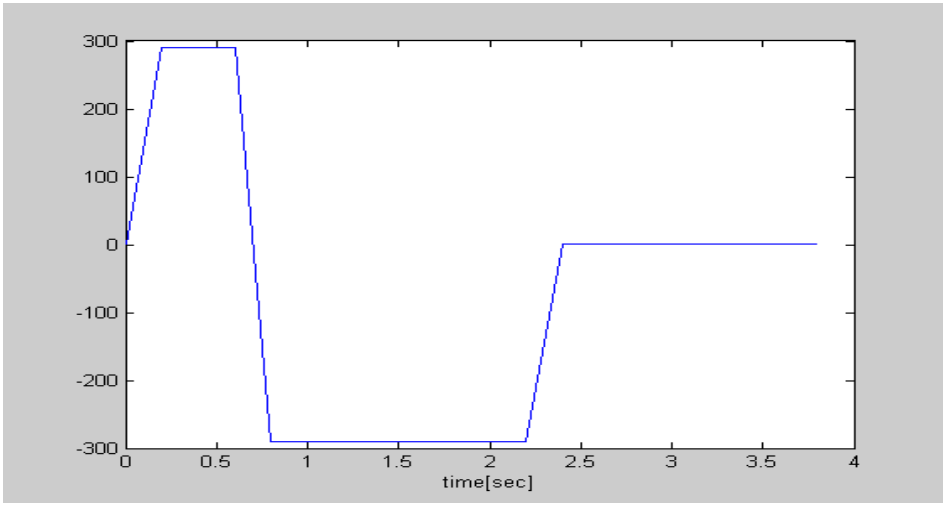

Figure 4.11 The initial point obtained from the impulse-response based WAPBD approach.

Table 4-3 The WCSE results using three different initial points (NHTSA tests and WAPBD) in small and large SUVs @ initial vehicle speed: 80[kph]

		Small SUV	Large SUV
Initial points	NHTSA Fishhook	**Rollover**	**Rollover**
	NHTSA sine-dwell	**Rollover**	**Rollover**
	WAPBD method	**Rollover**	**Rollover**

For broad searches, candidates for the initial points can be generated via simplified vehicle model-based iterative dynamic programming (IDP), which is designed in the MATLAB environment. First, we create initial trajectories and generate the transitional cost and the terminal state values from the simulation of the simple vehicle model. The results are then stored in a database. The optimal costs are calculated backwards based on the information in the database, and the final optimal input is recomposed through the simulation of the simple vehicle model. The above procedures are repeated until the final optimal solutions converge to the given tolerance. It should be noted that vehicle models in the IDP approach must be in an open state form as the developed nonlinear vehicle model in Section 2.1.1 .i.e. the states must be arbitrarily initialized. Even though the simple model has limits in representing real vehicle motion, the searching results can provide the candidate maneuvers for initial points a higher number of broad searches.

Figure 4.12 shows the WCSE procedure, where the IDP WCSE based on the nonlinear 3 DOF model provides the SQP WCSE based on the CarSim model with initial points, and the final optimal solutions are obtained through the SQP WCSE. The Fishhook maneuver is used to obtain initial points of the IDP WCSE. The maneuvers sequentially obtained from the IDP WCSE are used for initial points of the SQP WCSE via the CarSim model. Figure 4.13 shows simple results of the WCSE procedures.

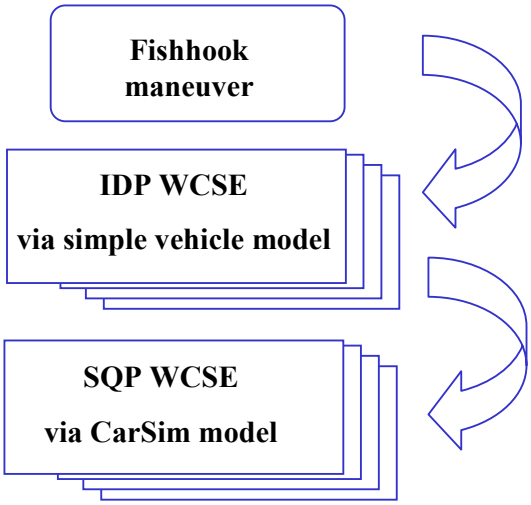

Figure 4.12 The WCSE procedure via SQP and IDP methods

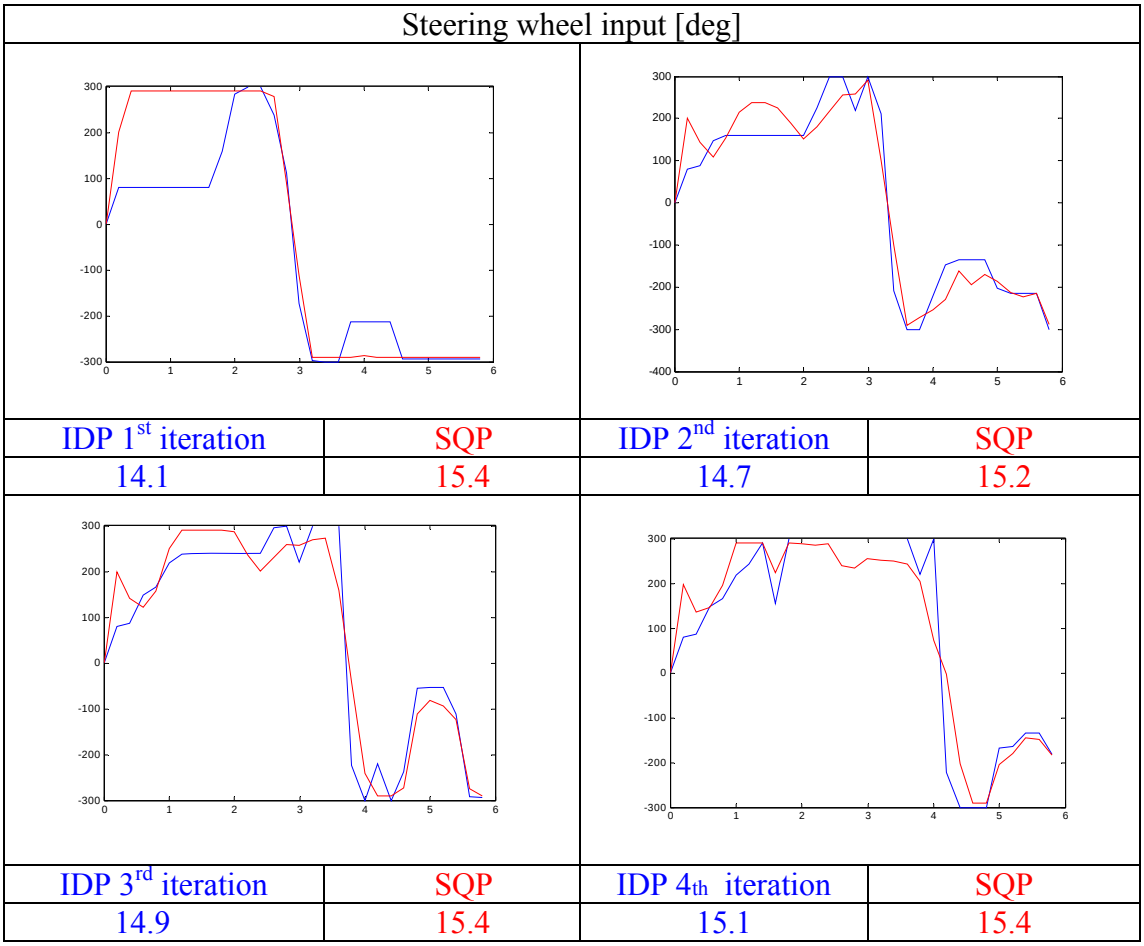

Figure 4.13 The IDP and SQP methods based WCSE search results: maximum roll angle

In MADS method, random options is selected for direction, order, and center types of the poll that is the local exploration in the space of optimization variables (Audet, 2006) for the purpose of broad searches as shown in Figure 4.14. Various initial points can be applied in the MADS search. MADS search depends on initial points as shown in Figure 4.11. Two initial points (NHTSA sine-with-dwell maneuver and WAPBD method) generates different type of steering inputs as the WCSE solutions.

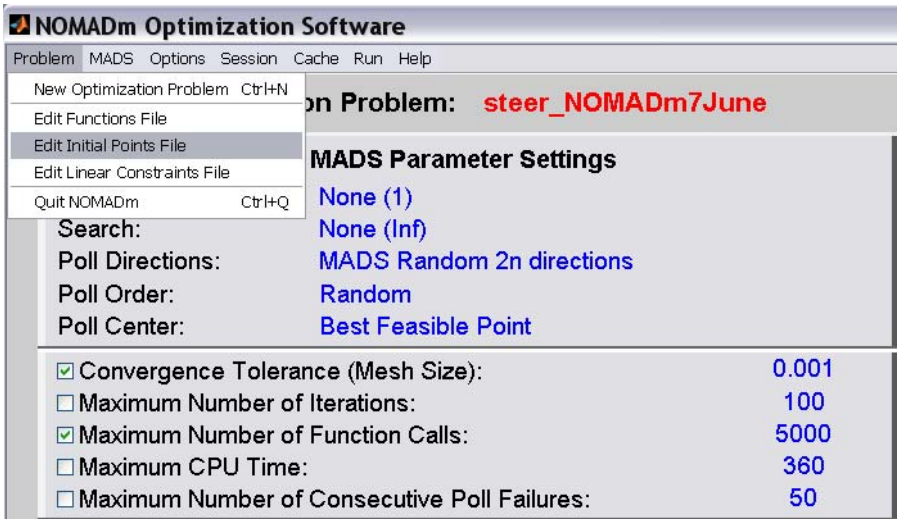

Figure 4.14 Snap shot of poll options and initial points in MDAS

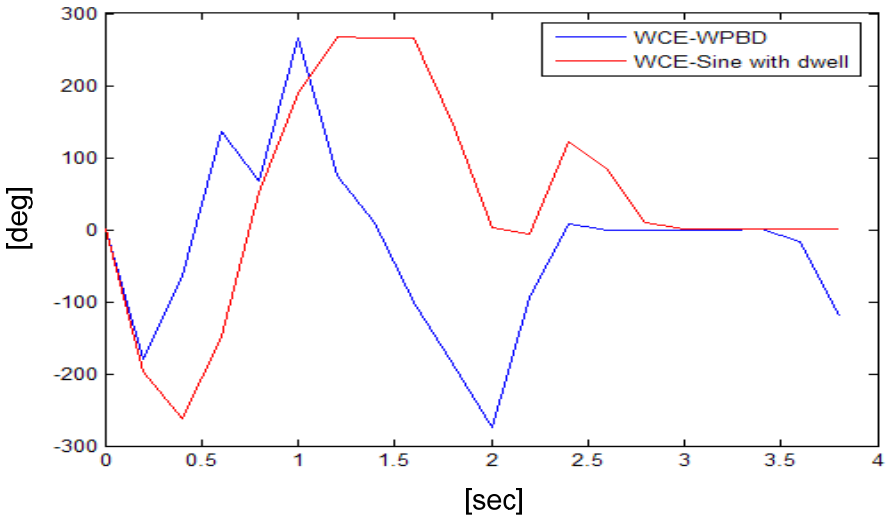

Figure 4.15 MADS search results from two different initial points (sine-with-dwell and WAPBD)

The WCSE results obtained from various initial points attempted in our research are shown in Table 4-4. All the searched maneuvers generate large roll angle, which almost leads to rollovers. The initial point from WAPBD leads to rollover after the local search. These initial points are applied for the WCSE approach in the following research. It should be noted that the maximum roll angle corresponds to the best solution in each initial point type.

Table 4-4 WCSE search results starting from various initial points of middle size SUV @ initial vehicle speed: 80[kph]

Initial point types	ϕ_{max} :Maximum roll angle
NHTSA Fishhook tests	14.6
NHTSA sine with dwell tests	13.9
Sinusoidal inputs :0.1~0.5[Hz]	13.8
IDP WCSE results	14.7
WAPBD method	**Rollover**

4.4 THE WORST-CASE SCENARIO EVALUATION OF VEHICLES

The WCSE is applied to the evaluation of rollover propensity of two different sizes of SUVs without control systems. In the WCSE programs, two optimization methods (MADS and SQP) are used with the initial points in Section 4.3.4. The overall procedures of both optimizations methods-based WCSE are explained in Appendix B. The steering angle and rates are constrained at the level specified in the NHTSA Fishhook test (δ_{max} :290[deg] and $\dot{\delta}_{max}$:1000[deg/s]). The convergence tolerance of the numerical methods is defined by a value as 0.001 for a terminal condition. The best solutions among the solutions obtained from two optimization methods with different initial points is selected as the final solution.

Figure 4.16 shows "The minimum steering angle" necessary to induce rollover under various initial longitudinal speeds; the data are obtained from the WCSE process. The basic idea is that when the steering angle is limited below these steering values, no rollover can occur. In the WCSE evaluation, two SUV are compared, and their safety rating for rollover propensity can be determined. Additionally, the obtained results can help us to make critical engineering decisions. For example, in case of steer-by-wire systems, the results provide a way of determining the permitted limit of the steering input at the specific speed without rollover. It is difficult to establish this curve applying the standard tests such as NHTSA because the standard tests do not cause rollover at higher speeds (over 110[kph]). In other word, if the maneuvers are limited to the standard tests, the tendency to rollover cannot be monotonic with regard to the initial longitudinal speed.

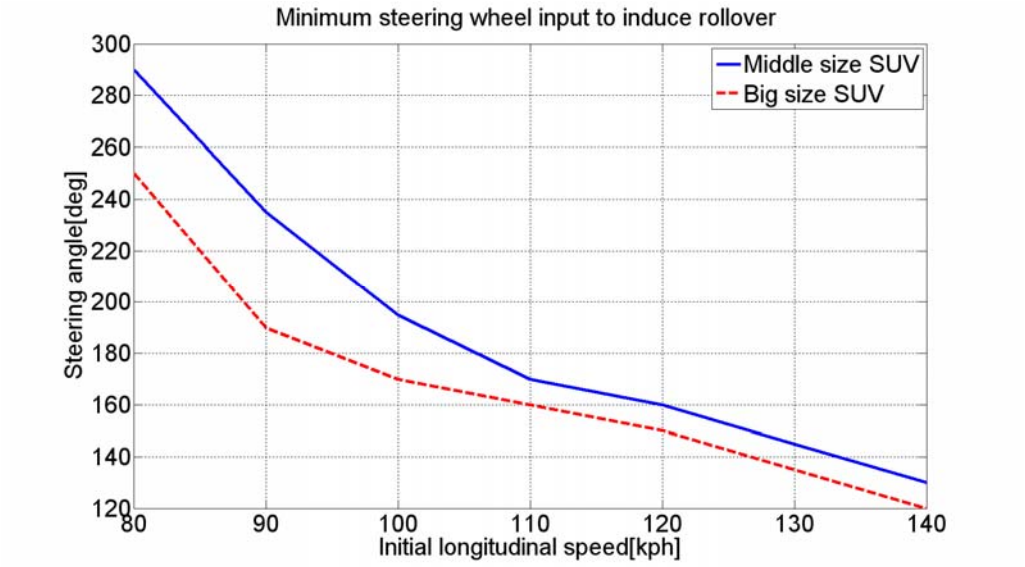

Figure 4.16 Characteristic curves of minimum steering wheel to induce rollover under various initial vehicle speeds

4.5 DESIGN FOR ROLLOVER PREVENTION (ROP) CONTROL

In this subsection, ROP prevention, one of the ICC objectives, is redesigned using the WCSE results. First, the original chassis control design is evaluated using the WCSE

method presented in the previous section. The maneuver that is identified exposes risks not addressed by the original design. It contributes to the design improvement by helping the evaluation procedure of chassis control systems (see Figure 4.17).

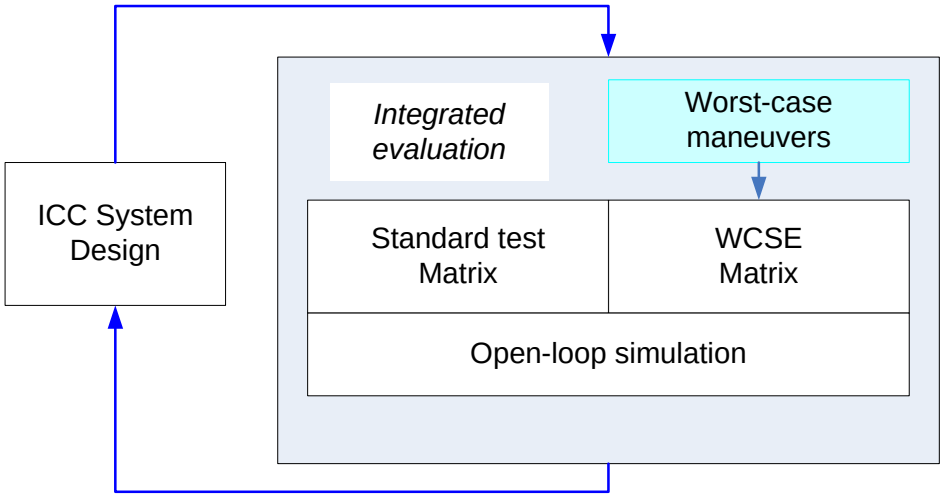

Figure 4.17 Design procedure of ICC via WCSE

The ESC is effective in rollover prevention (ROP) as shown in Figure 2.12 (p. 35). Furthermore, ROP function based on the determined control strategy must be given higher priority over various functionalities for other vehicle control objectives such as desired yaw rate following and lateral stability.

The ROP function can be realized in different ways; (i) single wheel(SW) braking, (ii) multiple wheel (MW) braking with anti wheel locking features (generated by ABS), and (iii) MW braking without ABS, which means allowing wheel-locking as shown in Figure 4.18. Design of these ROP strategies is based on the following consideration. The SW braking at the front outside tire is used for yaw moment stabilization. Rear wheel braking at the outside encompasses the following two functions with respect to the stabilization of the vehicle planar yaw motion. One function is increasing of yaw moment via generated braking force and the other is decreasing of yaw moment via reduced lateral force. Therefore, application of MW braking for increase of

the number of the braking wheels to regulate vehicle roll motion must be determined through a rigorous verification procedure. Both SW braking and MW braking are based on ABS. Another important decision for the ROP control is the decision of whether wheel locking is allowed during the generation of braking forces or not. The wheel locking may have negative effects on the vehicle handling response because of tire force saturation. However, given the fact that rollover events are potentially fatal, wheel locking can be allowed for the generation of sufficient braking force in the effective ROP control strategy. This is based on the assumption that brake pressure to generate sufficient brake forces cannot be maintained while ABS control releases brake pressure for the purpose of preventing wheel locking. Finally, the MW braking without ABS is proposed as a candidate ROP control strategy.

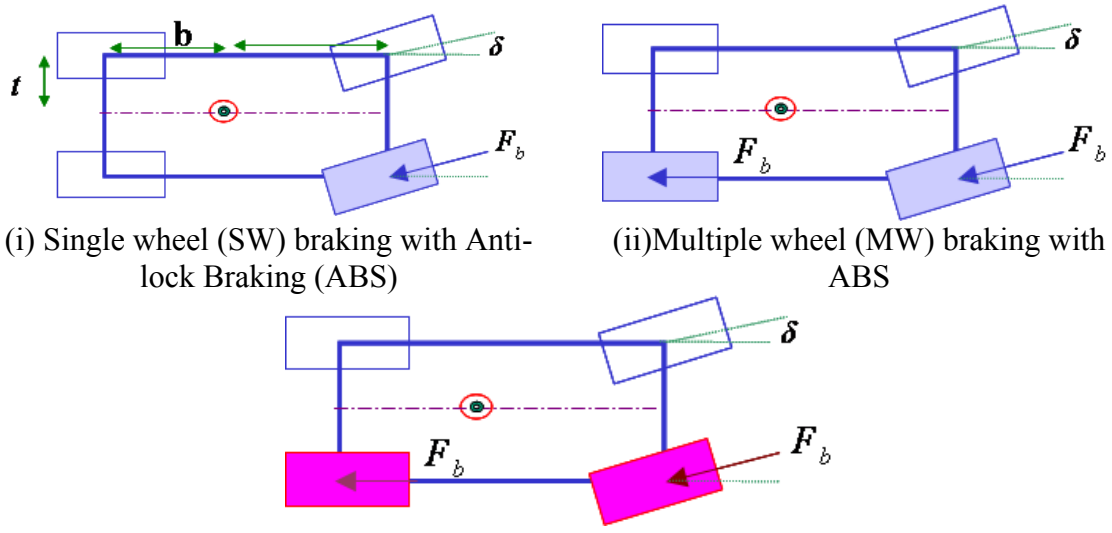

(i) Single wheel (SW) braking with Anti-lock Braking (ABS)

(ii)Multiple wheel (MW) braking with ABS

(iii) MW braking without ABS

Figure 4.18 Three rollover prevention control (ROP) strategies

In the WCSE of ESC ROP, the test specification, the limit of the steering angle and steering rate, are all based on the NHTSA sine-with-dwell test. It is because the sine-with-dwell test is developed to enable us to observe ESC's contribution to a target

vehicle's resistance to rollover. Simulations are executed iteratively with increasing initial longitudinal speed from 80[kph]. To determine the ROP control strategy suitable for a big SUV, comparison simulations of the respective control strategies were performed by the WCSE procedure with regard to rollover.

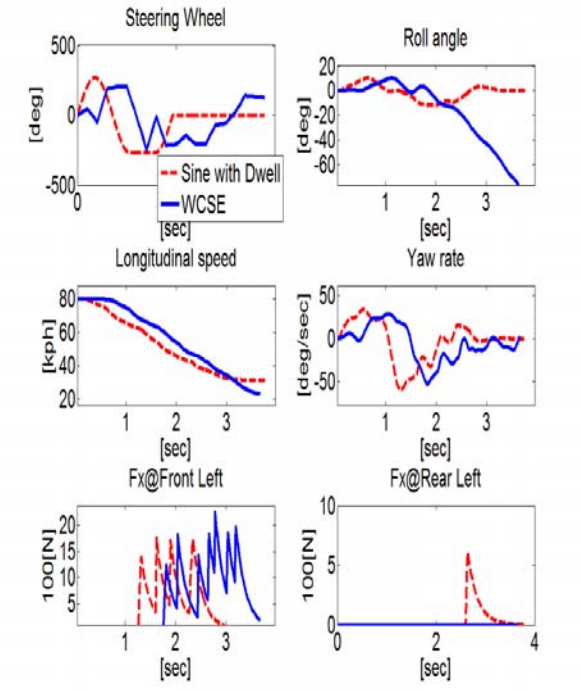

(a)Rollover does not occur in the NHTSA sine with dwell test @ 80 [kph]

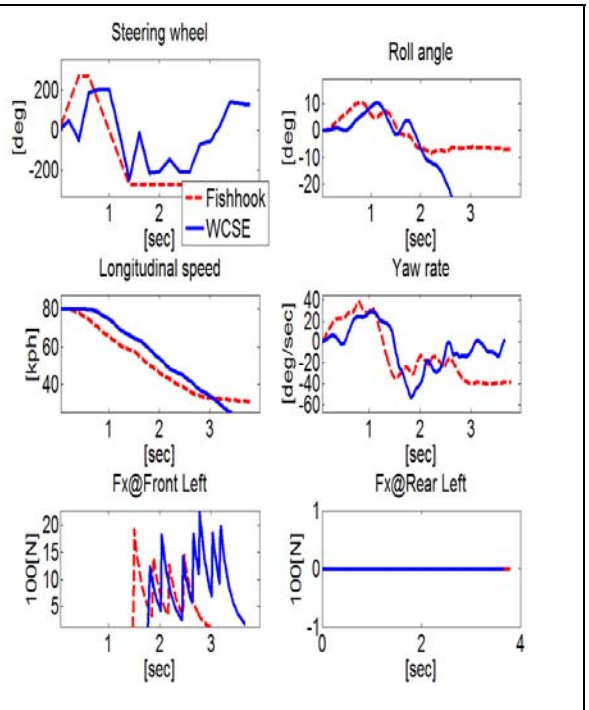

(b)Rollover does not occur in the NHTSA Fishhook test @ 80 [kph]

Figure 4.19 Comparison between the WCSE and NHTSA standard tests for evaluation of SW braking ROP control

First, the performance of SW ROP control is evaluated applying two NHTSA rollover propensity tests (sine-with-dwell and Fishhook test) and the proposed WCSE method.

Figure 4.19 shows that SW ROP fails to stabilize the vehicle under the worst-case maneuver, which is not identified by the NHTSA test maneuvers. The performance of "MW ROP control with ABS" is investigated by applying the previous WCSE. We

cannot find any problem of "MW ROP control with ABS" under the given conditions as shown in Figure 4.20. Therefore, the WCSE method is applied to the "MW ROP control with ABS" and "without ABS" (sees Figure 4.21). The results show that "SW ROP control with ABS" fails to stabilize the vehicle under the WCSE maneuver whereas "MW ROP control without ABS" succeeds in stabilizing the vehicle.

Through these studies, we can learn two features of the WCSE method. One is that the WCSE is more effective than the NHTSA tests in finding weakness of control systems, and the other is that the WCSE should be customized. In other words, the maneuver that is obtained through the WCSE for "SW ROP control" cannot be the solution of the WCSE for "MW ROP control" even though it can be valid.

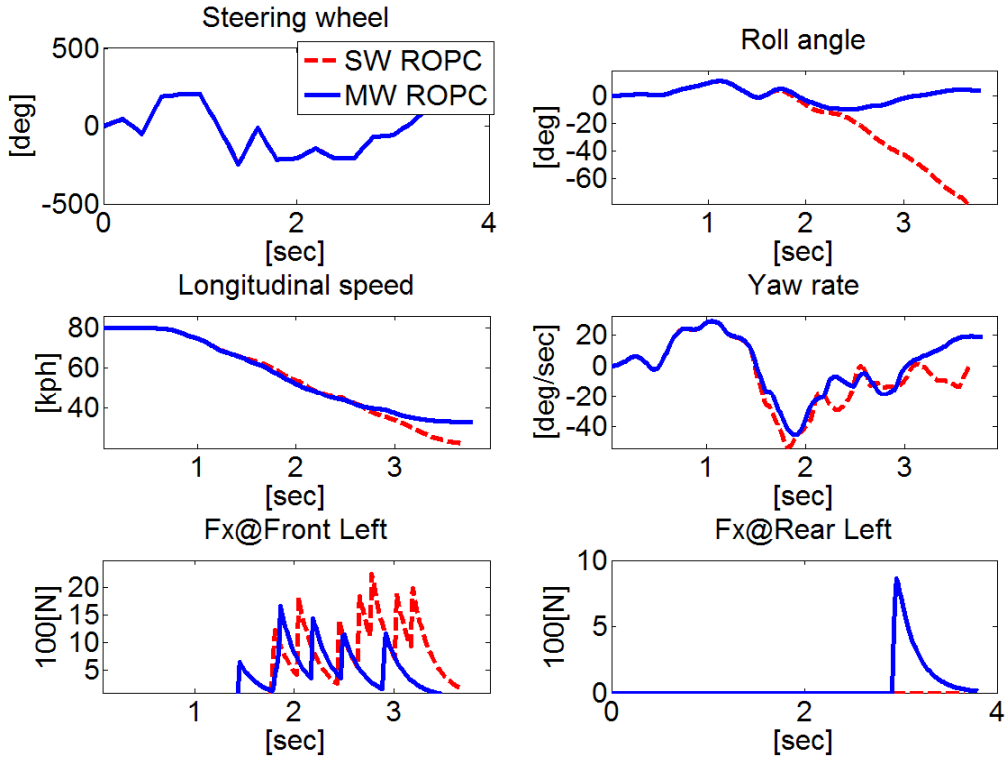

Figure 4.20 Comparison between the SW braking and MW braking ROP with ABS

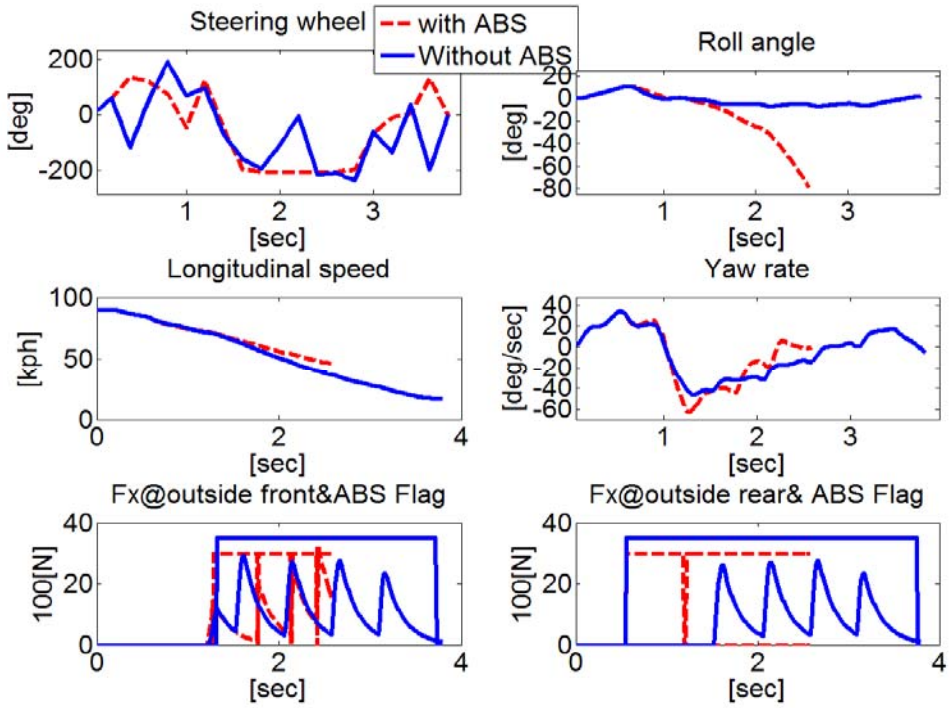

Figure 4.21 Comparison test simulation of MW ROP control with ABS and without ABS

The representative WCSE results are presented on the basis of the above study. First, the SW braking with ABS (i) is evaluated as Figure 4.22, which shows that the worst-case maneuver causes rollover but the sine-with-dwell maneuver does not. Through the WCSE procedure, we can in fact find that the SW braking fails to prevent rollover of the SUV. As shown in Figure 4.23, the MW braking with ABS (ii) is investigated. The result shows that the control strategy fails to prevent rollover because the wheel-locking command blocks the braking force generation at the outside wheels. MW braking without ABS (iii) succeeded in preventing rollover by generation of the sufficient braking force, which leads to reduction of cornering forces and creation of compensated yaw moment regardless of wheel-locking phenomena. We can observe that the braking forces are generated during the wheel-locking situation through braking control outputs, F_x and the wheel locking flag in the third row of Figure 4.23.

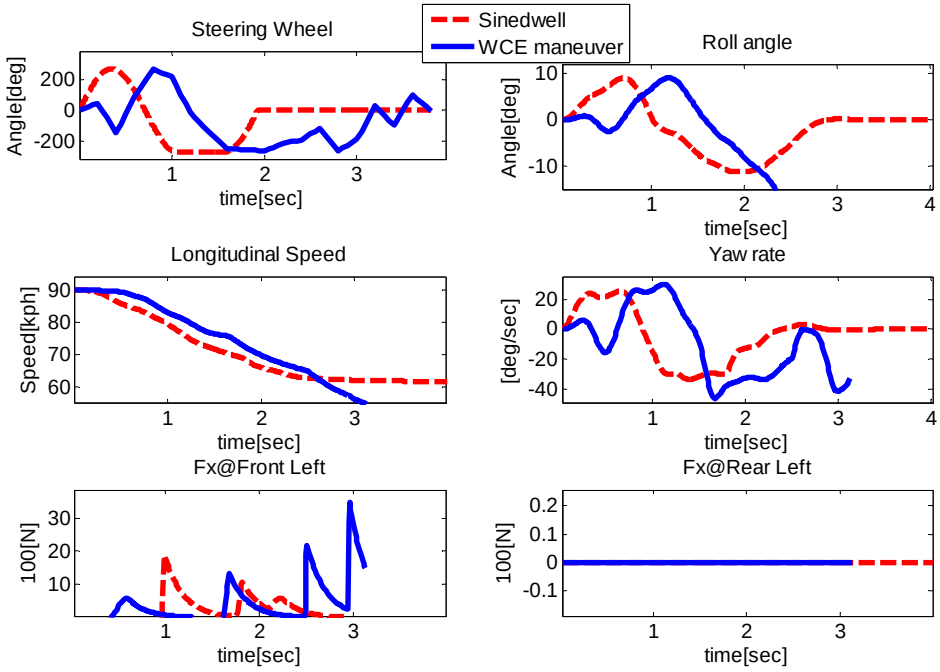

Figure 4.22 Comparison test simulation of NHTSA sine-with-dwell and the WCSE regarding SW braking-based ROP

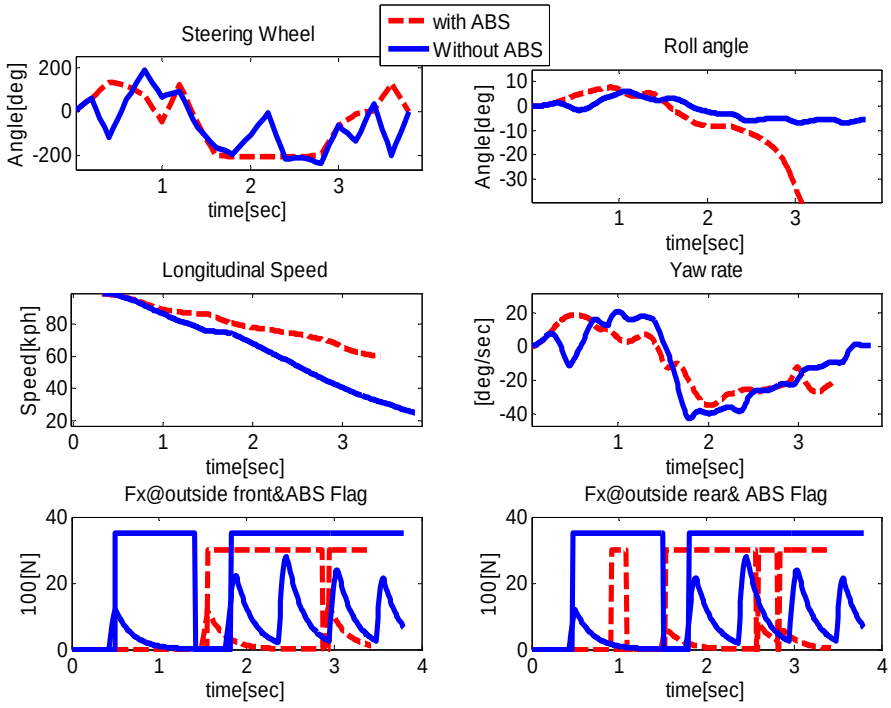

Figure 4.23 WCSE results for comparing the MW braking ROP with ABS and without ABS

Table 4-5 summarizes the WCSE results at various initial speed and different ROP strategies including the CDC system. The maximum roll angles according to the corresponding control strategies and given speeds are reported in the table—which represent the effectiveness of the worst-case maneuvers that promotes rollover. To compare the effectiveness of the WCSE with the standard test, simulation results from the NHTSA sine with dwell and Fishhook tests are reported in the "standard test" columns. As shown in this table, CDC is not very effective in preventing rollover, but ESC is able to stabilize vehicle roll motion under the NHTSA standard test maneuver. Through the WCSE, we can identify two ROP control strategies: The SW braking and the MW braking with ABS, both of which fail to prevent rollover for the target vehicle under the given initial speeds. The ROP strategy of the MW braking without ABS shows successful ROP performances. Therefore, it can be seen that MW braking without ABS stabilizes the vehicle better than other control strategies.

Table 4-5 WCSE results at various initial speed and different ROP control strategies

$\lvert\phi_{max}\rvert$	WCSE				Standard Test Simulation (NHTSA sine-dwell & Fishhook)			
Speed[kph] / Control strategy	80	90	100	110	80	90	100	110
CDC control	**Roll over**	**Roll over**	**Roll over**	**Roll over**	**Roll over**	**Roll over**	**Roll over**	**Roll Over**
SW braking with ABS	**Roll over**	**Roll over**	**Roll over**	**Roll over**	10.1	11.2	13.4	13.13
MW braking with ABS	**Roll over**	**Roll over**	**Roll over**	**Roll over**	9.5	10.0	**Roll over**	**Roll Over**
MW braking without ABS	10.2	10.8	10.8	11.3	9.1	9.9	10.7	11.0

Based on the above ROP control strategy study, we can obtain the characteristic curves of the minimum steering wheel input under different control strategies as shown in

Figure 4.24. The allowable steering input is limited at 360 [deg]. The steering wheel inputs can be allowed to the limit values in the MW ROP control without ABS under the given speed range.

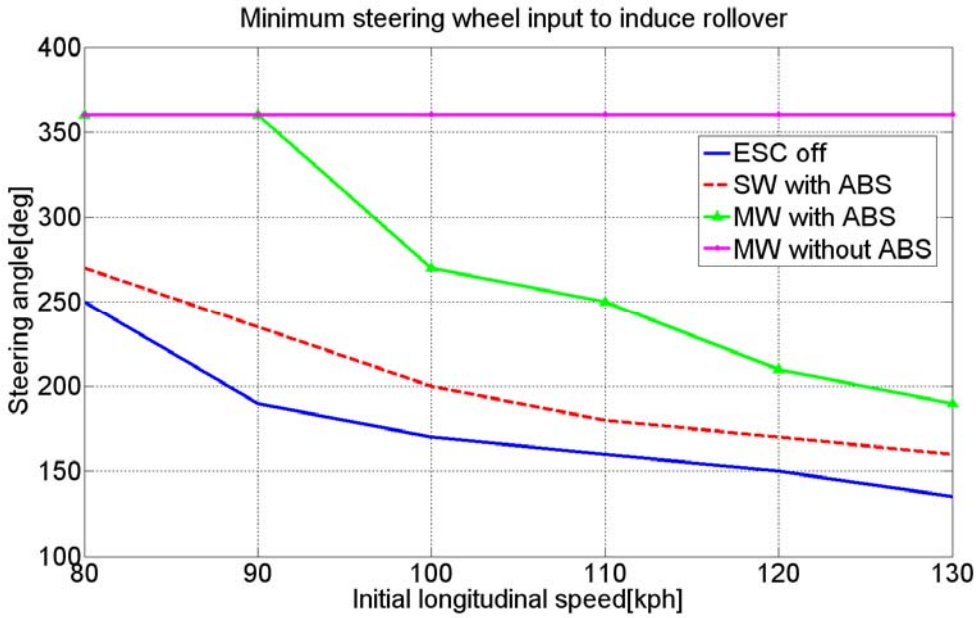

Figure 4.24 Characteristic curves of minimum steering wheel inputs to induce rollover under different ROP control strategies

4.6 SUMMARY

To demonstrate the necessity of the worst-case scenario evaluation, three significant problems of the conventional experimental evaluations are identified: high cost, low repeatability, and limited customization. The WCSE is based on extensive numerical searches via simulation models. The proposed WCSE procedure aims to find worst possible disturbances (in this study, driver's steering input) for selected vehicle motion (e.g., rollover). This study can be considered as the preliminary development of an evaluation procedure for the rollover prevention functionality of ICC.

The basic architecture and major components of the worst-case scenario evaluation are described. The major pre-process of the WCSE program is the application

of constraints and an initial point allocation. In these processes, constraints such as magnitude saturation and rate limits of the steering wheel input are imposed.

Because of the high nonlinearity of vehicle motions and control systems, two local search methods, sequential quadratic programming method and mesh adaptive direct search method are used. Since the applied algorithm identifies only local optimal points, multiple initial steering profiles must be used to ensure that the obtained results are close to the global optimal results. The obtained results represent a close approximation of the global optimal value, and the difference between local and global optimal values could be compensated for by use of safety factor.

A procedure motivated by control theories is proposed for generation of initial points. The worst allowable persistent bounded disturbance theory provided an effective starting point in searching the worst-case maneuver for rollover.

To verify the effectiveness of the WCSE, rollover prevention (ROP) performances of chassis control systems are assessed. Through this WCSE, the performance of ESC's ROP is compared with that of CDC because both ESC and CDC include rollover prevention function. The results of the WCSE show that multiple wheel braking without ABS is most robust in preventing rollover. The developed WCSE method provides evaluation results enabling us to identify the failure modes of ESC that cannot be monitored in the standard tests, and furthermore, it provides results that can help designers in improving the ROP control strategy.

The application of the WCSE approach can be extended with enhanced development environments. Experimental verifications of the case studies will strengthen the arguments behind the methodology by applying hardware in the loop system.

CHAPTER 5

CONCLUSION AND FUTURE STUDY

5.1 CONCLUSION

The focus of this Ph.D. research is the development and evaluation of integrated chassis control systems (ICC). Concerning ICC development, this research focuses on a decentralized design that coordinates the commands from sub-chassis control systems. This approach takes into account prevailing industry practices, in which different sub control systems may be individually developed by suppliers and then integrated for synergy in combination. For the evaluation of ICC, a development and extension of the worst-case scenario evaluation method via simulation-based optimization scheme is proposed to examine ICC performance under driver's steering disturbance. The evaluation method can ensure that ICC meet performance requirements and design criteria, and it provides an alternative to expensive and risky field tests for ultimately guaranteeing safe system performance.

The representative decentralized approach, diagonal decoupling control, is not suitable for ICC on the basis of the relative gain array analysis and thus that new coordination approach is necessary for decentralized ICC design. The proposed methodology is the design of coordinator to be placed downstream of individual chassis control systems to intercept and modify sub-control commands. The hybrid approach combining an offline model predictive control and an online control allocation (CA) was applied to ensure minimal real-time computational load and reconfigurable control. The fixed-point (FP) iteration method used in solving the CA problem showed computational efficiency for an on-board controller. In the online CA computation, the final control

inputs are calculated by applying sub-control commands as good initial points and as upper bounds.

The effectiveness of the decentralized ICC system is verified via the CarSim simulation. The simulation results showed that ICC resolved conflicts among subsystem, and achieved improved stability even while using reduced control commands. This ICC system demonstrates the capacity for reconfiguration of the control in response to actuator failure in the sub-control systems, and it shows robust control under uncertainties such as vehicle weight and road friction changes. It should be noted that control robustness of the decentralized ICC is affected by the feedback control in ESC as well as by the coordination control.

For regarding the evaluation of ICC, the worst-case scenario evaluation (WCSE) method was applied to find the worst possible disturbances. Two optimization schemes, the selected sequential quadratic programming and mesh adaptive direct searching methods, demonstrated convergence and computation efficiency in the simple linear quadratic control problem. Both displayed robust searching performance in dynamic optimization problems including a nonlinear system model with complex controllers.

The worst allowable persistent bounded disturbance theory provided an appropriate initial guess in searching for the worst-case disturbance to vehicles. This theoretical approach was found to give good results even though it is based on a linear-system analysis. This WCSE provided technical grounds for ESC rollover control that cannot be easily analyzed due to significant nonlinear dynamics. Multiple wheel control and admissible maximum longitudinal slip in a wheel lock control module of ESC were selected through these WCSE results. Although for the most part, only vehicle rollover prevention is considered, extensions of the application to other active safety systems evaluation and their logic improvement have been shown to be possible.

5.2 FUTURE STUDY

My dissertation research may lead to future tasks. They include

- Extended application of different ICC combination and coordinate control configurations

To demonstrate the viability of the proposed concept, more case studies may be explored. As an example, we might examine integrated active front steer (AFS) and ESC. It would be a useful case to study because AFS could contribute to the stabilization of vehicles. Coordination control configurations can vary according to the determination of control inputs (e.g. optimal longitudinal slip or braking torque). In the possible different configurations, the effective coordination design will be investigated through the application of modular control theories regarding stability and robustness.

- Experimental tests of the ICC design via on-board system

The practical implementation of the proposed controller will be investigated using potential on-board systems. The implementation of the real controller must be based on the appropriate electronic hardware design and the interface design involving signal processing.

- Extended application of the worst case scenario evaluation (WCSE) for ICC design

Another important issue that will be addressed is analysis and prioritization of the design goals of ICC, including rollover prevention, sideslip regulation, yaw rate responsiveness, and wheel slip regulation. These control objectives have different safety and performance implications, and their prioritization has not been discussed adequately in the literature. A performance index will be defined to ensure clear assessment of these performance objectives under a wide variety of driving conditions, and the trade-off between stability and responsiveness will be investigated. The WCSE will be used for performance prioritization and trade-offs in ICC design.

- Analytical study of the proposed coordinator for the decentralized ICC design

Even though the proposed coordinator design for the ICC system yields favorable results, this dissertation does not provide a rigorous stability and robustness analysis of the coordinator. Furthermore, some open questions and challenges remain unaddressed because this design is based on nonlinear systems, and the MPC and the CA approach relies on optimization methods, rather than a closed-form control law (Vermillion, 2009). Any future study of the analysis of coordinator design will be based on the MPC stability constraints (Morari and Lee, 1999; De Oliveira Kothare and Morari, 2000) and the stability analysis of modular control (Vermillion, 2009). Additionally, a different servomechanism (e.g. braking torque or longitudinal slip) of the sub-control systems will be investigated. The criteria for sampling times of the coordinator and sub-controller of sub-systems will be studied as preliminaries to the foundation of design guidelines for the ICC systems.

APPENDICES

APPENDIX A VEHICLE MODEL PARAMETERS

a	1.014 m	distance of c.g to front axle
b	1.676 m	distance of c.g to rear axle
t_{wf} , t_{wr}	(0.77, 0.77) m	half track of front and rear axle
g	9.81 m/s^2	gravitational acceleration
h_{cg}	0.677 m	c.g height above ground
h_0	0.085 m	ground to roll axis distance below c.g
h_1	0.4569 m	distance of h_{cg} to h_0
h_{rf}	0.42 m	height of front roll center above ground
h_{rr}	0.57 m	height of rear roll center above ground
I_{xx}	1000.kg-m^2	roll moment of inertia w.r.t. x-axis
I_{zz}	4000.6 kg-m^2	yaw moment of inertia w.r.t. z-axis
I_{xz}	0 kg-m^2	product of inertia w.r.t. x and z-axis
$K_{\varphi f}$, $K_{\varphi r}$	$(5.08\times10^4, 3.83\times10^4)$ N-m/rad	front and rear roll stiffness
K_{pf} , K_{pr}	$(2000\times10^4, 4\times10^4)$ N-m-s/rad	front and rear damping rate
m	1966 kg	vehicle sprung mass
R_w	0.301 m	effective wheel rolling radius
w_F	1100 kg	Weight at front side
w_R	866 kg	Weight at rear side

APPENDIX B WORST-CASE SCENARIO EVALUATION

Program information :

1) CarSim ver. 6.05 http://www.CarSim.com
2) Matlab ver.7.04 http://www.mathworks.com/
3) fmincon in Matlab library
4) NOMADm ver. 4.02

This sub-section presents the overall procedure of the worst-case scenario evaluation. The WCSE method is based on an integrated CarSim and Matlab/SIMULINK.

First, we select “data set”, in which vehicle parameters and test conditions are set up (see Figure B.1.). The SIMULINK model is opened after the set-up is ready. The corresponding execution files of the optimization method (SQP and MADS) are called in the SIMULINK model as shown in Figure B.2.

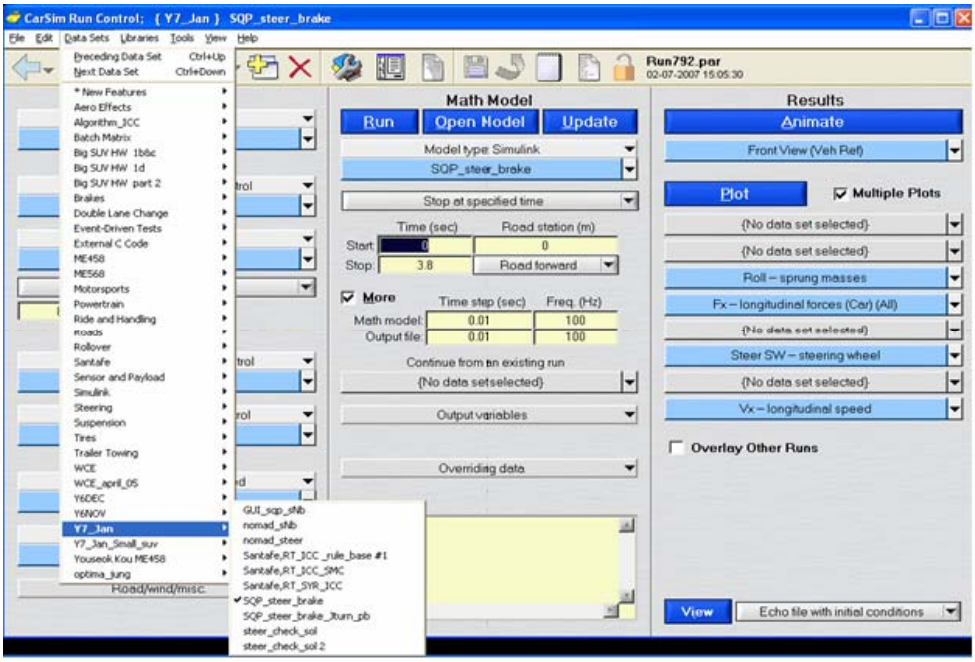

Figure B.1 Selection of data set in CarSim

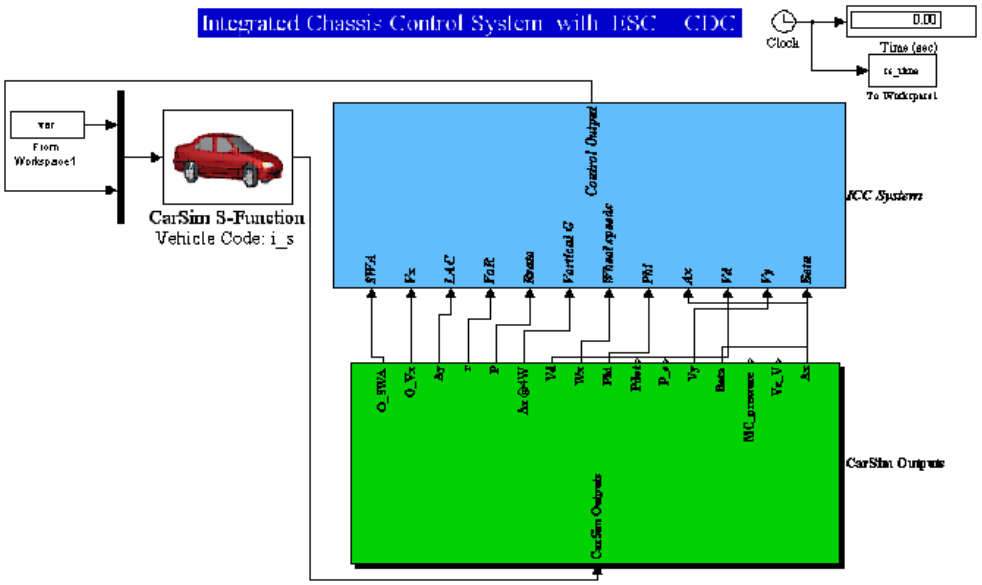

Figure B.2 ICC SIMULINK model for the WCSE

We run the SQP based WCSE through the batch process, which is designed on the basis of Matlab program function, fmincon. The search results of this SQP based WCSE is composed of four windows that correspond to four types of initial guess point sets (WAPBD method (Impulse response) + Sinusoidal inputs(5 frequencies) + Fishhook + Sine-with-dwell) as shown in Figure B.3.

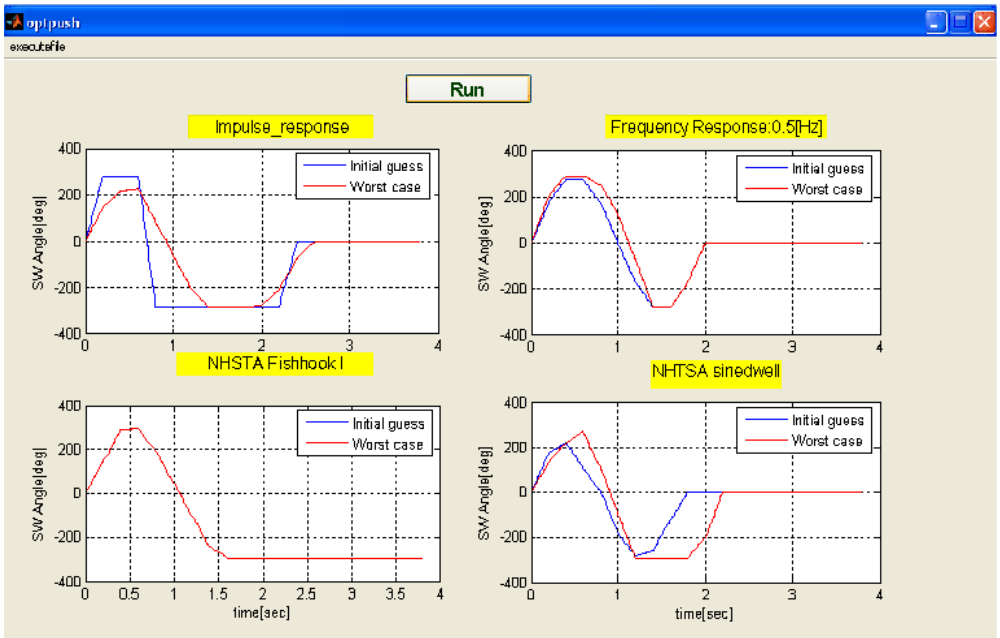

Figure B.3 Simulation results of the SQP based on WCSE

We run the MADS based WCSE through nomadm, the graphic user interface, which is developed in the Matlab environments. In this nomadm, various search conditions such as search options, terminal conditions and alternative search strategies (random generation and genetic algorithms) can be set up as shown in Figure B.4. The search results of this MADS based WCSE are displayed with setting including directions, order and center of poll (see Figure B.5).

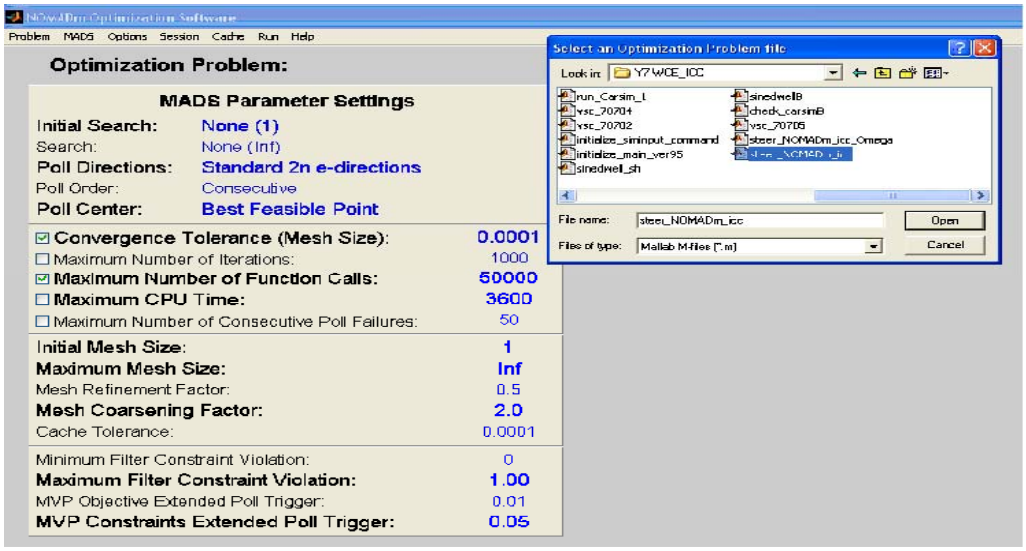

Figure B.4 MADS based WCSE: nomadm

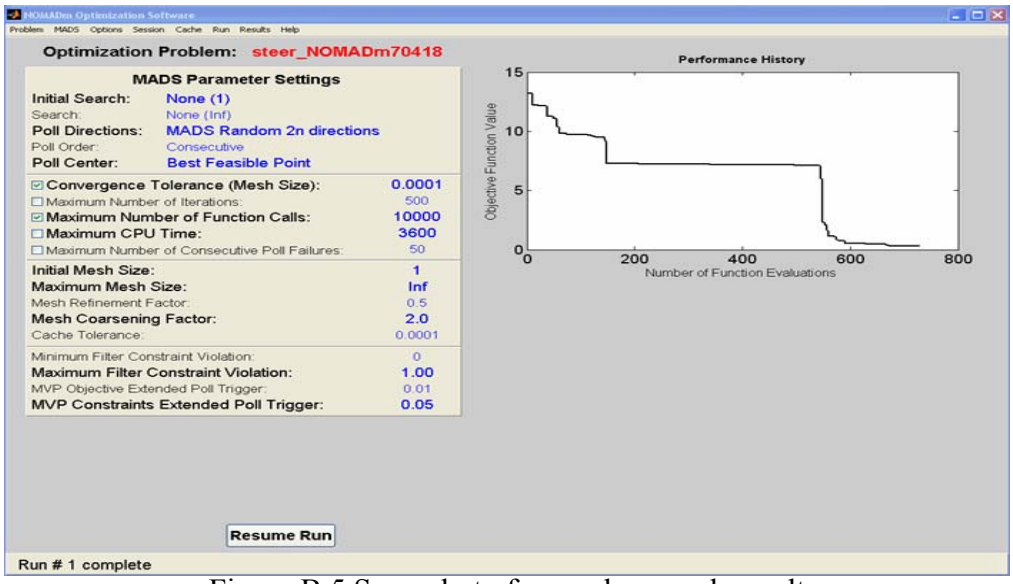

Figure B.5 Snap-shot of nomadm search result

APPENDIX C RELATIVE GAIN ARRAY ANALYSIS

The effective use of a decentralized controller requires some element of decoupling. Loosely speaking, independent design is used when the system is decoupled in space (G(s) is close to diagonal). The relative gain array (RGA) analysis is a very useful tool for a diagonal decoupling control. The RGA analysis provides a measure of interactions. Let u_j and y_i denote a particular input-output pair for the multivariable plant $G(s)$, and assume that my task is to use u_j to control y_i. The relationship between the input and output are investigated on the basis of the two conditions, in which all other loops except the pairing relationship are open: $u_k = 0, \forall k \neq j$ and all other loops are at the same way closed with perfect control: $y_k = 0, \forall k \neq i$. Perfect control is only possible at steady state, but it is a good approximation at frequencies within the bandwidth of each loop.

We now evaluate "our" gain $\partial y_i / \partial u_i$ for the two extreme cases:

$$\left(\frac{\partial y_i}{\partial u_j}\right)_{u_k=0,k\neq j} \triangleq g_{ij} \quad \text{and} \quad \left(\frac{\partial y_i}{\partial u_j}\right)_{y_k=0,k\neq i} \triangleq \hat{g}_{ij} \tag{A.1}$$

The following RGA analysis example is based on 2x2 MIMO system (Tham, 1999). An analytical determination is possible if a steady-state model of the system is available. Thus if:

$$y_1 = K_{11}u_1 + K_{12}u_2 \text{ and } y_2 = K_{21}u_1 + K_{22}u_2 \tag{A.2}$$

Where the K_{ij} are the steady state gains of the process transfer function matrix.

$$\left.\frac{\partial y_1}{\partial u_1}\right|_{u_2=0} = K_{11} \tag{A.3}$$

Eliminating u_2 in Eq. (A.2) yields

$$y_1 = K_{11}u_1 + K_{12}(y_2 - K_{21}u_1)/K_{22} \tag{A.4}$$

Differentiating this w.r.t u_1 while keep y_2 constant then yields:

$$\left.\frac{\partial y_1}{\partial u_1}\right|_{y_2=0} = K_{11} - K_{12}K_{21}/K_{22} \tag{A.5}$$

The relative gain λ_{11} is given by

$$\lambda_{11} = \left(\left.\frac{\partial y_1}{\partial u_1}\right|_{u_2=0}\right) \Big/ \left(\left.\frac{\partial y_1}{\partial u_1}\right|_{y_2=0}\right) = 1/\left(1-\left(K_{12}K_{21}\right)/\left(K_{11}K_{22}\right)\right) \tag{A.6}$$

Major remarks of the RGA are as follows

(i) If $0<\lambda_{11}<0.5$, For example, where $\lambda_{11}=0.25$, the diagonal elements of the RGA equal 0.25 while the off-diagonal elements are 0.75. The larger elements indicate the more suitable input-output pairings, Viz. y_1 with u_2, and y_2 with u_1.

(ii) If $0.5<\lambda_{11}<1$, then the larger diagonal elements of the RGA indicate the suitable input-output pairing.

(ii) If $\lambda_{11}>1$, then the off-diagonal elements of the RGA will be negative. The alternative pairings y_1 with u_2, and y_2 with u_1 are, however, unsuitable because the corresponding relative gains are negative. This means that the resulting interactions will take controlled outputs in a direction away from that which the control is trying to achieve. As a result, control will eventually be lost.

APPENDIX D CONTRACTION MAPPING THEOREM (UBC.CA, 2009)

Let $B_a = \left\{ \vec{x} \in R^d \mid \left\| \vec{x} \right\| \le a \right\}$ denote the open ball of radius a centered on the origin in R^d. If the function

$$\vec{g} : B_a \to R^d$$

Satisfies

Assumption [i]: there is a constant $G < 1$ such that $\left\| \vec{g}(\vec{x}) - \vec{g}(\vec{y}) \right\| \le G \left\| \vec{x} - \vec{y} \right\|$ for all $\vec{x}, \vec{y} \in B_a$

Assumption [ii]: $\left\| \vec{g}\left(\vec{0}\right) \right\| < (1-G)a$

then the equation, $\vec{x} = \vec{g}(\vec{x})$ has exactly one solution.

Assumption [i] is responsible for the word “Contraction" in the name of the theorem. Because G < 1 (and it is crucial that G < 1) the distance between the images $\vec{g}(\vec{x})$ and $\vec{g}(\vec{y})$ of $\vec{x}$ and $\vec{y}$ is smaller than the original distance between $\vec{x}$ and $\vec{y}$.

Assumption [ii]: If $\vec{g}(\vec{x})$ only takes values that are outside of B_a, then $\vec{x} = \vec{g}(\vec{x})$ cannot possibly have any solution. So there has to be a requirement that $\vec{g}(\vec{x})$ lies in B_a for at least some values of $\vec{x} \in B_a$. Our assumptions are actually somewhat stronger than this:

$$\vec{g}(\vec{x}) = \left\| \vec{g}(\vec{x}) - \vec{g}\left(\vec{0}\right) + \vec{g}\left(\vec{0}\right) \right\| \le \left\| \vec{g}(\vec{x}) - \vec{g}\left(\vec{0}\right) \right\| + \left\| \vec{g}\left(\vec{0}\right) \right\| \le G \left\| \vec{x} - \vec{0} \right\| + (1-G)a$$

With our assumptions: $\vec{g} : B_a \to B_a$ Roughly speaking, (A [ii]) requires that $\vec{g}(\vec{x})$ be sufficiently small for at least one, $\vec{x}$.

Figure D.1 shows a search procedure for solution via a fixed-point iteration. The fixed point iteration $x_{n+1} = g(x_n)$ converges to the unique fixed point of the function $x = g(x)$ for any starting point x_n.

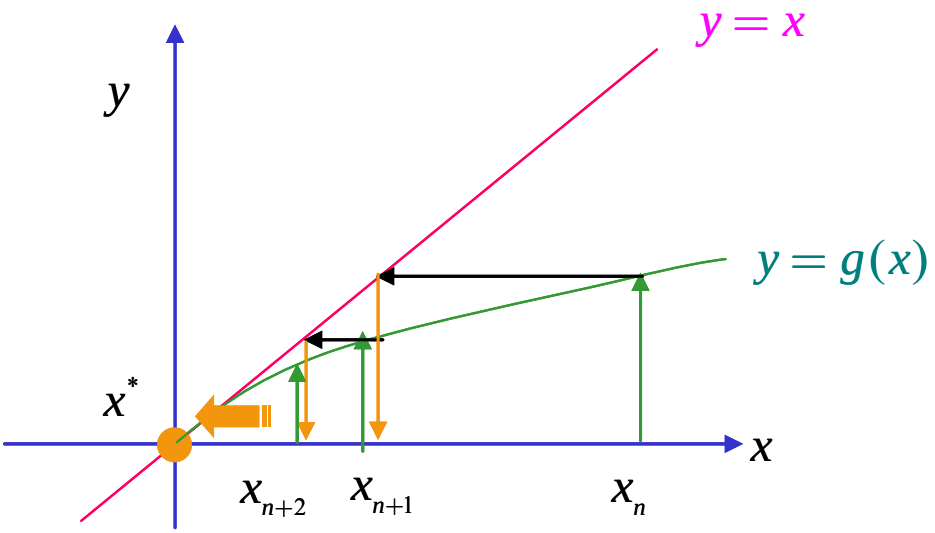

Figure D.1 Fixed-point iterations example; $x_{n+1} = g(x_n)$

BIBLIOGRAPHY

BIBLIOGRAPHY

A Hac, D. D., M Oppenheimer (2006). "Unified Control of Brake-and Steer-by-Wire Systems Using Optimal Control Allocation Methods." 2006 SAE World Congress Detroit.

An, F., and Sauer, A. (2004). "Comparison of Passenger Vehicle Fuel Economy and GHG Emission Standards around the World." the Pew Center on Global Climate Change.

Audet, C. (2006). "Mesh Adaptive Direct Search Algorithm for Constrained Optimization." *SIAM Journal on Optimization Archive*, 17, 188-217.

Bedner, E., and Chen, H. H. (2004). "A Supervisory Control to Manage Brakes and Four-Wheel-Steer Systems." 2004 SAE World Congress, Detroit.

Bedner, E., Fulk, D., and Hac, A. (2007). "Exploring the Trade-Off of Handling Stability and Responsiveness with Advanced Control Systems." 2007 SAE World Congress, Detroit.

Bellman, R. E., and Kalaba, R. (1966). *Dynamic Programming and Modern Control Theory*, Academic Press.

Bemporad, A., Morari, M., Dua, V., and Pistikopoulos, E. N. (2003). "The Explicit Linear Quadratic Regulator for Constrained Systems." *Automatica*, 39(10), 1845-1846.

Borrelli, F., Falcone, P., Keviczky, T., Asgari, J., and Hrovat, D. (2005). "MPC-based Approach to Active Steering for Autonomous Vehicle Systems." *International Journal of Vehicle Autonomous Systems*, 3(2-4), 265-291.

Brooks, R. A. (1990). "Elephants Don't Play Chess." *Robotics and Autonomous Systems*, 6(2), 3-15.

Brooks, R. A. (1991). "Integrated Systems Based on Behaviors." *ACM Sigart Bulletin*, 2(4), 46-50.

Burken, J. J., Lu, P., Wu, Z., and Bahm, C. (2001). "Two Reconfigurable Flight-Control Design Methods: Robust Servomechanism and Control Allocation." *Journal of Guidance, Control and Dynamics*, 24(3), 482-493.

Buskensa, C. (2000). "SQP-Methods for Solving Optimal Control Problems with Control and State Constraints: Adjoint Variables, Sensitivity Analysis and Real-time Control " *Journal of Computational and Applied Mathematics*, 120(1-2), 85-108.

Chandy, A. (2003). "System and Method Incorporating Feedforward for Motor Vehicle Chassis Control." US Patent 6,567,731.

Chang, S. (2007). "A Flexible Hierarchical Model-Based Control Methodology for Vehicle Active Safety Systems," Ph. D. Dissertation, University of Michigan, Ann Arbor.

Commission, E. (2005). "Road safety: Road Safety Action Programme (2003-2010)." Activities of the European Union: Summaries of Legislation.

Corno, F., Tosato, S., and Gabrielli, P. (2003). "System-level Analysis of Fault Effects in an Automotive Environment." 18th IEEE International Symposium 529-536.

Costlow, T. (2008). "Automakers Explore New Ways to Spread Computing around The Vehicle, with An Eye toward Centralized Architectures." Automotive Engineering International 20~23.

Davidson, J. B. (2001). "Real-Time Adaptive Control Allocation Applied to a High Performance Aircraft." 5th SIAM Conference on Control & Its Applications.

De Oliveira Kothare, S. L., and Morari, M. (2000). "Contractive Model Predictive Control for Constrained Nonlinear Systems." *IEEE Transactions on Automatic Control*, 45(6), 1053-1071.

DeCicco, J., An, F., and Ross, M. (2001). "Technical Options for Improving the Fuel Economy of U.S. Cars and Light Trucks by 2010–2015." A Report Prepared for The Energy Foundation.

Doman, D. B., and Oppenheimer, M. W. (2002). "Improving Control Allocation Accuracy for Nonlinear Aircraft Dynamics." AIAA Guidance, Navigation, and Control Conference and Exhibit.

Falcone, P., Borrelli, F., Asgari, J., Tseng, H. E., and Hrovat, D. (2007). "Predictive Active Steering Control for Autonomous Vehicle Systems." *IEEE Transactions on Control Systems Technology*, 15(3), 566-580.

Falcone, P., Borrelli, F., Asgari, J., Tseng, H. E., and Hrovat, D. . (2007 b). "MPC-based Yaw Stabilization via Active Front Steering and Braking." IAVSD 20th Symposium: Dynamics of Vehicles on Roads and Tracks.

Fletcher, R. (1989). *Practical Methods of Optimization* Willey, New York.

Forkenbrock, G. J., Elsasser, D., and O'Harra, B. (2005). "NHTSA'S Light Vehicle Handling and ESC Effectiveness Research Program."

Frazzoli, E. (2001). "Robust Hybrid Control for Autonomous Vehicle Motion Planning," Ph. D. Dissertation, Massachusetts Institute of Technology.

Furukawa, Y., and Abe, M. (1997). "Advanced Chassis Control Systems for Vehicle Handling and Active Safety." *Vehicle System Dynamics*, 28, 59-86.

Furukawa, Y., Yuhara, N., Sano, S., Takeda, H., and Matsushita, Y. (1989). "A Review of Four-Wheel Steering Studies from the Viewpoint of Vehicle Dynamics and Control." Taylor & Francis, 151-186.

Georgiou, T. T., and Fialho, I., J. (1999). "Worst-case Analysis of Nonlinear Systems." *IEEE Transactions on Automatic Control*, 44(6), 1180-1196.

Ghoneim, Y. A., Lin, W. C., Sidlosky, D. M., Chen, H. H., Chin, Y.-K., and Tedrake, M. J. (2000). "Integrated Chassis Control System to Enhance Vehicle Stability." *International Journal of Vehicle Design*, 23(1-2), 124-144.

Girard, A. R. (2005). "Hybrid Supervisory Control for Real-Time Embedded Bus Rapid Transit Applications." *IEEE Transaction on Vehicular Technology*, 54(5), 1684-1696.

Gordon, T., Howell, M., and Brandao, F. (2003). "Integrated Control Methodologies for Road Vehicles." *Vehicle System Dynamics*, 40(1-3), 157-190.

Hac, A., and Bodie, M. O. (2002). "Improvements in Vehicle Handling through Integrated Control of Chassis Systems." *International Journal of Vehicle Design*, 29(1-2), 23-50.

He, Crolla, J., Levesley, D. A., Manning, M. C., and J, W. (2004). "Integrated Chassis Control through Coordination of Active Front Steering and Intelligent Torque Distribution." Advanced Vehicle Control 04, Arnhem.

Inagaki, S., Kushiro, I., and Yamamoto, M. (1995). "Analysis on Vehicle Stability in Critical Cornering Using Phase-Plane Method." *JSAE Review*, 16(2), 216-216.

Jayasuriya, S. (1995). "On The Determination of the Worst Allowable Persistent Bounded Disturbance for A System with Constraints." *ASME Journal of Dynamic Systems, Measurement, and Control*, 117(2), 126-134.

Kade, A., Hopkins, H. G., and Salman, M. A. (1987). "Anti-Lock Brake Control System ", US Patent 4,664,453.

Karbalaei, R., Ghaffari, A., Kazemi, R., and Tabatabaei, S. H. (2007). "Design of An Integrated AFS/DYC Based on Fuzzy Logic Control." Vehicular Electronics and Safety, 2007. ICVES. IEEE International Conference.

Karnopp, D. (1983). "Active Damping in Road Vehicle Suspension Systems." *Vehicle System Dynamics*, 12(6), 291-311.

Kimbrough, Scott S, W., and Hallman, S. J. (1988). "Four Wheel Steering System With Closed-loop Feed back and Open-loop Feedforward " US Patent 4842089.

Kitajima, K., and Peng, H. (2000). "Control for Integrated Side-slip, Roll and Yaw Controls for Ground Vehicles." Advanc Vehicle Control 2000.

Kleimaier, A., and Schroder, D. (2000). "Optimization Strategy for Design and Control of a Hybrid Vehicle." Advanced Motion Control 6th International Workshop, Nagoya.

Koehn, P., Eckrich, M., Smakman, H., and Schaffert, A. (2006). "Integrated Chassis Management: Introduction into BMW's Approach to ICM." 2006 SAE World Congress, Detroit.

Komatsu, A., Gordon, T., and Best, M. (2000). "4WS Control of Handling Dynamics Using a Linear Optimal Reference Model." Advanc Vehicle Control 2000, Ann Arbor.

Lim, E. H. M., and Hedrick, J. K. (1999). "Lateral and Longitudinal Vehicle Control Coupling for Automated Vehicle Operation." American Control Conference, San Diego.

Lin, C. C., Peng, H., Grizzle, J. W., and Kang, J. M. (2003). "Power Management Strategy for a Parallel Hybrid Electric Truck." *IEEE Transactions on Control Systems Technology* 11(6), 839-849

Lu, P. (1996). "Constrained Tracking Control of Nonlinear Systems." *Systems &Control Letters*, 27(5), 305–314.

Ma, W. H. (1998). "Worst-case Evaluation Methods for Vehicles and Vehicle Control Systems," Ph. D. Dissertation, University of Michigan, Ann Arbor.

Maciejowski, J. M. (2002). *Predictive Control: With Constraints*, Prentice Hall.

Mokhiamar, O., and Abe, M. (2005). "Simultaneous Optimal Distribution of Lateral and Longitudinal Tire Forces for the Model Following Control." *Journal of Dynamic Systems, Measurement, and Control*, 126(4), 753-764.

Morari, M., and Lee, J. H. (1999). "Model Predictive Control: Past, Present and Future." *Computers and Chemical Engineering*, 23(4-5), 667-682.

MSC. (2009). "CarSim Reference Manual." Mechanical Simulation Corporation.

Nagai, M., Shino, M., and Gao, F. (2002). "Study on Integrated Control of Active Front Steer Angle and Direct Yaw Moment." *JSAE Review*, 23(3), 309-315.

NHTSA. (2003). "Consumer Information. New Car Assessment Program: Rollover Resistance." Federal Register.

NHTSA. (2007a). "Federal Motor Vehicle Safety Standards Electronic Stability Control Systems Control and Display." Federal Register.

NHTSA. (2007b). "FMVSS No. 126 Electronic Stability Control Systems." NHTSA Final Regulatory Impact Analysis, Federal Register.

Oppenheimer, M. W., Doman, D. B., and Bolender, M. A. (2006). "Control Allocation for Over-actuated Systems." 14th Mediterranean Conference on Control and Automation, Ancona.

Saberi, A., Stoorvogel, A. A., and Sannuti, P. (2004). "Decentralized Control with Input Saturation." American Control Conference Boston.

Skogestad, S., and Postlethwaite, I. (2005). *Multi-variable Feedback Control: Analysis and Design*, John Wiley & Sons.

Storkaas, E. (2002). "Model Predictive Control: Online Optimization versus Explicit Pre-computed Controller." Norwegian University of Science and Technology.

Tham, M. T. (1999). "Multi-variable Control: An Introduction to Decoupling Control." Department of Chemical and Process Engineering, University of Newcastle upon Tyne.

Tondel, P., and Johansen, T. A. (2005). "Control Allocation for Yaw Stabilization in Automotive Vehicles Using Multi-parametric Nonlinear Programming." American Control Conference, Portland.

Trachtler, A. (2004). "Integrated Vehicle Dynamics Control Using Active Brake, Steering and Suspension Systems." *International Journal of Vehicle Design* 36(1), 1-12.

UBC.CA. (2009). "www.math.ubc.ca/~feldman/m227/contraction.pdf."

Ungoren, A. Y. (2003). "Worst-case Evaluation Methods for Rollover Prevention System," Ph. D. Dissertation, University of Michigan, Ann Arbor.

Vermillion, C. R. (2009). "Optimal Modular Control of Overactuated Systems - Theory and Applications," University of Michigan, Ann Arbor.

Wang, J. (2006). "Coordinated Vehicle Dynamics Control with Control Distribution," Ph. D. Dissertation, University of Texas at Austin.

Wang, J. (2007). "On the Control Allocation for Coordinated Ground Vehicle Dynamics Control Systems." American Control Conference, New York.

Wang, Y. Q., and Nagai, M. (1999). "Improvement of Vehicle Handling and Stability by an Integrated Four-Wheel-Steer and Yaw Moment Control System." *Progress in Technology*, 77, 173–182.

Webers, K., and Busch, R. (2003). "Ford Integrated Vehicle Dynamics Control: Realization." Ford Forschungszentrum Aachen.

WorldAutoSteel. (2009). "Mass Reduction and Fuel Efficiency ".

Xiong, Q., Wen-Jian, C., Mao-Jun, H., and He, M. (2006). "Decentralized Control System Design for Multivariable Processes : A Novel Method Based on Effective Relative Gain Array." *Industrial & Engineering Chemistry Research*, 45(8), 2769-2776.

Yoshimura, T., and Emoto, Y. (2003). "Steering and Suspension System of a Full Car Model Using Fuzzy Reasoning Based on Single Input Rule Modules." *International Journal of Vehicle Autonomous Systems* 1(3-4), 363-386.

Zanten, V. (2000). "Bosch ESP Systems: 5 Years of Experience." *SAE Transactions*, 109(7), 428-436.

Zeyada, Y. F., ElBeheiry, E. M., and ElArabi, M. E. (2000). "Fault Diagnosis and Mu-estimation for Integrated Chassis Control of Vehicles in Emergency Maneuvers." *Journal of Engineering and Applied Science* 47, 665–682.

Zhou, J. (2008). "Active Safety Measures for Vehicles Involved in Light Vehicle-to-Vehicle Impacts," Ph. D. Dissertation, University of Michigan, Ann Arbor.